Available online at www.sciencedirect.com
SCIENCE DIRECT®
Progress in Particle and Nuclear Physics 54 (2005) 193–288
Progress in Particle and Nuclear Physics
www.elsevier.com/locate/ppnp

Review

Strange quark matter and compact stars

F. Weber*

Department of Physics, San Diego State University, 5500 Campanile Drive, San Diego, CA 92182, USA

Abstract

Astrophysicists distinguish between three different kinds of compact stars. These are white dwarfs, neutron stars, and black holes. The former contain matter in one of the densest forms found in the Universe which, together with the unprecedented progress in observational astronomy, makes such stars superb astrophysical laboratories for a broad range of most striking physical phenomena. These range from nuclear processes on the stellar surface to processes in electron degenerate matter at subnuclear densities to boson condensates and the existence of new states of baryonic matter—such as color superconducting quark matter—at supernuclear densities. More than that, according to the strange matter hypothesis strange quark matter could be more stable than nuclear matter, in which case neutron stars should be largely composed of pure quark matter possibly enveloped in thin nuclear crusts. Another remarkable implication of the hypothesis is the possible existence of a new class of white dwarfs. This article aims at giving an overview of all these striking physical possibilities, with an emphasis on the astrophysical phenomenology of strange quark matter. Possible observational signatures associated with the theoretically proposed states of matter inside compact stars are discussed as well. They will provide most valuable information about the phase diagram of superdense nuclear matter at high baryon number density but low temperature, which is not accessible to relativistic heavy ion collision experiments.

Keywords: Nuclear matter; Strange matter; Quarks; Phase transitions; Neutron stars

Contents

1. Introduction 194

* Tel.: +1 619 594 0239; fax: +1 619 594 5485.
E-mail address: fweber@sciences.sdsu.edu.

0146-6410/$ - see front matter © 2004 Elsevier B.V. All rights reserved.
doi:10.1016/j.ppnp.2004.07.001

2. Confined hadronic matter 197
2.1. Effective nuclear field theories 198
2.2. Non-relativistic treatments 202
3. Primer on quark matter 204
3.1. Models for the equation of state 204
3.2. Color superconductivity 210
3.3. The strange quark matter hypothesis 212
3.4. Searches for strange quark matter 217
3.5. Unusual seismographic events 222
3.6. AMS and ECCO 223
4. Relativistic stellar models 224
4.1. Particles in curved space–time 224
4.2. Stellar structure equations of non-rotating stars 225
4.3. Rotating star models 227
4.4. Kepler frequency 228
4.5. Moments of inertia of rotating compact stars 230
5. Strangeness in compact stars 232
5.1. Neutron stars 232
5.1.1. Hyperons 232
5.1.2. K^- meson condensate 232
5.1.3. Strange quarks 234
5.1.4. H-dibaryons 240
5.2. Strange stars 241
5.2.1. General properties 241
5.2.2. SAX J1808.4-3658 246
5.2.3. RX J1856.5-3754 248
5.2.4. The neutron star in 3C58 250
5.2.5. X-ray, gamma ray burst, and SGR associations 250
5.2.6. Rotational instabilities 252
5.2.7. Surface properties of strange stars 253
5.3. Strange dwarfs 254
6. Neutrino emission and stellar cooling 258
7. Signals of quark matter in rotating neutron stars 264
7.1. Isolated pulsars 265
7.2. Accreting neutron stars 274
8. Summary 279
Acknowledgments 280
References 280

1. Introduction

It is often stressed that there has never been a more exciting time in the overlapping areas of nuclear physics, particle physics, and relativistic astrophysics than today. This comes at a time where new orbiting observatories such as the Hubble Space Telescope, Rossi X-ray Timing Explorer (RXTE), Chandra x-ray satellite, and X-ray Multi Mirror Mission (XMM) have extended our vision tremendously, allowing us to see vistas with an

unprecedented clarity and angular resolution that previously were only imagined, enabling astrophysicists for the first time ever to perform detailed studies of large samples of galactic and extragalactic objects. On the Earth, radio telescopes (e.g., Arecibo, Green Bank, Parkes, VLA) and instruments using adaptive optics and other revolutionary techniques have exceeded previous expectations of what can be accomplished from the ground. The gravitational wave detectors LIGO, LISA, VIRGO, and Geo-600 are opening up a window for the detection of gravitational waves emitted from compact stellar objects such as neutron stars and black holes.

Neutron stars are dense, neutron-packed remnants of massive stars that blew apart in supernova explosions. They are typically about twenty kilometers across and spin rapidly, often making several hundred rotations per second. Many neutron stars form radio pulsars, emitting radio waves that appear from the Earth to pulse on and off like a lighthouse beacon as the star rotates at very high speeds. Neutron stars in x-ray binaries accrete material from a companion star and flare to life with a burst of x-rays. Measurements of radio pulsars and neutron stars in x-ray binaries comprise most of the neutron star observations. Improved data on isolated neutron stars (e.g. RX J1856.5-3754, PSR $0205+6449$) are now becoming available, and future investigations at gravitational wave observatories such as LIGO and VIRGO will focus on neutron stars as major potential sources of gravitational waves. Depending on star mass and rotational frequency, gravity compresses the matter in the core regions of pulsars up to more than ten times the density of ordinary atomic nuclei, thus providing a high pressure environment in which numerous subatomic particle processes compete with each other. The most spectacular ones stretch from the generation of hyperons and baryon resonances ($\Sigma, \Lambda, \Xi, \Delta$) to quark ($u, d, s$) deconfinement to the formation of boson condensates (π^-, K^-, H matter) [1–3]. There are theoretical suggestions of even more exotic processes inside neutron stars, such as the formation of absolutely stable strange quark matter [4–6], a configuration of matter more stable than the most stable atomic nucleus, ^{62}Ni.[1] In the latter event, neutron stars would be largely composed of strange quark matter [7–9] possibly enveloped in thin nuclear crusts [10] whose density is less than neutron drip. Another striking implication of the hypothesis is the possible existence of a new class of white dwarfs [11,12]. An overview of the conjectured composition of neutron stars is shown in Fig. 1. Because of their complex interior structures, the very name neutron star is almost certainly a misnomer. Instead these objects should be named nucleon stars, since relatively isospin symmetric nuclear matter—in equilibrium with condensed K^- mesons—may prevail in their interiors [13], hyperon stars if hyperons (Σ, Λ, Ξ, possibly in equilibrium with the Δ resonance) become populated in addition to the nucleons [14], quark hybrid stars if the highly compressed matter in the centers of neutron stars were to transform into u, d, s quark matter [15], or strange stars if strange quark matter were to be more stable than nuclear matter. The idea that quark matter may exist in the cores of neutron stars is not new but has already been suggested by several authors [16–21,326]. For many years it has been thought that the deconfined phase of quarks and hadrons is strictly excluded from neutron stars. Theoretical

[1] It is common practice to compare the energy of strange quark matter to ^{56}Fe. The energy per particle of ^{56}Fe, however, comes in only third after ^{62}Ni and ^{58}Fe.

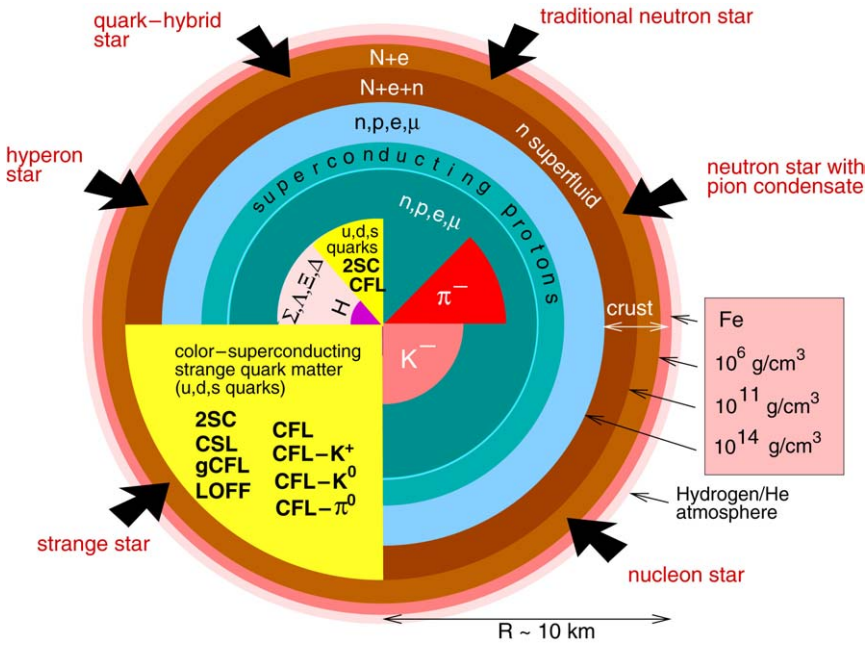

Fig. 1. Competing structures and novel phases of subatomic matter predicted by theory to make their appearance in the cores ($R \lesssim 8$ km) of neutron stars [1].

studies, however, have shown that this was due to seemingly innocuous idealizations [22,23]. Thus neutron stars may very well contain quark matter in their cores, which ought to be in a color superconducting state [24–27]. This fascinating possibility has renewed tremendous interest in the physics and astrophysics of quark matter.

Of course, at present one does not know from experiment at what density the expected phase transition to quark matter occurs. Neither do lattice Quantum ChromoDynamical (QCD) simulations provide a conclusive guide yet. From simple geometrical considerations it follows that, for a characteristic nucleon radius of $r_N \sim 1$ fm, nuclei begin to touch each other at densities of $\sim(4\pi r_N^3/3)^{-1} \simeq 0.24$ fm^{-3}, which is less than twice the baryon number density of ordinary nuclear matter, $\rho_0 = 0.16$ fm^{-3} (energy density $\epsilon_0 = 140$ MeV/fm^3). Depending on the rotational frequency and stellar mass, such densities are easily surpassed in the cores of neutron stars so gravity may have broken up the neutrons (n) and protons (p) in the centers of neutron stars into their constituents. Moreover, since the mass of the strange quark (s) is rather small, probably less than 100 MeV as indicated by the latest lattice results [28], highly energetic up (u) and down (d) quarks may readily transform to strange quarks at about the same density at which unconfined up and down quarks appear.

The phase diagram of quark matter, expected to be in a color superconducting phase, is very complex [24,25]. At asymptotic densities the ground state of QCD with a vanishing strange quark mass is the color–flavor locked (CFL) phase. This phase is electrically charge

neutral without any need for electrons for a significant range of chemical potentials and strange quark masses [29]. (Technically, there are no electrons only at zero temperature. At finite temperature the electron population is exponentially ($\exp(-\Delta/T)$) suppressed, where Δ denotes the superconducting gap.) If the strange quark mass is heavy enough to be ignored, then up and down quarks may pair in the two-flavor superconducting (2SC) phase. Other possible condensation patterns include the CFL-K^0 phase [30] and the color–spin locked (CSL) phase [31]. The magnitude of the gap energy lies between ∼50 and 100 MeV. Color superconductivity, which modifies the equation of state at the order $(\Delta/\mu)^2$ level [32,33], thus changes the volume energy by just a few per cent. Such a small effect can be safely neglected in present determinations of models for the equation of state of neutron star matter and strange star matter. The situation is different for phenomena involving the cooling by neutrino emission, the pattern of the arrival times of supernova neutrinos, the evolution of neutron star magnetic fields, rotational (r-mode) instabilities, and glitches in rotation frequencies of pulsars (see Refs. [24,25,34–38] and references therein). Aside from neutron star properties, an additional test of color superconductivity may be provided by upcoming cosmic ray space experiments such as AMS [39] and ECCO [40]. As shown in Ref. [41], finite lumps of color–flavor locked strange quark matter, which should be present in cosmic rays if strange matter is the ground state of the strong interaction, turn out to be significantly more stable than strangelets [327,328] without color–flavor locking for wide ranges of parameters. In addition, strangelets made of CFL strange matter obey a charge–mass relation that differs significantly from the charge–mass relation of strangelets made of ordinary strange quark matter [9,41]. This difference may allow an experimental test of CFL locking in strange quark matter [41].

In this review I will describe the current status of our understanding of the phases of superdense nuclear matter inside compact stars, putting special emphasis on the role of strange quark matter in astrophysics. This is accompanied by a discussion of possible observable signatures of the competing states of superdense matter in the cores of compact stars. These signatures will provide most valuable information about the phase diagram of superdense nuclear matter at high baryon number density but low temperature, which is not accessible to relativistic heavy ion collision experiments.

The article is organized as follows. Section 2 discusses the properties and representative models for the equation of state of confined hadronic matter. This is followed by a brief primer on quark matter presented in Section 3. Relativistic stellar models are discussed in Section 4. The possible role of strange quarks for compact stars and astrophysical phenomena associated with such stars are reviewed in Section 5. Neutrino emission from compact stars and their cooling behavior are discussed in Section 6. Finally, possible astrophysical signals of quark matter in compact stars are reviewed in Section 7, and this is followed by general concluding remarks provided in Section 8.

2. Confined hadronic matter

The equation of state of neutron star matter below neutron drip, which occurs at densities around 4×10^{11} g/cm^3, and at densities above neutron drip but below the saturation density of nuclear matter is relatively well known. This is to a lesser extent

the case for the equation of state in the vicinity of the saturation density of normal nuclear matter. Finally the physical properties of matter at still higher densities are highly uncertain and the models derived for the equation of state of such matter differ considerably as regards the functional dependence of pressure on density. This has its origin in various sources, which concern the many-body technique used to determine the equation of state, the model of the nucleon–nucleon interaction, the alteration of hadron properties by immersion in dense matter, the fundamental constituents of neutron star matter (including phase transitions to meson condensates and quark matter), and the theoretical possibility that strange quark matter may be the true ground state of the strong interaction rather than nuclear matter. In the subsection below we introduce a collection of relativistic models for the equation of state which account for these uncertainties. Non-relativistic models for the equation of state will be studied in Section 3.

2.1. *Effective nuclear field theories*

Up until the mid-1970s nearly all dense nuclear matter studies were based on non-relativistic potential models for describing the nucleon–nucleon interaction. The relativistic, field-theoretical approach to nuclear matter was pioneered primarily by Walecka and collaborators [42,43]. The generalization of Walecka's model Lagrangian to superdense neutron star matter has the following form [1,14,44]:

$$\begin{aligned}\mathcal{L} = {} & \sum_B \bar{\psi}_B (i\partial\!\!\!/ - m_B)\psi_B + \frac{1}{2}(\partial^\mu \sigma \partial_\mu \sigma - m_\sigma^2 \sigma^2) \\ & - \frac{1}{4} F^{\mu\nu} F_{\mu\nu} + \frac{1}{2} m_\omega^2 \omega^\nu \omega_\nu + \frac{1}{2}(\partial^\mu \boldsymbol{\pi} \cdot \partial_\mu \boldsymbol{\pi} - m_\pi^2 \boldsymbol{\pi} \cdot \boldsymbol{\pi}) \\ & - \frac{1}{4} \mathbf{G}^{\mu\nu} \cdot \mathbf{G}_{\mu\nu} + \frac{1}{2} m_\rho^2 \boldsymbol{\rho}^\mu \cdot \boldsymbol{\rho}_\mu - \sum_B \Bigg(g_{\sigma B} \bar{\psi}_B \sigma \psi_B + g_{\omega B} \bar{\psi}_B \phi\!\!\!/ \psi_B \\ & + \frac{f_{\omega B}}{4m_B} \bar{\psi}_B \sigma^{\mu\nu} F_{\mu\nu} \psi_B + \frac{f_{\pi B}}{m_\pi} \bar{\psi}_B \gamma^5 \partial\!\!\!/ \boldsymbol{\tau} \cdot \boldsymbol{\pi} \psi_B \\ & + g_{\rho B} \bar{\psi}_B \gamma^\mu \boldsymbol{\tau} \cdot \boldsymbol{\rho}_\mu \psi_B + \frac{f_{\rho B}}{4m_B} \bar{\psi}_B \sigma^{\mu\nu} \boldsymbol{\tau} \cdot \mathbf{G}_{\mu\nu} \psi_B \Bigg) \\ & - \frac{1}{3} m_N b_N (g_{\sigma N} \sigma)^3 - \frac{1}{4} c_N (g_{\sigma N} \sigma)^4 + \sum_L \bar{\psi}_L (i\partial\!\!\!/ - m_L)\psi_L \end{aligned} \tag{1}$$

where B denotes baryons (p, n, Σ, Λ, Ξ), L stands for leptons (e^-, μ^-), and $\phi = \gamma^\mu \omega_\mu$, $\partial\!\!\!/ = \gamma^\mu \partial_\mu$, $\sigma^{\mu\nu} = i[\gamma^\mu, \gamma^\nu]/2$. The baryons are described as Dirac particles which interact via the exchange of σ, ω, π, and ρ mesons. The σ and ω mesons are responsible for nuclear binding while the ρ meson is required to obtain the correct value for the empirical symmetry energy. The cubic and quartic σ terms in Eq. (1) are necessary (at the relativistic mean-field level) for obtaining the empirical incompressibility of nuclear matter [45]. The field equations for the baryon fields follow from (1) as follows [1,44]:

$$(i\gamma^\mu\partial_\mu - m_B)\psi_B = g_{\sigma B}\sigma\psi_B + \left(g_{\omega B}\gamma^\mu\omega_\mu + \frac{f_{\omega B}}{4m_B}\sigma^{\mu\nu}F_{\mu\nu}\right)\psi_B + \left(g_{\rho B}\gamma^\mu\boldsymbol{\tau}\cdot\boldsymbol{\rho}_\mu + \frac{f_{\rho B}}{4\,m_B}\sigma^{\mu\nu}\boldsymbol{\tau}\cdot\mathbf{G}_{\mu\nu}\right)\psi_B + \frac{f_{\pi B}}{m_\pi}\gamma^\mu\gamma^5(\partial_\mu\boldsymbol{\tau}\cdot\boldsymbol{\pi})\psi_B. \quad (2)$$

The meson fields in (2) are obtained as solutions of the following field equations:

$$(\partial^\mu\partial_\mu + m_\sigma^2)\sigma = -\sum_B g_{\sigma B}\bar\psi_B\psi_B - m_N b_N g_{\sigma N}(g_{\sigma N}\sigma)^2 - c_N\, g_{\sigma N}(g_{\sigma N}\sigma)^3, \quad (3)$$

$$\partial^\mu F_{\mu\nu} + m_\omega^2\omega_\nu = \sum_B\left(g_{\omega B}\bar\psi_B\gamma_\nu\psi_B - \frac{f_{\omega B}}{2m_B}\partial^\mu(\bar\psi_B\sigma_{\mu\nu}\psi_B)\right), \quad (4)$$

$$(\partial^\mu\partial_\mu + m_\pi^2)\boldsymbol{\pi} = \sum_B\frac{f_{\pi B}}{m_\pi}\partial^\mu(\bar\psi_B\gamma_5\gamma_\mu\boldsymbol{\tau}\psi_B), \quad (5)$$

$$\partial^\mu\mathbf{G}_{\mu\nu} + m_\rho^2\boldsymbol{\rho}_\nu = \sum_B\left(g_{\rho B}\bar\psi_B\boldsymbol{\tau}\gamma_\nu\psi_B - \frac{f_{\rho B}}{2m_B}\partial^\mu(\bar\psi_B\boldsymbol{\tau}\sigma_{\mu\nu}\psi_B)\right), \quad (6)$$

with the field tensors $F_{\mu\nu}$ and $\mathbf{G}_{\mu\nu}$ defined as $F_{\mu\nu} = \partial_\mu\omega_\nu - \partial_\nu\omega_\mu$ and $\mathbf{G}_{\mu\nu} = \partial_\mu\boldsymbol{\rho}_\nu - \partial_\nu\boldsymbol{\rho}_\mu$. For neutron star matter, Eqs. (2) through (6) are to be solved subject to the conditions of electric charge neutrality and chemical equilibrium. The condition of electric charge neutrality reads

$$\sum_B q_B^{\rm el}(2J_B+1)\frac{k_{F_B}^3}{6\pi^2} - \sum_L\frac{k_{F_L}^3}{3\pi^2} - \rho_M\,\Theta(\mu^M - m_M) = 0, \quad (7)$$

where J_B and $q_B^{\rm el}$ denote the spin and electric charge number of a baryon B, respectively. The last term in (7) accounts for the electric charge carried by condensed bosons. The only mesons that may plausibly condense in neutron star matter are the π^- or, alternatively, the more favored K^- [46,47]. Eq. (7) constrains the Fermi momenta of baryons and leptons, k_{F_B} and k_{F_L} respectively. Leptons in neutron star matter are treated as free relativistic particles:

$$(i\gamma^\mu\partial_\mu - m_L)\psi_L = 0. \quad (8)$$

The baryon and lepton Fermi momenta are further constrained by the condition of chemical equilibrium. Since neutron star matter is characterized by the existence of two conserved charges, electric charge and baryon charge, the chemical potential of an arbitrary baryon, B, created in a neutron star can be expressed in terms of two independent chemical potentials. Choosing μ^n and μ^e as the independent chemical potentials, one has

$$\mu^B = q_B\mu^n - q_B^{\rm el}\mu^e, \quad (9)$$

with q_B the baryon number of particle B. Since $q_B \equiv q_f = \frac{1}{3}$ for quark flavors $f = u, d, s$, the chemical potentials of quarks follow from (9) as

$$\mu^f = \frac{1}{3}\mu^n - q_f^{\rm el}\mu^e. \quad (10)$$

Relativistic Green's functions constitute an elegant and powerful technique which allows one to derive from (2) to (6) a set of three coupled equations which are numerically tractable [1]. The first one of these equations is the Dyson equation which determines the two-point baryon Green function S^B in matter:

$$S^B = S_0^B - S_0^B \Sigma^B S^B. \tag{11}$$

The second equation determines the effective baryon–baryon scattering amplitude in matter, $T^{BB'}$, which is given by

$$T^{BB'} = V^{BB'} - V_{\rm ex}^{BB'} + \int V^{B\bar{B}} \Lambda^{\bar{B}\bar{B}'} T^{\bar{B}'B'}. \tag{12}$$

Here V and $V_{\rm ex}$ denote the direct and exchange terms of a given one-boson-exchange potential, which serves as an input, and the quantity $\Lambda^{\bar{B}\bar{B}'} \propto S^{\bar{B}} S^{\bar{B}'}$ describes the propagation of baryons $\bar{B}$ and $\bar{B}'$ in intermediate scattering states. A popular and physically most suggestive choice for Λ is the so-called Brueckner propagator [1,48]. This propagator describes the propagation of two baryons in intermediate scattering states in terms of the full single-particle energy–momentum relation and, in addition, guarantees that these particles obey the Pauli principle too. The system of equations is closed by the expression for the self-energy of a baryon in matter, Σ^B, given by

$$\Sigma^B = i \sum_{B'} \int (\mathrm{Tr}(T^{BB'} S^{B'}) - T^{BB'} S^{B'}). \tag{13}$$

The one-boson-exchange potentials, $V^{BB'}$, sum the contributions arising from different kinds of mesons that exchanged among the baryons:

$$\langle 12|V^{BB'}|34\rangle = \sum_{M=\sigma,\omega,\pi,\rho,\ldots} \delta^4(1,3)\delta^4(2,4)\Gamma^M(1,3)\Gamma^M(2,4)\Delta^M(1,2), \tag{14}$$

where Γ^M denote meson–nucleon vertices, and Δ^M free meson propagators.

Relativistic models for the equation of state of neutron star matter are obtained by solving Eqs. (11) through (13) self-consistently in combination with Eqs. (7) and (9) for electric charge neutrality and chemical equilibrium. This has been accomplished for several different approximation schemes. With increasing level of complexity, these are the relativistic Hartree (RH), the relativistic Hartree–Fock (RHF), and the relativistic Brueckner–Hartree–Fock (RBHF) approximations [1]. The first two approximations are obtained by keeping only the Born term in the T-matrix equation (12), that is, by setting $T = V - V_{\rm ex}$ (and readjusting the parameters for the boson-exchange potential). The mass operator (13) is then given by

$$\Sigma^B(p) = -i \sum_{B'} g_{\sigma B} g_{\sigma B'} \int \frac{\mathrm{d}^4 q}{(2\pi)^4} \mathrm{e}^{\mathrm{i}\eta q^0} \times (\Delta^\sigma(0) S^{B'}(q) - \delta_{BB'} \Delta^\sigma(p-q) S^B(q)) \pm \ldots \tag{15}$$

where the T-matrix is replaced, according to Eq. (14), by free meson propagators. This simplifies the solution of the many-body equations considerably. Because of this approximation, however, the coupling constants of the theory need to be adjusted to fit the

properties of infinite nuclear matter, hypernuclear data, and neutron star properties (see, for instance, Refs. [1,15,49,50]). The five nuclear matter properties are the binding energy E/A, the effective nucleon mass $m_{\rm N}^*/m_{\rm N}$, the incompressibility K, and the symmetry energy $a_{\rm s}$ at nuclear matter saturation density ρ_0 ($=0.16$ fm^{-3}):

$$E/A = -16.0 \text{ MeV}, \quad m_N^*/m_N = 0.79, \quad K \simeq 225 \text{ MeV}, \quad a_s = 32.5 \text{ MeV}. \tag{16}$$

Of the five, the value for the incompressibility of nuclear matter carries the biggest uncertainty [2]. Its value is currently believed to lie in the range between about 220 and 250 MeV. In contrast to the RH and RBHF ones, the RBHF approximation makes use of one-boson-exchange potentials whose parameters are adjusted to the properties of the deuteron and relativistic nucleon–nucleon scattering data. This approximation is therefore referred to as parameter free. In passing we mention that in recent years a new class of effective field theories was developed which treat the meson–nucleon couplings as density dependent. These field theories provide a very good description of the properties of nuclear matter, atomic nuclei, as well as neutron stars [52–56]. We conclude this section with a brief discussion of the total energy density of the system which follows from the stress–energy density tensor, $T_{\mu\nu}$, as [1]

$$\epsilon = \langle T_{00} \rangle = \sum_{\chi=B,L} \partial_0 \psi_\chi \frac{\partial \mathcal{L}}{\partial(\partial^0 \psi_\chi)} - g_{00}\mathcal{L}. \tag{17}$$

The pressure, and thus the equation of state, are obtained from Eq. (17) as

$$P = \rho^2 \partial/\partial\rho(\epsilon/\rho). \tag{18}$$

Finally, the energy per particle is given in terms of the energy density and baryon number density as

$$\epsilon = (E/A + m_{\rm N})\rho. \tag{19}$$

Fig. 2 shows several model equations of state based on RH and RBHF assuming different particle compositions of neutron star matter [1]. Of particular interest later (Section 7) will be the equation of state in Fig. 2 accounting for quark deconfinement [49] which, for this model, sets in at 230 MeV/fm^3, which is less than two times the energy density of nuclear matter, $\epsilon_0 = 140$ MeV/fm^3. Pure quark matter exists for densities greater than 950 MeV/fm^3, which is around seven times ϵ_0. Of key importance for the possible occurrence of a quark–hadron phase in neutron stars is that pressure in the mixed phase of quarks and hadrons varies with density [22]. If this is not the case, hydrostatic equilibrium would strictly exclude the mixed phase from neutron stars. Table 1 shows the properties of nuclear matter computed for different many-body techniques as well as nuclear forces. In addition to the saturation properties listed in (16) this table also shows the symmetry energy density derivative, L, and the slope, y, of the saturation curve of isospin asymmetric nuclear matter, defined as $L = 3\rho_0(\partial a_{\rm s}/\partial\rho)_{\rho_0}$ and $y = -K a_{\rm s}(3\rho_0 L)^{-1}$, for several models, which vary considerably from one model to another.

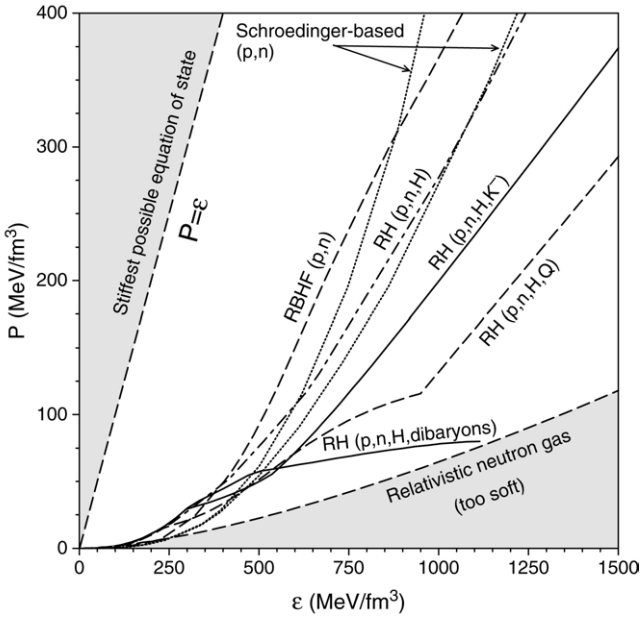

Fig. 2. Models for the equation of state of neutron star matter computed for different compositions and many-body techniques described in the text [1]. (p, n denote protons and neutrons; H, K^-, Q stand for hyperons, K^- condensate, and quarks, respectively.)

2.2. Non-relativistic treatments

The most frequently used non-relativistic treatments of dense nuclear matter studies are the hole–line expansion (Brueckner theory) [57,58], the coupled cluster method, self-consistent Green functions, the variational approach (Monte Carlo techniques), the semiclassical Thomas–Fermi method [59,60], and the density functional approach based on Skyrme effective interactions (for an overview of these methods and additional references, see Refs. [2,61]). Apart from in the density functional approach, the starting point in each case is a phenomenological nucleon–nucleon interaction, which, in some cases, is supplemented with a three-nucleon interaction V_{ijk} introduced to achieve the correct binding energy of nuclear matter at the empirical saturation density, $\rho_0 = 0.15$ nucleons/fm^3. Fig. 2 shows two Schrödinger based models for the equation of state which are obtained for variational calculations based on the Urbana V_{14} two-nucleon interaction supplemented with the three-body interaction UVII (left curve) and TNI (right curve) three-nucleon interaction [2,62,63]. The Hamiltonian is thus of the form

$$\mathcal{H} = \sum_i \frac{-\hbar^2}{2m}\nabla_i^2 + \sum_{i<j} V_{ij} + \sum_{i<j<k} V_{ijk}. \tag{20}$$

In the variational approach the Schrödinger equation $\mathcal{H}|\Psi\rangle = E|\Psi\rangle$ is solved using a variational trial function $|\Psi_v\rangle$, which is constructed from a symmetrized product of two-body correlation operators (F_{ij}) acting on an unperturbed ground state (Fermi gas

Table 1
Saturation properties of nuclear matter computed for numerous different nuclear forces and many-body techniques [1,44,51]

Method/Force	ρ_0 (fm^{-3})	E/A (MeV)	K (MeV)	a_s (MeV)	L (MeV)	y (MeV fm^3)
SG-0	0.168	−16.7	253	35.6	41.6	−430
SGI	0.154	−15.8	261	28.3	64.1	−250
SGII	0.158	−15.6	215	26.8	37.6	−322
SkM	0.160	−15.8	217	30.7	49.3	−281
SkM*	0.160	−15.8	217	30.0	45.8	−296
E_σ	0.163	−16.0	249	26.4	−36.9	364
Z_σ	0.163	−15.9	233	26.7	−29.4	432
Z^*_σ	0.163	−16.0	235	28.8	−4.58	3030
R_σ	0.158	−15.6	238	30.6	85.7	−179
G_σ	0.158	−15.6	237	31.4	94.0	−167
SkT6	0.161	−16.0	236	30.0	30.8	−475
SkP	0.163	−16.0	201	30.0	19.5	−632
SkSC4	0.161	−15.9	235	28.8	−2.17	6460
SkX	0.155	−16.1	271	31.1	33.2	−545
MSk7	0.158	−15.8	231	27.9	9.36	−1460
BSk1	0.157	−15.8	231	27.8	7.15	−1908
SLy4	0.160	−16.0	230	32.0	45.9	−335
SLy7	0.158	−15.9	230	32.0	47.2	−328
TM1	0.145	−16.3	281	37.9	114	−215
NL 1	0.152	−16.4	212	43.5	140	−145
FRDM	0.152	−16.3	240	32.7	–	–
HV	0.145	−15.98	285	32.5		
Bro *A*	0.174	−16.5	280	34.4	81.9	−225
Bro *B*	0.172	−15.7	249	32.8	90.2	−175
Bro *C*	0.170	−14.4	258	31.5	76.1	−209
UV_{14} + TNI	0.157	−16.6	261	30.8	–	–
UV_{14} + UVII	0.175	−11.5	202	29.3	–	–
AV_{14} + UVII	0.194	−12.4	209	27.6	–	–
$\mathrm{A}_{18} + \delta v$ + UIX	0.16	−16.00	–	–	–	–
TF96	0.161	−16.04	234	32.0	–	–

wave function) $|\Phi\rangle$,

$$|\Psi_v\rangle = \left(S\prod_{i<j} F_{ij}\right)|\Phi\rangle. \tag{21}$$

The antisymmetrized Fermi gas wave function is given by $|\Phi\rangle = A(\prod_{i<\mathrm{F}}|i\rangle)$. The correlation operator contains variational parameters (14 for the UV_{14} and AV_{14} models [62] and 18 for the more recent A_{18} model [64]) which are varied to minimize the energy per baryon for a given density ρ,

$$E(\rho) = \min\frac{\langle\Psi_v|\mathcal{H}|\Psi_v\rangle}{\langle\Psi_v|\Psi_v\rangle}, \tag{22}$$

which constitutes an upper bound to the ground state energy of the system. The pressure and energy density of the stellar matter are obtained from relations (18) and (19), respectively. The new Thomas–Fermi approach of Myers and Swiatecki, TF96, is based on a Seyler–Blanchard potential generalized by the addition of one momentum dependent and one density dependent term [59]:

$$V_{12} = -\frac{2T_0}{\rho_0} Y(r_{12}) \times \left(\frac{1}{2}(1 \mp \xi)\alpha - \frac{1}{2}(1 \mp \zeta) \left(\beta \left(\frac{p_{12}}{k_{F_0}} \right)^2 - \gamma \frac{k_{F_0}}{p_{12}} + \sigma \left(\frac{2\bar{\rho}}{\rho_0} \right)^{\frac{2}{3}} \right) \right). \tag{23}$$

The upper (lower) sign in (23) corresponds to nucleons with equal (unequal) isospin. The quantities k_{F_0}, $T_0\,(=k_{F_0}^2/2m)$, and ρ_0 are the Fermi momentum, the Fermi energy, and the saturation density of symmetric nuclear matter. The potential's radial dependence is described by a Yukawa-type interaction of the form

$$Y(r_{12}) = \frac{1}{4\pi a^3} \frac{\mathrm{e}^{-r_{12}/a}}{r_{12}/a}. \tag{24}$$

Its strength depends both on the magnitude of the particles' relative momentum, p_{12}, and on an average of the densities at the locations of the particles. The parameters ξ and ζ were introduced in order to achieve better agreement with asymmetric nuclear systems. The behavior of the optical potential is improved by the term $\sigma(2\bar{\rho}/\rho_0)^{2/3}$ with the average density defined as $\overline{\rho}^{2/3} = (\rho_1^{2/3} + \rho_2^{2/3})/2$, and ρ_1 and ρ_2 the densities of interacting neutrons or protons at points 1 and 2. The seven free parameters of the theory are adjusted to the properties of finite nuclei, the parameters of the mass formula, and the behavior of the optical potential [59]. The nuclear matter properties at saturation density obtained for TF96 are listed in Table 1.

3. Primer on quark matter

3.1. Models for the equation of state

The field theory of quarks and gluons, Quantum ChromoDynamics (QCD), is a non-Abelian gauge theory with $\mathrm{SU(3)_c}$ as a gauge group. The QCD Lagrangian has the form

$$\mathcal{L} = \bar{\psi}_f^a (i\gamma_\mu D_{ab}^\mu - m_f)\psi_f^b - \frac{1}{4} F_{\mu\nu}^i F_i^{\mu\nu}, \tag{25}$$

where ψ_f^a are the quark fields for each flavor f and m_f the current quark masses (see Table 2). In color space, the fields ψ_f^a are three-component columns with $a = 1, 2, 3$. The color gauge-covariant derivative D^μ is given by

$$D_{ab}^\mu = \delta_{ab}\partial^\mu - i\frac{g_s}{2}[\lambda_i]_{ab} G_i^\mu, \tag{26}$$

where g_s is the strong interaction coupling constant. The quantities G_i^μ are the gluon fields with color indices $i = 1, \ldots, 8$, and λ_i the Gell-Mann $\mathrm{SU(3)_c}$ matrices. The quantity $F_{\mu\nu}^i$

is the gluon field tensor defined as

$$F^i_{\mu\nu} = \partial_\mu G^i_\nu - \partial_\nu G^i_\mu + g_s\, f_{ijk} G^j_\mu G^k_\nu, \tag{27}$$

where f_{ijk} are the $SU(3)_c$ structure constants. The equations of motion of the coupled quark and gluon fields derived from Eq. (25) are then as follows:

$$(i\gamma_\mu \partial^\mu - m_f)\psi^a_f = -g_s \gamma_\mu \left(\frac{\lambda_i}{2}\right)_{ab} \psi^b_f G^\mu_i, \tag{28}$$

$$\partial^\mu F^i_{\mu\nu} + g_s\, f_{ijk} G^{j\mu} F^k_{\mu\nu} = -g_s \bar{\psi}^a_f \gamma_\nu \left(\frac{\lambda_i}{2}\right)_{ab} \psi^b_f. \tag{29}$$

Considerable efforts are made to solve the QCD equations of motion on the lattice. At present, however, such simulations do not provide a guide at finite baryon number density, and it is necessary to rely on non-perturbative QCD models for quark matter which incorporate the basic properties expected for QCD. Three different categories of models have emerged. These are (1) phenomenological models (MIT bag models) where quark masses are fixed and confinement is described in terms of a bag constant, and more advanced (2) dynamical models and (3) Dyson–Schwinger equation models where the properties of quarks (matter) are determined self-consistently. The most widely used of these models is the MIT bag model [65,66,329]. For this model, the pressure P^i of the individual quarks and leptons contained in the bag is counterbalanced by the total external bag pressure $P + B$ according to

$$P + B = \sum_f P^f, \tag{30}$$

while the total energy density of the quark flavors confined in the bag is given by

$$\epsilon = \sum_f \epsilon^f + B. \tag{31}$$

The quantity B denotes the bag constant, and ϵ^f are the contributions of the individual quark to the total energy density. The condition of electric charge neutrality among the quarks reads

$$3\sum_f q^{\rm el}_f k^3_{F_f} - \sum_L k^3_{F_L} = 0, \tag{32}$$

where $q^{\rm el}_f$ denotes the electric charge number of a quark of flavor f, listed in Table 2. The contributions of each quark flavor to pressure, energy density, and baryon number density are determined by the thermodynamic potentials $\mathrm{d}\Omega^f = -S^f \mathrm{d}T - P^f \mathrm{d}V - A^f \mathrm{d}\mu^f$, from which one obtains

$$P^f = \frac{\nu_i}{6\pi^2} \int_0^{k_{F_f}} \mathrm{d}k \frac{k^4}{\sqrt{k^2 + m_f^2}},$$

$$\epsilon^f = \frac{\nu_f}{2\pi^2} \int_0^{k_{F_f}} \mathrm{d}k\, k^2 \sqrt{k^2 + m_f^2}, \qquad \rho^f = \frac{\nu_f}{6\pi^2} k^3_{F_f}. \tag{33}$$

Table 2
Approximate masses, m_f, and electric charge numbers, $q_f^{\rm el}$ of quarks

Quark flavor (f)	u	d	c	s	t	b
m_f (GeV)	0.005	0.01	1.5	0.1	180	4.7
$q_f^{\rm el}$	$+\frac{2}{3}$	$-\frac{1}{3}$	$+\frac{2}{3}$	$-\frac{1}{3}$	$+\frac{2}{3}$	$-\frac{1}{3}$

The quantity μ^f denotes the chemical potential of quark flavor f, and m_f stands for its mass. The phase space factor ν_f is equal to 2(spin) $\times$ 3(color) $= 6$. Chemical equilibrium among the quark flavors and the leptons is maintained by the following weak reactions:

$$d \leftrightarrow u + e^- + \bar{\nu}^e, \qquad s \leftrightarrow u + e^- + \bar{\nu}^e, \qquad s \leftrightarrow c + e^- + \bar{\nu}^e,$$
$$s + u \leftrightarrow d + u, \qquad c + d \leftrightarrow u + d. \tag{34}$$

Since neutron stars lose the neutrinos within the first few seconds after birth, the chemical potentials of neutrinos and antineutrinos obey $\mu^\nu = \mu^{\bar{\nu}} = 0$ and one obtains from the weak reactions (34)

$$\mu^d = \mu^u + \mu^e, \qquad \mu^c = \mu^u, \qquad \mu \equiv \mu^d = \mu^s. \tag{35}$$

The equation of state of relativistic quark matter at zero temperature made up of massless, non-interacting particles is readily calculated from (33). One obtains

$$P^f = \frac{\nu_f}{24\pi^2}(\mu^f)^4 = \frac{1}{3}\epsilon^f, \qquad \rho^f = \frac{\nu_f}{6\pi^2}(\mu^f)^3, \tag{36}$$

with $\nu_f = 6$. The equation of state of such matter is obtained from equations (30) and (31) as

$$P = (\epsilon - 4B)/3. \tag{37}$$

From Eq. (37) one sees that the external pressure acting on a bag filled with quarks vanishes for $\epsilon = 4B$. The mass contained inside the bag is given by $M = \int_0^R \epsilon \mathrm{d}V = (4\pi/3)\epsilon R^3$, which is the generic mass–radius relation of self-bound matter. The consequences of this relation for strange quark matter systems are illustrated in Fig. 3. The condition of electric charge neutrality of stellar quark matter, Eq. (32), leads to

$$2\rho^u - \rho^d - \rho^s = 0. \tag{38}$$

Since $\mu^u = \mu^d = \mu^s$ for massless quarks, one finds from Eq. (30) that for zero external pressure, P, the bag constant is related to the quark chemical potential as $B = 3\mu^4/4\pi^2$. The energy per baryon number of quark matter follows as

$$\frac{E}{A} \equiv \frac{\epsilon}{\rho} = 4\frac{B}{(\rho^u + \rho^d + \rho^s)/3} = 4\frac{B}{\rho^u} = 4\pi^2\frac{B}{\mu^3}, \tag{39}$$

with ρ the total baryon number density defined as

$$\rho = \sum_f \rho^f/3. \tag{40}$$

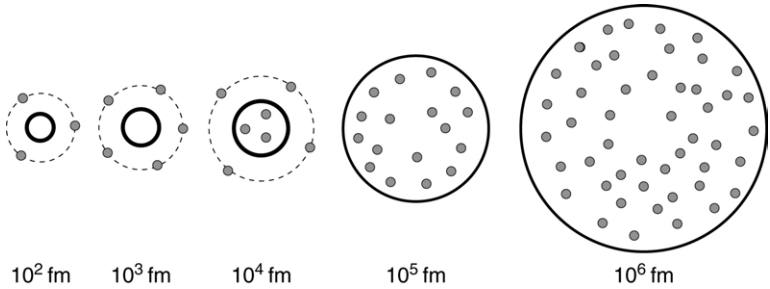

Fig. 3. Radii of quark bags [67]. For masses less than 10^9 GeV the electrons (gray dots) are outside the quark bags (indicated by thick solid circles) and the core + electron system has a size of $\sim 10^5$ fm. For masses between 10^9 and 10^{15} GeV the electrons are partially inside the core. For masses greater than 10^{15} GeV all electrons are inside the core.

In the next step we turn to the determination of the equation of state if the charm and strange quarks are given their finite mass values listed in Table 2. In this case Eq. (33) leads for the pressure, mass density, and baryon number density of quark matter to the following expressions:

$$P^f = \frac{\nu_f (\mu^f)^4}{24\pi^2}\left(\sqrt{1-z_f^2}\left(1-\frac{5}{2}z_f^2\right)+\frac{3}{2}z_f^4 \ln\frac{1+\sqrt{1-z_f^2}}{z_f}\right), \tag{41}$$

$$\rho^f = \frac{\nu_f (\mu^f)^3}{6\pi^2}(1-z_f^2)^{\frac{3}{2}}, \tag{42}$$

$$\epsilon^f = \frac{\nu_f (\mu^f)^4}{8\pi^2}\left(\sqrt{1-z_f^2}\left(1-\frac{1}{2}z_f^2\right)-\frac{z_f^4}{2}\ln\frac{1+\sqrt{1-z_f^2}}{z_f}\right), \tag{43}$$

with z_i defined as $z_f = m_f/\mu^f$. Ignoring the two most massive quark flavors, t and b, which are far too heavy to become populated in compact stars (see Fig. 4), the condition of electric charge neutrality, expressed in Eq. (32), reads

$$2(\rho^u+\rho^c)-(\rho^d+\rho^s)-3(\rho^e+\rho^\mu)=0. \tag{44}$$

Upon substituting (42) into (44), this relation can be written as

$$\begin{aligned}&2(1-(\mu^e/\mu)^3)(1+(1-z_c^2)^{\frac{3}{2}})-(1+(1-z_s^2)^{\frac{3}{2}})\\&\quad-(\mu^e/\mu)^3(1+(1-z_\mu^2)^{\frac{3}{2}})=0.\end{aligned} \tag{45}$$

An expression for the pressure of the system is obtained by substituting (41) into (30). This leads to

$$P+B=\frac{\mu^4}{4\pi^2}((1-(\mu^e/\mu)^4)\Phi(z_c)+\Phi(z_s)), \tag{46}$$

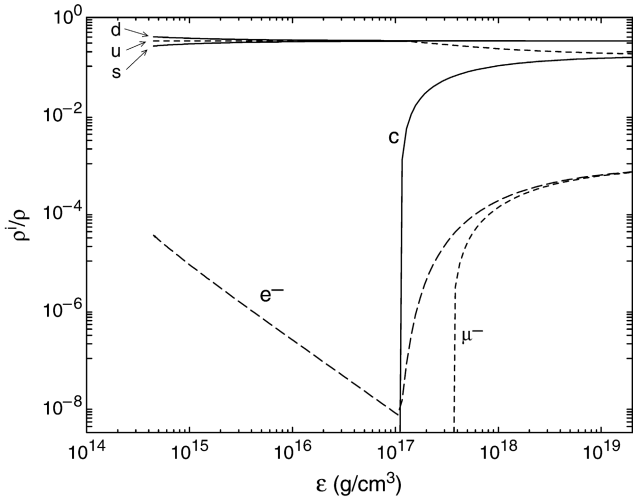

Fig. 4. Relative quark and lepton densities in quark star matter as a function of mass density (from Ref. [68]).

with Φ defined as

$$\Phi(z_f) = 1 + \sqrt{1 - z_f^2}\left(1 - \frac{5}{2}z_f^2\right) + \frac{3}{2}z_f^2 \ln\frac{1 + \sqrt{1 - z_f^2}}{z_f}. \tag{47}$$

The total energy density follows from (31) as

$$\epsilon = (3P + 4B) + \frac{1}{4\pi^2}\sum_{f=s,c} \nu_f (\mu^f)^4 z_f^{-2}\left(\sqrt{1 - z_f^2} - z_f^2 \ln\frac{1 + \sqrt{1 - z_f^2}}{z_f}\right). \tag{48}$$

The first term on the right-hand side of Eq. (48) represents the equation of state of a relativistic gas of massless quarks derived in Eq. (37) while the second term accounts for finite strange and charm quark masses. Finally, the total baryon number density of such quark matter is given by

$$\rho = \frac{\mu^3}{3\pi^2}((1 - (\mu^e/\mu)^3)(1 + (1 - z_c^2)^{\frac{3}{2}}) + (1 + (1 - z_s^2)^{\frac{3}{2}})). \tag{49}$$

The relative quark–lepton composition of absolutely stable ($B^{1/4} = 145$ MeV) quark star matter at zero temperature is shown in Fig. 4. All quark flavor states that become populated in such matter up to densities of 10^{19} g/cm^3 are taken into account. Since the Coulomb interaction is so much stronger than gravity, quark star matter in the lowest energy state must be charge neutral to very high precision [8]. Therefore, any net positive quark charge must be balanced by a sufficiently large number of negatively charged quarks and leptons, which determines the lepton concentration shown in Fig. 4. Because of their relatively large masses, the presence of charm quarks requires densities greater than 10^{17} g/cm^3 in order to be present. Stellar sequences containing strange and charm quarks

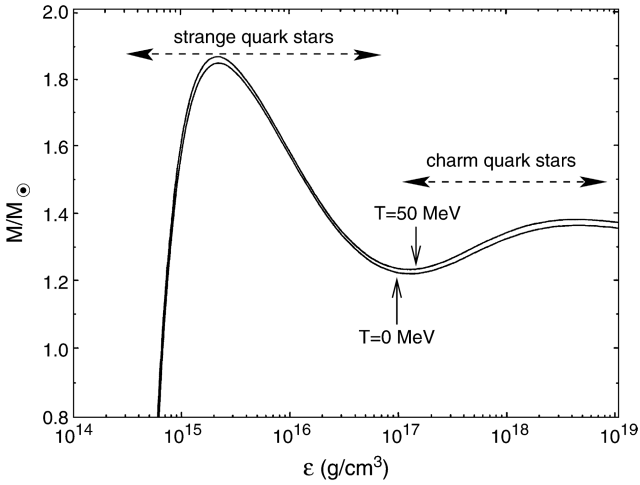

Fig. 5. Masses of quark stars at zero and finite temperature versus the central star density [68].

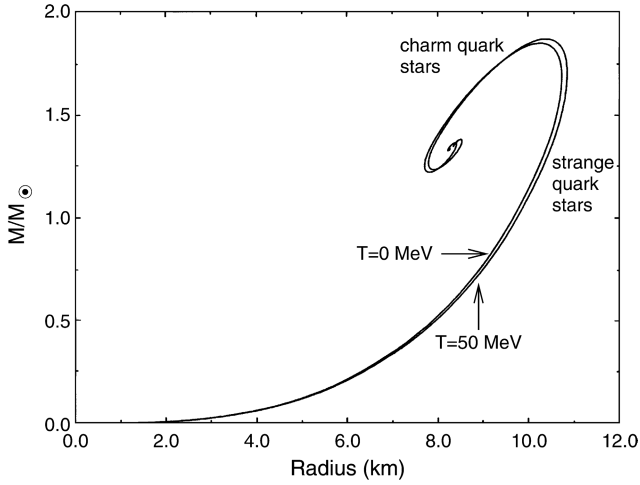

Fig. 6. Mass versus radius for the quark star sequences shown in Fig. 5 [68].

are shown in Figs. 5 and 6. An analysis of the stability of these sequences against radial oscillations (see Section 5.3), however, shows that only the strange star sequence is stable and not the charm star sequence. Finally, we mention that a value for the bag constant of $B^{1/4} = 145$ MeV places the energy per baryon number of (non-interacting) strange quark matter at $E/A = 829$ MeV [329], which corresponds to strange quark matter strongly bound with respect to ^{56}Fe whose energy per baryon is $M(^{56}\mathrm{Fe})c^2/56 = 930.4$ MeV, with $M(^{56}\mathrm{Fe})$ the mass of the ^{56}Fe atom.

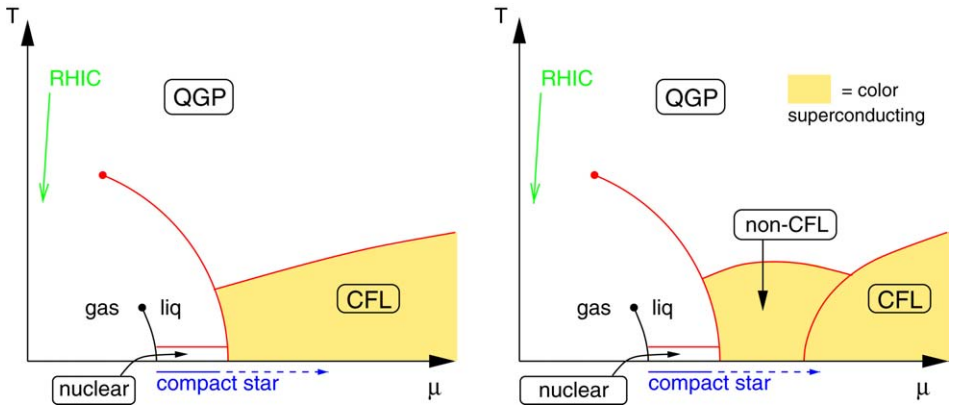

Fig. 7. The conjectured phase diagram for QCD [33]. For small m_s^2/Δ there is a direct transition from nuclear matter to CFL color superconducting quark matter. For large m_s^2/Δ there is an intermediate phase where condensation patterns such as the CFL-K^0, CFL-K^+, CFL-π^0, gCFL, 2SC, 1SC, CSL, and LOFF phases (see the text) may exist. Figure reprinted with permission from M. Alford, J. Phys. G 30 (2004) S441.

3.2. Color superconductivity

There has been much recent progress in our understanding of quark matter, culminating in the discovery that if quark matter exists it ought to be in a color superconducting state [24–27]. This is made possible by the strong interaction among the quarks which is very attractive in some channels. Pairs of quarks are thus expected to form Cooper pairs very readily. Since pairs of quarks cannot be color neutral, the resulting condensate will break the local color symmetry and form what is called a color superconductor. The phase diagram of such matter is expected to be very complex [24,25], as can be seen from Figs. 7 and 8. This is caused by the fact that quarks come in three different colors, different flavors, and different masses. Moreover, bulk matter is neutral with respect to both electric and color charge, and is in chemical equilibrium under the weak interaction processes that turn one quark flavor into another. To illustrate the condensation pattern briefly, we note the following pairing ansatz for the quark condensate [70]:

$$\langle \psi^{\alpha}_{f_a} C\gamma_5 \psi^{\beta}_{f_b} \rangle \sim \Delta_1 \epsilon^{\alpha\beta 1}\epsilon_{f_a f_b 1} + \Delta_2 \epsilon^{\alpha\beta 2}\epsilon_{f_a f_b 2} + \Delta_3 \epsilon^{\alpha\beta 3}\epsilon_{f_a f_b 3}, \tag{50}$$

where $\psi^{\alpha}_{f_a}$ is a quark of color $\alpha = (r, g, b)$ and flavor $f_a = (u, d, s)$. The condensate is a Lorentz scalar, antisymmetric in Dirac indices, antisymmetric in color, and thus antisymmetric in flavor. The gap parameters Δ_1, Δ_2, and Δ_3 describe d–s, u–s, and u–d quark Cooper pairs, respectively. The following pairing schemes have emerged. At asymptotic densities ($m_s \to 0$ or $\mu \to \infty$) the ground state of QCD with a vanishing strange quark mass is the color–flavor locked (CFL) phase (color–flavor locked quark pairing), in which all three quark flavors participate symmetrically. The gaps associated with this phase are

$$\Delta_3 \simeq \Delta_2 = \Delta_1 = \Delta, \tag{51}$$

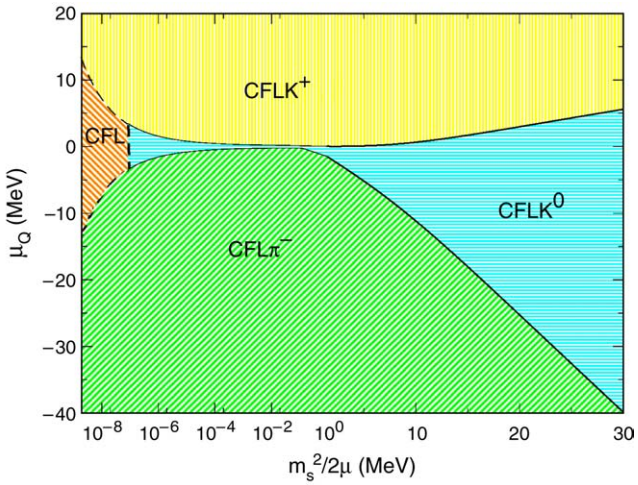

Fig. 8. Possible meson condensed phases in the neighborhood of the symmetric CFL state for a strange quark mass of $m_s = 150$ MeV. μ is the quark chemical potential and μ_Q the chemical potential for positive electric charge. Solid and dashed lines indicate first- and second-order transitions respectively [69]. Figure reprinted with permission from D.B. Kaplan and S. Reddy, Phys. Rev. D 65 (2002) 054042.

and the quark condensates of the CFL phase are approximately of the form

$$\langle \psi^{\alpha}_{f_a} C\gamma_5 \psi^{\beta}_{f_b} \rangle \sim \Delta \epsilon^{\alpha\beta X} \epsilon_{f_a f_b X}, \tag{52}$$

with color and flavor indices all running from 1 to 3. Since $\epsilon^{\alpha\beta X}\epsilon_{f_a f_b X} = \delta^{\alpha}_{f_a}\delta^{\beta}_{f_b} - \delta^{\alpha}_{f_b}\delta^{\beta}_{f_a}$ one sees that the condensate (52) involves Kronecker delta functions that link color and flavor indices. Hence the notion of color–flavor locking. The CFL phase has been shown to be electrically neutral without any need for electrons for a significant range of chemical potentials and strange quark masses [29]. If the strange quark mass is heavy enough to be ignored, then up and down quarks may pair in the two-flavor superconducting (2SC) phase. Other possible condensation patterns are CFL-K^0 [30], CFL-K^+, and CFL-$\pi^{0,-}$ [69], gCFL (a gapless CFL phase) [70], 1SC (single-flavor pairing) [70–72], CSL (a color–spin locked phase) [31], and the LOFF (crystalline pairing) [35,73,74] phase, depending on m_s, μ, and the electric charge density. Calculations performed for massless up and down quarks and a very heavy strange quark mass ($m_s \to \infty$) agree that the quarks prefer to pair in the two-flavor superconducting (2SC) phase where

$$\Delta_3 > 0, \qquad \text{and} \qquad \Delta_2 = \Delta_1 = 0. \tag{53}$$

In this case the pairing ansatz (50) reduces to

$$\langle \psi^{\alpha}_{f_a} C\gamma_5 \psi^{\beta}_{f_b} \rangle \propto \Delta \epsilon_{ab} \epsilon^{\alpha\beta 3}. \tag{54}$$

Here the resulting condensate picks a color direction (3 or blue in the example (54) above), and creates a gap Δ at the Fermi surfaces of quarks with the other two out of three colors

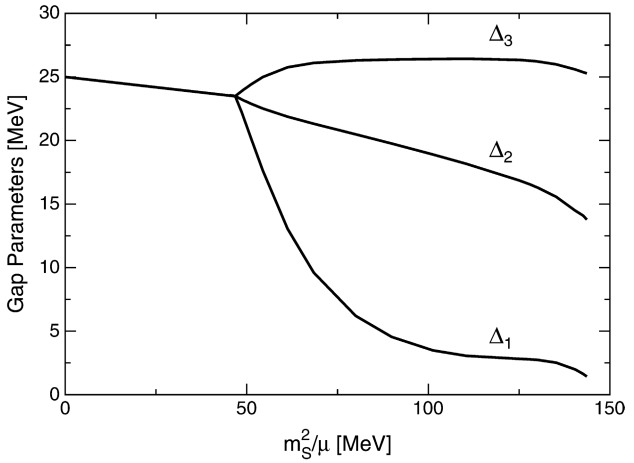

Fig. 9. Gap parameters Δ_1, Δ_2, and Δ_3 as a function of m_s^2/μ for $\mu = 500$ MeV, in an NJL model [70]. There is a second-order phase transition between the CFL phase and the gapless CFL (gCFL) phase at $m_s^2/\mu = 2\Delta$. Figure reprinted with permission from M. Alford, C. Kouvaris, and K. Rajagopal, Phys. Rev. Lett. 92 (2004) 222001.

(red and green). The gapless CFL phase (gCFL) may prevail over the CFL and 2SC phases at intermediate values of m_s^2/μ with gaps given obeying the relation (see Fig. 9)

$$\Delta_3 > \Delta_2 > \Delta_1 > 0. \tag{55}$$

As shown in Fig. 10, for chemical potentials that are of astrophysical interest (see Section 5 through 7), $\mu < 1000$ MeV, the gap is between 50 and 100 MeV. The order of magnitude of this result agrees with calculations based on phenomenological effective interactions [27,75] as well as with perturbative calculations for $\mu > 10$ GeV [76]. We also note that superconductivity modifies the equation of state at the order of $(\Delta/\mu)^2$ [32,33], which is even for such large gaps only a few per cent of the bulk energy. Such small effects may be safely neglected in present determinations of models for the equation of state of quark hybrid stars. There has been much recent work on how color superconductivity in neutron stars could affect their properties. (See Refs. [24,25,34–37] and references therein.) These studies reveal that possible signatures include the cooling by neutrino emission, the pattern of the arrival times of supernova neutrinos, the evolution of neutron star magnetic fields, rotational stellar instabilities, and glitches in rotation frequencies. Several of these issues will be discussed in Section 5 to 7.

3.3. The strange quark matter hypothesis

The theoretical possibility that strange quark matter may constitute the true ground state of the strong interaction rather than ^{56}Fe was proposed by Bodmer [4], Witten [5], and Terazawa [6]. A schematic illustration of this so-called strange matter hypothesis is given in Fig. 11, which compares the energy per baryon of ^{56}Fe and infinite nuclear matter with

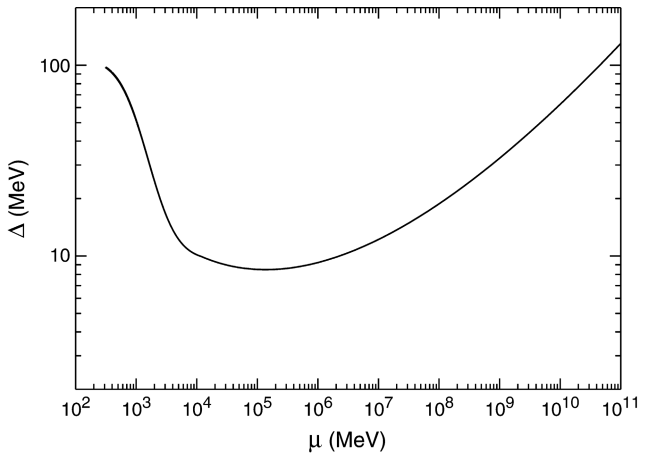

Fig. 10. Superconducting gap Δ versus quark chemical potential μ [69]. Figure reprinted with permission from D.B. Kaplan and S. Reddy, Phys. Rev. D 65 (2002) 054042.

the energy per baryon of two- and three-flavor quark matter. Three-flavor quark matter is always lower in energy than two-flavor quark matter due to the extra Fermi well that is accessible to the strange quarks. Theoretical arguments indicate that the energy of three-flavor quark matter may be even smaller than 930 MeV in which case strange matter would be more stable than nuclear matter and atomic nuclei. This peculiar feature makes the strange matter hypothesis one of the most startling speculations of modern physics, which, if correct, would have implications of fundamental importance for our understanding of the early universe, its evolution in time to the present day, astrophysical compact objects, and laboratory physics, as summarized in Table 3 [7,9,77]. In the following we describe the possible absolute stability of strange quark matter for a gas of massless u, d, s quarks inside a confining bag at zero temperature [329]. For a massless quark flavor f, the Fermi momentum, p_{F_f}, equals the chemical potential, μ^f. The number densities, energy densities, and corresponding pressures, therefore, follow from Eq. (36) as

$$\rho^f = (\mu^f)^3/\pi^2, \qquad \epsilon^f = 3(\mu^f)^4/4\pi^2, \qquad P^f = (\mu^f)^4/4\pi^2 = \epsilon^f/3. \tag{56}$$

For a gas of massless u and d quarks the condition of electric charge neutrality $2\rho^u - \rho^d = 0$, which follows from Eq. (32), requires that $\rho^d = 2\rho^u$. Hence the chemical potential of two-flavor quark matter is given by $\mu_2 \equiv \mu^u = \mu^d/2^{1/3}$. The corresponding two-flavor quark pressure then follows as $P_2 \equiv P^u + P^d = (1 + 2^{4/3})\mu_2^4/4\pi^2 = B$. From the expressions for the total energy density, $\epsilon_2 = 3P_2 + B = 4B$, and baryon number density, $\rho_2 = (\rho^u + \rho^d)/3 = \mu_2^3/\pi^2$, one then obtains for the energy per baryon of two-flavor quark matter

$$\left.\frac{E}{A}\right|_2 \equiv \frac{\epsilon_2}{\rho_2} = \frac{4B}{\rho_2} = 934 \text{ MeV} \times B_{145}^{1/4}, \tag{57}$$

where $B_{145}^{1/4} \equiv B^{1/4}/145$ MeV. Values for $B^{1/4}$ smaller than 145 MeV are excluded. Otherwise two-flavor quark matter would have a lower energy than ^{56}Fe, which then would be made up of up and down quarks, in contradiction to what is observed. In the next step we add massless strange quarks to the system. The three-flavor quark gas is electrically neutral for $\rho^u = \rho^d = \rho^s$, i.e. $\mu_3 \equiv \mu^u = \mu^d = \mu^s$. For a fixed bag constant, the three-flavor quark gas should exert the same pressure as the two-flavor gas, that is $P_3 = P_2$. This implies for the chemical potentials $\mu_3 = ((1 + 2^{4/3})/3)^{1/4}\mu_2$. Hence, the total baryon number in this case can be written as $\rho_3 = \mu_3^3/\pi^2 = ((1 + 2^{4/3})/3)^{3/4}\rho_2$. The energy per baryon is therefore given by

$$\left.\frac{E}{A}\right|_3 \equiv \frac{\epsilon_3}{\rho_3} = \frac{4B}{1.127\rho_2} = 829 \text{ MeV} \times B_{145}^{1/4}, \tag{58}$$

since $\epsilon_3 = 3P_3 + B = 4B = \epsilon_2$. It thus follows that the energy per baryon of a massless non-interacting three-flavor quark gas is of order 100 MeV per baryon lower than for two-flavor quark matter. The difference arises from the fact that baryon number can be packed more densely in three-flavor quark matter, $\rho_2/\rho_3 = (3/(1 + 2^{4/3}))^{3/4} \simeq 0.89$, due to the extra Fermi well that is accessible to the strange quarks. The energy per baryon in a free gas of neutrons is equal to the neutron mass, $E/A = 939.6$ MeV. For an ^{56}Fe nucleus the energy per baryon is $E/A = (56m_N - 56 \times 8.8 \text{ MeV})/56 = 930$ MeV, where $m_N = 938.9$ denotes the nucleon mass. Stability of two-flavor quark matter relative to neutrons thus corresponds to $(E/A)_2 < m_n$, or $B^{1/4} < 145.9$ MeV ($B^{1/4} < 144.4$ MeV for stability relative to ^{56}Fe). The stability argument is often turned around because one observes neutrons and ^{56}Fe in Nature rather than two-flavor quark matter. Hence the bag constant must be larger than about 145 MeV. Bulk three-flavor quark matter is absolutely stable relative to ^{56}Fe for $B^{1/4} < 162.8$ MeV, metastable relative to a neutron gas for $B^{1/4} < 164.4$ MeV, and metastable relative to a gas of Λ particles for $B^{1/4} < 195.2$ MeV. These numbers are upper limits. A finite strange quark mass as well as a non-zero strong coupling constant decrease the limits on $B^{1/4}$ [9,329]. The presence of ordinary nuclei in nature is not in contradiction to the possible absolute stability of strange matter, the reason being that conversion of an atomic nucleus of baryon number A into a lump of strange quark matter requires the simultaneous transformation of roughly A up and down quarks into strange quarks. The probability for this to happen involves a weak transition $\propto G_F^{2A}$ which makes nuclei with $A \gtrsim 6$ stable for more than 10^{60} y. The conversion of very light nuclei into strange matter is determined by finite-size and shell effects which dominate over the volume energy of strange matter at small A values. An example for the mass formula of strange matter is [9,327]

$$\frac{E}{A} \simeq (829 \text{ MeV} + 351 \text{ MeV } A^{-2/3})B_{145}^{1/4}, \tag{59}$$

in which case strange matter becomes absolutely stable for $A > 6$. If quark matter is in the CFL phase, metastability or even absolute stability of strange quark matter may become more likely than hitherto thought since the binding energy from pairing of the quarks should reduce the energy of the system by a contribution proportional to Δ^2 [41]. Fig. 12 shows the energy per baryon for ordinary quark matter and CFL quark matter. For high A values a bulk value is approached, but for low A the finite-size contributions

Table 3
Strange matter phenomenology

Phenomenon	References[a]
Centauro cosmic ray events	[78–81]
High energy gamma ray sources: Cyg X-3 and Her X-3	[82,83]
Strange matter hitting the Earth:	
1. Strange meteors	[84]
2. Nuclearite-induced earthquakes	[84,85]
3. Unusual seismic events	[86]
4. Strange nuggets in cosmic rays	[87–92]
Strange matter in supernovae	[93–95]
Strange star phenomenology	[1,7,8,10,11,68,77,96–98]
Strange dwarfs:	
1. Static properties and stability	[11,99,100]
2. Thermal evolution	[101]
Strange planets	[11,12,99]
Strange MACHOS	[102]
Strangeness production in dense stars	[103]
Burning of neutron stars to strange stars	[104–106]
Gamma ray bursts, soft gamma repeaters	[7,97,107–113]
Cosmological aspects of strange matter	[5,114–117]
Strange matter as a compact energy source	[118]
Strangelets in nuclear collisions	[119–121]

[a]Numerous additional references are provided in the text.

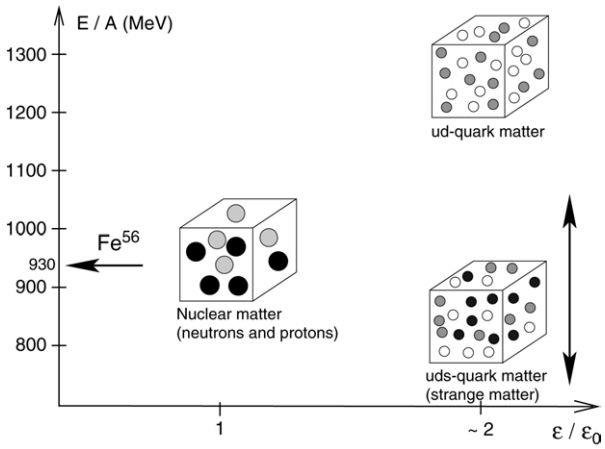

Fig. 11. Comparison of the energy per baryon of ^{56}Fe and nuclear matter with the energy per baryon of two-flavor (u, d quarks) and three-flavor (u, d, s quarks) strange quark matter. Theoretically the energy per baryon of strange quark matter may be below 930 MeV, which would render such matter more stable than nuclear matter.

(surface tension and curvature) increase the energy per baryon significantly. The pairing contribution is on the order of 100 MeV per baryon for $\Delta \approx 100$ MeV for fixed values

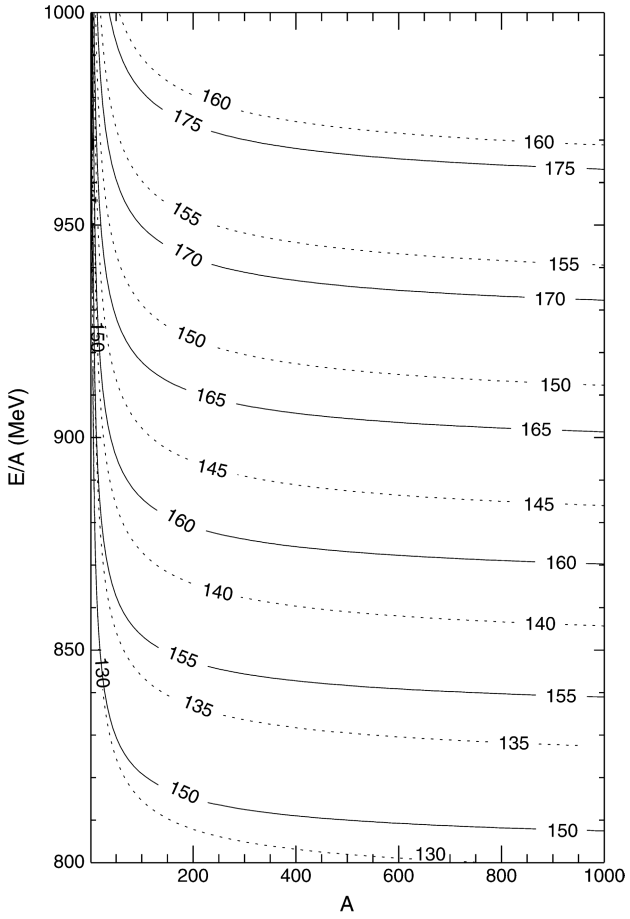

Fig. 12. Energy per baryon in MeV as a function of A for ordinary strangelets (dashed curves) and CFL strangelets (solid curves) for $B^{1/4}$ in MeV as indicated, $m_s = 150$ MeV, and $\Delta = 100$ MeV [41]. Figure reprinted with permission from J. Madsen, Phys. Rev. Lett. 87 (2001) 172003.

of the strange quark mass and bag constant. Another crucial difference between non-CFL and CFL quark matter is the equality of all quark Fermi momenta in CFL quark matter which leads to charge neutrality in bulk without any need for electrons [29]. This has most important consequences for the charge to mass ratios of strangelets. For non-CFL strangelets one has

$$Z \approx 0.1 \left(\frac{m_s}{150\ \text{MeV}}\right)^2 A \text{ for } A \ll 10^3, \qquad \text{and}$$
$$Z \approx 8 \left(\frac{m_s}{150\ \text{MeV}}\right)^2 A^{1/3} \text{ for } A \gg 10^3, \tag{60}$$

while, in contrast to this, CFL strangelets have a charge to mass ratio of [41]

$$Z \approx 0.3 \left(\frac{m_s}{150\ \text{MeV}}\right) A^{2/3}. \tag{61}$$

This difference may provide a test of color superconductivity in upcoming cosmic ray space experiments such as AMS [39] and ECCO [40] (see Section 3.6 and Table 4).

3.4. Searches for strange quark matter

Experimental physicists have searched unsuccessfully for stable or quasistable strange matter systems over the past two decades. These searches fall in three main categories: (a) searches for strange matter (strange nuggets or strangelets) in cosmic rays, (b) searches for strange matter in samples of ordinary matter, and (c) attempts to produce strange matter at accelerators. An overview of these search experiments is given in Table 4. The experiments searching for nuggets of strange matter which got stuck in terrestrial matter focus on objects whose masses can range from those of atomic nuclei to the upper limit of about 0.3×10^{-9} g. The latter carry a baryon number of $A \sim 2 \times 10^{14}$ and have a radius of $R \sim 10^{-8}$ cm. Strange nuggets heavier than 0.3×10^{-9} g will not be slowed down and stopped in the crust of the Earth. Finally, nuggets of more than $\sim 10^{22}$ quarks (i.e. $A \sim 10^{21}$) would have too much momentum to be stopped by the encounter and thus would pass through the Earth. Such encounters could take the form of unusual meteorite events, earthquakes, and peculiar particle tracks in ancient mica, in meteorites, and in cosmic ray detectors [84]. One distinguishing feature of unusual meteorite events caused by strange nuggets could be the apparent magnitude of -1.4 associated with a 20-g nugget at a distance of 10 km, which would rival that of the brightest star, Sirius. Another distinguishing feature could be the meteorite's velocity which is smaller than about 70 km/s for an ordinary meteorite bound to the solar system, but amounts to about 300 km/s for a strange meteorite of galactic origin. An upper limit on the flux of cosmic strange nuggets can be derived by assuming that the galactic dark matter halo consists entirely of strange nuggets. The expected flux at the Earth is then on the order of $10^6 A^{-1} v_{250} \rho_{24}$ cm^{-2} s^{-1} sr^{-1}, where $\rho_{24} = \rho/(10^{-24}\ \text{g/cm}^3)$ and v_{250} is the speed in units of 250 km/s [9]. Experiments sensitive at this flux level or better have been able to rule out quark nuggets as being the dark matter for baryon numbers $10^8 < A < 10^{25}$ [77, 147]. This however does not rule out a low flux level either left over from the Big Bang or arising from collisions of strange stars. If the strange matter hypothesis is valid, one should indeed expect a significant background flux of nuggets from collisions of strange stars in binary systems, which are ultimately colliding because of the loss of angular momentum emitted from the binary system as gravitational radiation. If such collisions spread as little as $0.1 M_\odot$ of strangelets with baryon number $A(\sim 10^3)$, a single collision will lead to a flux of $10^{-6} A^{-1} v_{250}$ cm^{-2} s^{-1} sr^{-1} [9], assuming that the nuggets are spread homogeneously in a galactic halo of radius 10 kpc. This would lead to a concentration of nuggets in our galaxy of less than 10^{-8} nuggets/cm^3, translating to a nugget concentration in terrestrial crust matter of at most 10^9 cm^{-3} (mass density $\sim 10^{-29}$ g/cm^3). Such a nugget density would correspond to a concentration of nuggets per nucleon, $N_{\text{strange}}/N_{\text{nucleons}}$, that is much less than 10^{-14} [148]. The upper limit on the concentration of strange nuggets per nucleon in terrestrial matter established experimentally by Brügger et al. [149] and

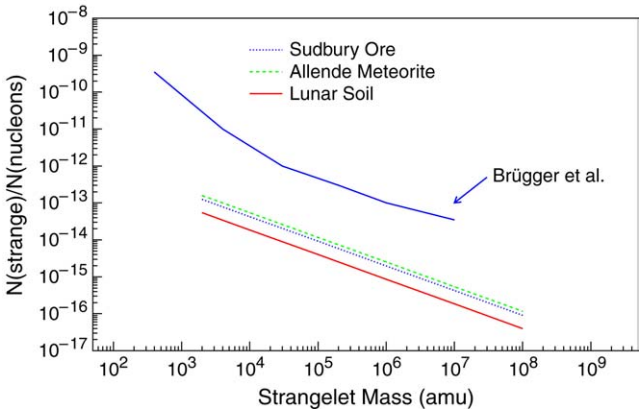

Fig. 13. Experimental limits on the concentration of strangelets per nucleon, $N_{\text{strange}}/N_{\text{nucleons}}$, contained in three samples studied [137]. These are a meteorite, terrestrial nickel ore, and lunar soil. The results from Brügger et al. [149] obtained with an iron meteorite are shown for comparison. Figure reprinted with permission from M.C. Perillo Isaac et al., Phys. Rev. Lett. 81 (1998) 2416.

Perillo Isaac et al. [137] is 10^{-14}, which falls short of the upper limits that follow from strange star–strange star collisions as well as the flux of strange nuggets in cosmic rays. Consequently the results of Brügger et al. [149] and Perillo Isaac et al. [137] shown in Fig. 13 do not rule out the existence of strange matter. This figure shows the results for three samples, a heavy ion activation experiment mostly sensitive to light strangelets ($A < 10^9$) which, if present as cosmic rays, would have been absorbed into the Earth's atmosphere. The situation would be different for the Moon, which has no atmosphere. Since its surface has been exposed to cosmic rays for millions of years, the upper limit of the concentration of strange matter in the lunar soil can be used to deduce a limit for the flux of impinging strangelets. The lunar sample was collected from the top 0.5 to 1 cm surface, at the base of the Sculptured Hills, Station 8. The presence of high cosmic ray track densities in the sample suggests that the integrated lunar surface exposure age is about 100 Myr. Using the range of strange matter in normal matter suggested in [84], a limit on the flux of strangelets on the surface of the Moon was deduced in [137] and is shown in Fig. 14.

A limit on the total amount of strange matter in the Universe follows from the observed abundance of light isotopes. This is so because the strange nuggets formed in the Big Bang would have absorbed free neutrons which reduces the neutron to proton ratio, N_n/N_p. This effect in turn would lower the rate of production of the isotope ^{4}He, whose abundance is well known from observation. For a given mass of the strange nuggets, this constrains their total surface area. To be consistent with the missing dark matter, assumed to be strange quark matter, and the observed abundance of light isotopes, the primordial quark nuggets had to be made of more than $\sim 10^{23}$ quarks. According to what has been said above, quark nuggets that massive are not stopped by the Earth.

As summarized in Table 4, during the past few years several experiments have been using high energy, heavy ion collisions to attempt to create strange quark matter

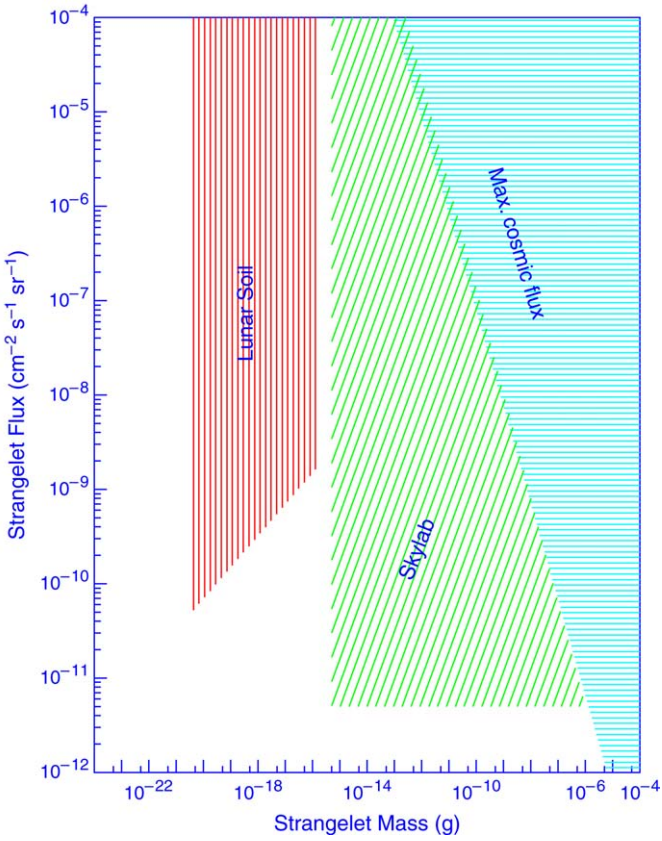

Fig. 14. Limits on the flux of strangelets impinging on the lunar surface [137]. Maximum cosmic flux refers to the cosmic flux of strangelets, assuming that all of the dark matter in the Universe is composed of strangelets. Figure reprinted with permission from M.C. Perillo Isaac et al., Phys. Rev. Lett. 81 (1998) 2416.

(strangelets) in the laboratory. The detection of strangelets in relativistic heavy ion collisions is conceptually rather simple, because of the strangelet's low Z/A ratio. Technically, however, such an attempt is very difficult for several reasons. First of all one has to defeat the finite-number destabilizing effect of strange nuggets; that is, the number of free quarks produced in a nuclear collision must be sufficiently large that surface and shell effects do not dominate over the volume energy of strange matter, destroying its possible absolute stability. Moreover, since the dense and hot matter is produced for $\sim 10^{-22}$ s, there is no time to develop a net strangeness. However, it is believed that strange nuggets will result from two kinds of simultaneous fluctuations that separate strange and antistrange quarks, and that also cool the nuggets with the result that they do not evaporate. Finally, we mention the huge multiplicity of particles produced in such collisions, which makes the particle identification rather onerous [150]. The NA52 (Newmass) experiment has been

Table 4
Past, present, and future search experiments for strange quark matter

Experiment	References
Cosmic ray searches for strange nuggets:	
AMS-02[a]	[39,122]
CRASH[b]	[123–125]
ECCO[c]	[40]
HADRON	[126]
IMB[d]	[127]
JACEE[e]	[128,129]
MACRO[f]	[130–133]
Search for strangelets in terrestrial matter:	[134]
1. Tracks in ancient mica	[84,135]
2. Rutherford backscattering	[136,137]
Search for strangelets at accelerators:	
1. Strangelet searches E858, E864, E878, E882-B, E896-A, E886	[138–140]
2. H-dibaryon search	[141,142]
3. Pb + Pb collisions	[143–146]

[a]AMS: Alpha Magnetic Spectrometer (scheduled for 2005–2008).
[b]CRASH: Cosmic Ray And Strange Hadronic matter.
[c]ECCO: Extremely heavy Cosmic-ray Composition Observer.
[d]IMB: Irvine Michigan Brookhaven proton decay detector (1980–1991).
[e]JACEE: Japanese–American Cooperative Emulsion Chamber Experiment.
[f]MACRO: Monopole, Astrophysics and Cosmic Ray Observatory (1989–2000).

searching for long lived strangelets as well as for antinuclei in Pb–Pb collisions at CERN SPS. No evidence for the production of long lived charged strangelets has been observed. One very intriguing candidate for a strangelet of mass $m = (7.4 \pm 0.3)$ GeV, electric charge $Z = -1$, and laboratory lifetime $\tau > 0.85 \times 10^{-6}$ sec was detected in the data of the 1996 run [151]. This object, which could not be confirmed however, could have been made of $6u + 6d + 9s$ quarks, carrying a baryon number of $A = 7$, or $7u + 7d + 10s$ quarks ($A = 8$).

Evidence for the possible existence of strange matter in cosmic rays may come from Centauro cosmic ray events [78–81,152]. Such events are seen in mountain top emulsion chamber experiments. The typical energy of such an event is of order $\sim 10^3$ TeV, and the typical particle multiplicity is 50 to 100 particles. Several intriguing Centauro events have been reported from a Brazilian–Japanese collaboration, the first several decades ago, where an interaction in the air 50 to about 500 m above the detector gave rise to a large number of charged hadrons and zero or very few photons or electrons [153]. In one particularly striking Centauro event, 49 hadrons were observed to interact in the detector but only one photon or electron. The typical transverse momentum (poorly determined) of about ~ 1 GeV seems to be larger than that for a typical event of the same energy. The striking feature is that there seem to be no photons produced in the primary interaction which makes the Centauro. This is unusual because in high energy collisions, π^0 mesons are always produced, and they decay into photons. A Centauro event is much like a nuclear fragmentation. If a nucleus were to fragment, then there would be many nucleons, and if the interaction which produced the fragmentation was sufficiently peripheral, there would

be few pions. This possibility is ruled out because the typical transverse momentum is so large, and more important because a nucleus would not survive to such a great depth in the atmosphere. Being much more tightly bound together than an ordinary nucleus, a strangelet with a baryon number around $A \sim 10^3$ explains many of these unusual features. So it is conceivable that a strangelet incident upon the top of the atmosphere or produced at the top of the atmosphere could survive to mountain altitude. It may have lost a significant amount of baryon number before getting to this depth however. A peripheral interaction might be sufficient to unbind it, since it certainly will not be so tightly bound with reduced baryon number. The problem with this explanation is that it does not explain the high transverse momenta. At transverse momenta of ∼1 GeV one would expect final state interactions to generate some pions, and therefore an electromagnetic component which, as mentioned above, is not observed [154]. Strange matter does not constitute the only explanation of Centauros. One alternative explanation would be that Centauro (and anti-Centauro) events are manifestations of disoriented chiral condensates [155]. Another interpretation (of the Chacaltaya Centauro events) suggests that they are due to fragments of heavy primary cosmic rays. However, the probability of survival of heavy primary nuclei to this depth in the atmosphere appears much too low to account for the number of Centauros reported.

Besides the peculiar Centauro events which may act as agents for strange matter, the high energy γ-ray sources Cygnus X-3 and Hercules X-1 may give additional independent support for the existence of strange matter. The reason is that air shower experiments on Her X-1 and Cyg X-3 indicate that these air showers have a muon content typical of cosmic rays. This muon content is a surprising result. Typical cosmic rays at energies between 10 and 10^5 TeV are protons. To arrive from the direction of Cyg X-1 or Her X-1, the particle must be electrically neutral. To survive the trip, it must be long lived. The only known particle which can quantitatively satisfy this constraint is the photon. Photon air showers however have only a small muon component. Photons shower by producing electron pairs. When only underground data was known, it was proposed that the most likely candidate for the initiating particle is a hadron, and in order for interstellar magnetic fields not to alter its direction relative to that of the source, the hadron—known in the literature as the cygnet—must be neutral. A natural candidate for the cygnet appears to be the H particle (see Section 5.1.4), the electrically neutral strangeness-2 dibaryons with the quantum numbers of two lambdas ($Z = 0$, $A = 2$) proposed by Jaffe [82]. In the theory of hadrons composed of colored quarks and antiquarks, combinations other than the usual qqq and $q\bar{q}$ are allowed as long as they are color singlets. Jaffe found that a six-quark $uuddss$ color singlet state (H) might have strong enough color–magnetic binding to be stable against strong decay. That is, m_{H} could be less than the strong decay threshold, twice the Λ^0 (uds) mass, $m_{\mathrm{H}} < 2m_{\Lambda^0}$. Estimated lifetimes for H range from $\sim 10^{-10}$ s for m_{H} near the $\Lambda^0\Lambda^0$ threshold to $>10^7$ for light H particles near the nn threshold. The potentially long lifetimes raise the possibility that H particles may be present as components of existing neutral particle beams (e.g. the E888 experiment listed in Table 4). To make the H long lived enough, it is necessary to make the H have a mass below single weak decay stability. To generate a large enough flux of H particles, the source is assumed to be a strange star. Studies of Her X-1 however seem to rule out this hypothesis, since studies of the correlation in arrival time with the known period of Her X-1 give an upper

limit of the particle mass of about 100 MeV. The source of radiation must be either due to anomalous interactions of photons or neutrinos, or from some exotic as yet undiscovered light mass, almost stable particles. The problem with Cyg X-3 may be that it is accreting mass and thus has a crust, such that there is no exposed strange matter surface where small strangelets could be produced and subsequently accelerated electrodynamically to high energies into the atmosphere of the companion star where H particles were created via spallation reactions.

Anomalously massive particles, which could be interpreted as strangelets, have been observed in a number of independent cosmic ray experiments [81]. Two such anomalous events, which are consistent with electric charge values $Z \simeq 14$ and baryon numbers $A \simeq 350$, have been observed by a balloon-borne counter experiment devoted to the study of primary cosmic rays by Saito et al. [123]. A balloon-borne experiment carried out by the Italian/Japanese CRASH (Table 4) collaboration, however, could not confirm the existence of such objects in cosmic rays [124]. Evidence for the presence of strangelets in cosmic rays has also been pointed out by Shaulov [126,156]. This experiment, known as HADRON, was carried out at Tien-Shan Station between 1985 and 1993. It is based on a combination of extensive air shower arrays and large emulsion chambers. The strangelet component in this experiment was estimated to be about 1 $\mathrm{m}^{-2}\ \mathrm{yr}^{-1}$. The data taken by HADRON indicates that some primary cosmic rays may contain non-nucleus components which generate extended air showers that contain both a large number of muons and very highly energetic photons [156]. Another group of data, associated with the absorption of high energy photons in the atmosphere, suggests that cosmic rays may contain an unusual component with an absorption length a few times greater than for ordinary nuclei [156]. These features are nicely explained if one assumes that they are caused by stable or metastable strangelets [156]. Besides that, the so-called Price event [157] with $Z \simeq 46$ and $A > 1000$, regarded previously as a possible candidate for the magnetic monopole, turned out to be fully consistent with the Z/A ratio for strange quark matter [158]. Finally we mention an exotic track event with $Z \simeq 20$ and $A \simeq 460$ observed in an emulsion chamber exposed to cosmic rays on a balloon as reported by Miyamura [125]. This exotic track event motivated the balloon-borne emulsion chamber experiment JACEE [128] and Concorde aircraft [159] experiments. JACEE was flown near the top of the atmosphere. At least two events have been observed which have been referred to as anti-Centauros [129].

3.5. Unusual seismographic events

As already described in Section 3.4, De Rújula and Glashow speculated about the presence of lumps of stable strange matter, also referred to as strange nuggets or nuclearites, in the cosmic radiation [127]. The seismic signals caused by these nuclearites passing through the Earth would be very different from the seismic signals caused by an earthquake or a nuclear explosion [85,127]. This follows from the rate of seismic energy produced by strange nuggets given by $\mathrm{d}E/\mathrm{d}t = f\sigma\rho v^3$, where σ is the nugget cross section, ρ the nominal Earth density, v the nugget speed, and f the fraction of nugget energy loss that results in seismic waves rather than other dissipation such as heat or breaking rock [86]. Underground nuclear explosions have $f \simeq 0.01$, chemical explosions $f \simeq 0.02$. In contrast to this, strange nuggets with a mass of several tons (size of 10^{-3} cm)

passing through the Earth would imply that $f \simeq 0.05$. Anderson et al. [86] looked at more than a million records collected by the US Geological Survey between 1990 and 1993 that were not associated with traditional seismic disturbances such as earthquakes. The seismic signature would be caused by the large ratio of the nuclearite speed, estimated to be around 400 km/s. Strange nuggets might thus pass through the Earth at 40 times the speed of seismic waves. Most interestingly, Anderson et al. were able to single out two seismic events exhibiting this behavior. One event occurred on 22 October 1993; the other event occurred on 24 November 1993. In the first case, an unknown object seems to have entered the Earth off Antarctica and left it south of India. It was recorded at seven monitoring stations in India, Australia, Bolivia, and Turkey. In the second case, an object seems to have entered in the South Pacific, south of Australia, and left the Earth 16.8 seconds later in the Ross Ice Shelf near the South Pole. This event was recorded at nine monitoring stations in Australia and Bolivia. The chord length between the entry and exit points of the 24 November 1993 event is 4204 km, so the duration measured for this event, if caused by the passage of an object through the Earth, would imply a velocity for the hypothetical object of 250 km/s. The interpretation of the data as being caused by strange nuggets penetrating the Earth is backed by a Monte Carlo study that was used to identify the extent to which nuclearites could be detected by seismographic stations [86,160]. The study showed that one would expect to detect as many as 25 four-ton nuclearite events per year if a four-ton strange nugget were to saturate the halo dark matter density. If 10% of the dark matter density were distributed in strange nuggets over the mass range from 0.25 to 100 tons one would expect about an event per year. Detection of a nuclearite would require at least six station sites to fix its impact time, location, and velocity, and seismic detection of signals by at least seven stations is required in order to separate strange nugget events from random spurious coincidences.

3.6. AMS and ECCO

As shown in Ref. [41], finite lumps of color–flavor locked strange quark matter, which should be present in cosmic rays if strange matter is the ground state of the strong interaction, turn out to be significantly more stable than strangelets without color–flavor locking for a wide range of parameters. In addition, strangelets made of CFL strange matter obey a charge–mass relation of $Z/A \propto A^{-1/3}$, which differs significantly from the charge–mass relation of strangelets made of ordinary strange quark matter, as discussed in Section 3.3. In the latter case, Z/A would be constant for small baryon numbers A, and $Z/A \propto A^{-2/3}$ for large A [9,41,77]. This difference may allow an astrophysical test of CFL locking in strange quark matter [41]. The test in question is the upcoming cosmic ray experiment AMS-02 scheduled on the International Space Station [39]. AMS-02 is a roughly a 1 m^2 sterad detector which will provide data from October 2005 for at least three years. AMS-02 will probe the dark matter content in various channels (antiprotons, antideuterons, e^+, γ), cosmic rays and γ astrophysics, and, as already mentioned, strangelets. The expected flux of strangelets of baryon number $A < 6 \times 10^6$ at AMS-02 is [41]

$$F \simeq 5 \times 10^5 \ (\mathrm{m^2\ y\ sr})^{-1} \times R_{-4} \times M_{-2} \times V_{100}^{-1} \times t_7, \tag{62}$$

where R_{-4} is the number of strange star collisions in our galaxy per 10^4 y, M_{-2} is the mass of strangelets ejected per collision in units of $10^{-2}M_\odot$, V_{100} is the effective galactic volume in units of 100 kpc^3 over which strangelets are distributed, and t_7 is the average confinement time in units of 10^7 y. All these factors are of order unity if strange matter is absolutely stable, though each with significant uncertainties [41].

Another intriguing instrument is ECCO (Table 4), whose primary goal will be the measurement of the abundances of the individual long lived actinides (Th, U, Pu, Cm) in the galactic cosmic rays with excellent resolution and statistics. ECCO is a large array of passive glass–track–etch detectors to be exposed in orbit for at least three years [40]. The detectors will passively record the tracks of relativistic ultraheavy galactic cosmic rays during exposure in orbit. After recovery, the detectors are calibrated, etched, and analyzed. ECCO is one of two instruments on the HNX (Heavy Nuclei eXplorer) spacecraft, which is under consideration as a Small Class Explorer Mission. The HNX mission is planned for launch in October 2005 into a 475 km circular orbit. Recovery is planned nominally for three years following launch.

4. Relativistic stellar models

4.1. Particles in curved space–time

Neutron stars are objects of highly compressed matter such that the geometry of space–time is changed considerably from flat space. Thus models of such stars are to be constructed in the framework of Einstein's general theory of relativity combined with theories of superdense matter. The effects of curved space–time are included by coupling the energy–momentum density tensor for matter fields to Einstein's field equations. The generally covariant Lagrangian density is

$$\mathcal{L} = \mathcal{L}_{\rm E} + \mathcal{L}_{\rm G}, \tag{63}$$

where the dynamics of particles are introduced through $\mathcal{L}_{\rm E}$ and the gravitational Lagrangian density $\mathcal{L}_{\rm G}$ is given by

$$\mathcal{L}_{\rm G} = g^{1/2}\, R = g^{1/2} g^{\mu\nu} R_{\mu\nu}, \tag{64}$$

where $g^{\mu\nu}$ and $R_{\mu\nu}$ denote the metric tensor and the Ricci tensor, respectively. The latter is given by

$$R_{\mu\nu} = \Gamma^{\sigma}_{\mu\sigma,\nu} - \Gamma^{\sigma}_{\mu\nu,\sigma} + \Gamma^{\sigma}_{\kappa\nu}\Gamma^{\kappa}_{\mu\sigma} - \Gamma^{\sigma}_{\kappa\sigma}\Gamma^{\kappa}_{\mu\nu}, \tag{65}$$

with the commas denoting derivatives with respect to space–time coordinates, e.g., $\nu = \partial/\partial x^\nu$. The Christoffel symbols Γ in (65) are defined as

$$\Gamma^{\sigma}_{\mu\nu} = \frac{1}{2} g^{\sigma\lambda}(g_{\mu\lambda,\nu} + g_{\nu\lambda,\mu} - g_{\mu\nu,\lambda}). \tag{66}$$

The connection between the two branches of physics is provided by Einstein's field equations:

$$G^{\mu\nu} \equiv R^{\mu\nu} - \frac{1}{2} g^{\mu\nu} R = 8\pi T^{\mu\nu}(\epsilon, P(\epsilon)) \tag{67}$$

($\mu, \nu = 0, 1, 2, 3$), which couple the Einstein curvature tensor, $G^{\mu\nu}$, to the energy–momentum density tensor, $T^{\mu\nu}$, of the stellar matter. The quantities $g^{\mu\nu}$ and R in (67) denote the metric tensor and the Ricci scalar (scalar curvature) [1]. The tensor $T^{\mu\nu}$ contains the equation of state, $P(\epsilon)$, of the stellar matter, discussed in Sections 2 and 3. In general, Einstein's field equations and the many-body equations were to be solved simultaneously since the baryons and quarks move in curved space–time whose geometry, determined by Einstein's field equations, is coupled to the total mass–energy density of the matter. In the case of neutron stars, as for all astrophysical situations for which the long range gravitational forces can be cleanly separated from the short range forces, the deviation from flat space–time over the length scale of the strong interaction, $\sim$1 fm, is however practically zero up to the highest densities reached in the cores of such stars (some 10^{15} g/cm^3). This is not to be confused with the global length scale of neutron stars, $\sim$10 km, for which $M/R \sim 0.3$, depending on the star's mass. That is to say, gravity curves space–time only on a macroscopic scale but leaves it flat to a very good approximation on a microscopic scale. To achieve an appreciable curvature on a microscopic scale set by the strong interaction, mass densities greater than $\sim 10^{40}$ g/cm^3 would be necessary [161]! This circumstance divides the construction of models of compact stars into two distinct problems. Firstly, the effects of the short range nuclear forces on the properties of matter are described in a co-moving proper reference frame (local inertial frame), where space–time is flat, by the parameters and laws of (special relativistic) many-body physics. Secondly, the coupling between the long range gravitational field and the matter is then taken into account by solving Einstein's field equations for the gravitational field described by the general relativistic curvature of space–time, leading to the global structure of the stellar configuration.

4.2. Stellar structure equations of non-rotating stars

For many studies of neutron star properties it is sufficient to treat neutron star matter as a perfect fluid. The energy–momentum tensor of such a fluid is given by

$$T^{\mu\nu} = u^\mu u^\nu (\epsilon + P) + g^{\mu\nu} P, \tag{68}$$

where u^μ and u^ν are four-velocities defined as

$$u^\mu \equiv \frac{\mathrm{d}x^\mu}{\mathrm{d}\tau}, \qquad u^\nu \equiv \frac{\mathrm{d}x^\nu}{\mathrm{d}\tau}. \tag{69}$$

They are the components of the macroscopic velocity of the stellar matter with respect to the actual coordinate system that is being used to derive the stellar equilibrium equations. The production of curvature by the star's mass is specified by Einstein's field equations:

$$G_{\mu\nu} = 8\pi T_{\mu\nu}, \qquad \text{where } G_{\mu\nu} \equiv R_{\mu\nu} - \frac{1}{2} g_{\mu\nu} R \tag{70}$$

is the Einstein tensor. The scalar curvature of space–time R in Eq. (70), also known as the Ricci scalar, follows from Eq. (65) as

$$R = R_{\mu\nu} g^{\mu\nu}. \tag{71}$$

Finally, we need to specify the metric of a non-rotating body in general relativity theory. Assuming spherical symmetry, the metric has the form

$$\mathrm{d}s^2 = -\mathrm{e}^{2\Phi(r)}\mathrm{d}t^2 + \mathrm{e}^{2\Lambda(r)}\mathrm{d}r^2 + r^2\mathrm{d}\theta^2 + r^2\sin^2\theta\,\mathrm{d}\phi^2, \tag{72}$$

where $\Phi(r)$ and $\Lambda(r)$ are radially varying metric functions. Introducing the covariant components of the metric tensor,

$$g_{tt} = -\mathrm{e}^{2\Phi(r)}, \qquad g_{rr} = \mathrm{e}^{2\Lambda(r)}, \qquad g_{\theta\theta} = r^2, \qquad g_{\phi\phi} = r^2\sin^2\theta, \tag{73}$$

the non-vanishing Christoffel symbols of a spherically symmetric body are

$$\begin{aligned} &\Gamma^r_{tt} = \mathrm{e}^{2\Phi(r)-2\Lambda(r)}\,\Phi'(r), \qquad \Gamma^t_{tr} = \Phi'(r), \qquad \Gamma^r_{rr} = \Lambda'(r), \qquad \Gamma^\theta_{r\theta} = r^{-1}, \\ &\quad \Gamma^\phi_{r\phi} = r^{-1}, \qquad \Gamma^r_{\theta\theta} = -r\,\mathrm{e}^{-2\Lambda(r)}, \\ &\Gamma^\phi_{\theta\phi} = \frac{\cos\theta}{\sin\theta}, \qquad \Gamma^r_{\phi\phi} = -r\sin^2\theta\,\mathrm{e}^{-2\Lambda(r)}, \qquad \Gamma^\theta_{\phi\phi} = -\sin\theta\cos\theta, \end{aligned} \tag{74}$$

where primes denote differentiation with respect to the radial coordinate. From Eqs. (68), (70) and (74) one derives the structure equations of spherically symmetric neutron stars known as Tolman–Oppenheimer–Volkoff equations [162,163]:

$$\frac{\mathrm{d}P}{\mathrm{d}r} = -\frac{\epsilon(r)m(r)}{r^2}\,\frac{(1+P(r)/\epsilon(r))(1+4\pi r^3P(r)/m(r))}{1-2m(r)/r}. \tag{75}$$

Note that we use units for which the gravitational constant and velocity of light are $G = c = 1$, so $M_\odot = 1.475$ km. The boundary condition for (75) is $P(r=0) \equiv P_c = P(\epsilon_c)$, where ϵ_c denotes the energy density at the star's center, which constitutes an input parameter. The pressure is to be computed out to that radial distance where $P(r=R)=0$ which determines the star's radius R. The mass contained in a sphere of radius r ($\leq R$), denoted by $m(r)$, follows as $m(r) = 4\pi\int_0^r \mathrm{d}r'\,r'^2\,\epsilon(r')$. The star's total gravitational mass is thus given by $M \equiv m(R)$.

Fig. 15 shows the gravitational mass of non-rotating neutron stars as a function of stellar radius for several sample equations of state discussed in Sections 2 and 3. Each star sequence is shown up to densities that are slightly larger than those of the maximum-mass star (indicated by tick marks) of each sequence. Stars beyond the mass peak are unstable against radial oscillations and thus cannot exist stably in Nature. One sees that all equations of state are able to support neutron stars of canonical mass, $M \sim 1.4M_\odot$. Neutron stars more massive than about $2M_\odot$, on the other hand, are only supported by equations of state that exhibit a very stiff behavior at supernuclear densities and disfavor exotic (e.g., K^- mesons, quark matter) degrees of freedom. Knowledge of the maximum possible mass of neutron stars is of great importance for two reasons. The first is that the largest known neutron star mass imposes a lower bound on the maximum mass of a theoretical model. The current lower bound is about $1.55M_\odot$ for neutron star Cyg X-2 [165], which does not exclude the existence of exotic phases of matter in the core of Cyg X-2. The situation could easily change if a future determination of the mass of this neutron star were to result in a value that is close to its present upper limit of $\sim 2M_\odot$. The second reason is that the maximum mass is essential in order to identify black hole candidates [168,169]. For example, if the mass of a compact companion of an optical star is determined to exceed

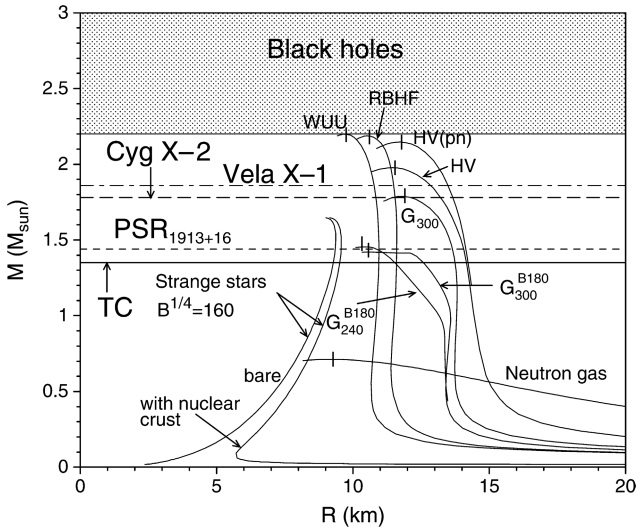

Fig. 15. Neutron star mass versus radius for different equations of state. The broken horizontal lines refer to the masses of Vela X-1 ($1.86 \pm 0.16 M_\odot$) [164], Cyg X-2 ($1.78 \pm 0.23 M_\odot$) [165], and PSR 1913+16 ($1.442 \pm 0.003 M_\odot$) [166]. The line labeled 'TC' denotes the average neutron star mass ($1.350 \pm 0.004 M_\odot$) derived by Thorsett and Chakrabarty [167].

the maximum mass of a neutron star it must be a black hole. Since the maximum mass of stable neutron stars studied here is $\sim 2.2 M_\odot$, compact companions more massive than that value would be black holes.

4.3. Rotating star models

The structure equations of rotating compact stars are considerably more complicated that those of non-rotating compact stars [1]. These complications have their cause in the rotational deformation, that is, a flattening at the pole accompanied with a radial blow-up in the equatorial direction, which leads to a dependence of the star's metric on the polar coordinate, θ, in addition to the mere dependence on the radial coordinate, r. Secondly, rotation stabilizes a star against gravitational collapse. It can therefore carry more mass than would be the case if the star were to be non-rotating. It being more massive, however, means that the geometry of space–time is changed too. This makes the metric functions associated with a rotating star depend on the star's rotational frequency. Finally, the general relativistic effect of the dragging of local inertial frames implies the occurrence of an additional non-diagonal term, $g^{t\phi}$, in the metric tensor $g^{\mu\nu}$. This term imposes a self-consistency condition on the stellar structure equations, since the extent to which the local inertial frames are dragged along in the direction of the star's rotation, indicated schematically in Fig. 16, is determined by the initially unknown stellar properties such as mass and rotational frequency. The covariant components of the metric tensor of a rotating compact star are thus given by [1,170]

$$g_{tt} = -\mathrm{e}^{2\nu} + \mathrm{e}^{2\psi}\omega^2,\ g_{t\phi} = -\mathrm{e}^{2\psi}\omega,\ g_{rr} = \mathrm{e}^{2\lambda},\ g_{\theta\theta} = \mathrm{e}^{2\mu},\ g_{\phi\phi} = \mathrm{e}^{2\psi}, \qquad (76)$$

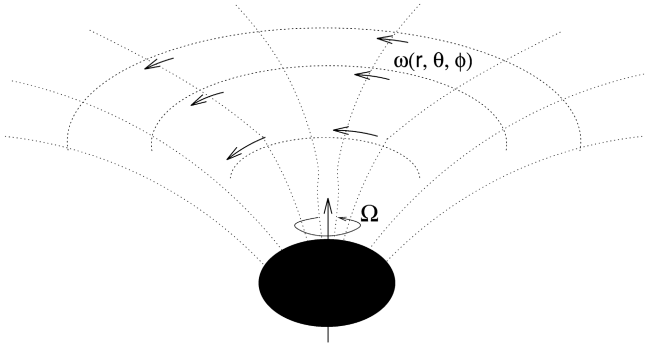

Fig. 16. Features of a rotating compact star in general relativity. Indicated is the deformation of the geometry of space–time and the dragging of the local inertial frames. The latter rotate at a position dependent angular frequency $\omega(r, \theta, \phi)$, which is to be calculated self-consistently from Einstein's field equations. The dragging frequencies inside three stellar configurations are shown in Fig. 17.

which leads for the line element to

$$ds^2 = g_{\mu\nu}dx^\mu dx^\nu = -e^{2\nu}dt^2 + e^{2\psi}(d\phi - \omega dt)^2 + e^{2\mu}d\theta^2 + e^{2\lambda}dr^2. \tag{77}$$

Here each metric function, i.e. ν, ψ, μ, and λ, as well as the angular velocities of the local inertial frames, ω, depend on the radial coordinate r and polar angle θ, and implicitly on the star's angular velocity Ω. Of particular interest is the relative angular frame dragging frequency, $\bar{\omega}$, defined as

$$\bar{\omega}(r, \theta, \Omega) \equiv \Omega - \omega(r, \theta, \Omega), \tag{78}$$

which is the angular velocity of the star, Ω, relative to the angular velocity of a local inertial frame, ω. It is this frequency that is of relevance when discussing the rotational flow of the fluid inside the star, since the magnitude of the centrifugal force acting on a fluid element is governed—in general relativity as well as in Newtonian gravitational theory—by the rate of rotation of the fluid element relative to a local inertial frame [171]. In contrast to Newtonian theory, however, the inertial frames inside (and outside) a general relativistic fluid are not at rest with respect to the distant stars, as pointed out just above. Rather, the local inertial frames are dragged along by the rotating fluid. This effect can be quite strong, as shown in Fig. 17. For a heavy neutron star rotating at its Kepler frequency, one sees that $\bar{\omega}/\Omega$ varies typically between about 15% at the surface and 60% at the center, where the mass density is highest.

4.4. Kepler frequency

No simple stability criteria are known for rapidly rotating stellar configurations in general relativity. However, an absolute upper limit on stable neutron star rotation is set by the Kepler frequency Ω_K, which is the maximum frequency a star can have before mass loss (mass shedding) at the equator sets in. In classical mechanics, the expression for the Kepler frequency, determined by the equality between the centrifugal force and gravity, is readily obtained as $\Omega_K = \sqrt{M/R^3}$. In order to derive its general relativistic counterpart,

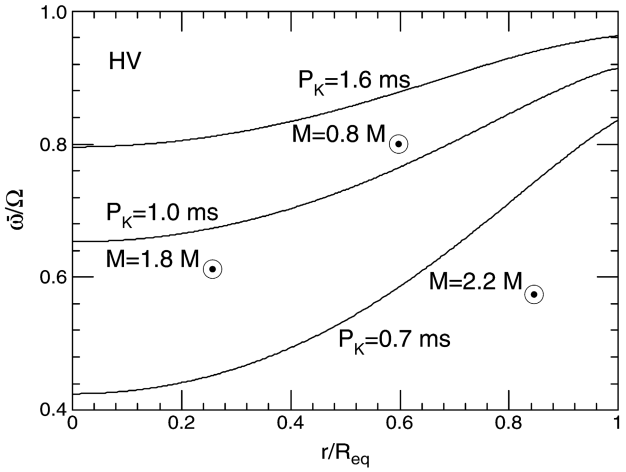

Fig. 17. Dragging of the local inertial frames inside rotating neutron stars in the equatorial direction. $P_{\rm K}$ and M denote the Kepler period, defined in Eq. (83), and the gravitational mass. (Taken from Ref. [1].)

one applies the extremal principle to the circular orbit of a point mass rotating at the star's equator. Since $r = \theta = \text{const}$ for a point mass there, one has $\mathrm{d}r = \mathrm{d}\theta = 0$. The line element (77) then reduces to

$$\mathrm{d}s^2 = (\mathrm{e}^{2\nu} - \mathrm{e}^{2\psi}(\Omega - \omega)^2)\mathrm{d}t^2. \tag{79}$$

Substituting this expression into $J \equiv \int_{s_1}^{s_2} \mathrm{d}s$, where s_1 and s_2 refer to points located at that particular orbit for which J becomes extremal, gives

$$J = \int_{s_1}^{s_2} \mathrm{d}t \sqrt{\mathrm{e}^{2\nu} - \mathrm{e}^{2\psi}(\Omega - \omega)^2}. \tag{80}$$

Applying the extremal condition $\delta J = 0$ to Eq. (80) and noticing that

$$V = \mathrm{e}^{\psi - \nu}(\Omega - \omega), \tag{81}$$

one obtains from Eq. (80)

$$\frac{\partial \psi}{\partial r}\mathrm{e}^{2\nu}V^2 - \frac{\partial \omega}{\partial r}\mathrm{e}^{\nu+\psi}V - \frac{\partial \nu}{\partial r}\mathrm{e}^{2\nu} = 0. \tag{82}$$

This constitutes a simple quadratic equation for the orbital velocity V of a particle at the star's equator. Solving (81) for $\Omega = \Omega_{\rm K}$ gives the fluid's general relativistic Kepler frequency in terms of V, the metric functions ν and ψ, and the frame dragging frequency ω, each quantity being a complicated function of all the other quantities. In this manner $\Omega_{\rm K}$ is given by [1]

$$\Omega_{\rm K} = \omega + \frac{\omega'}{2\psi'} + \mathrm{e}^{\nu-\psi}\sqrt{\frac{\nu'}{\psi'} + \left(\frac{\omega'}{2\psi'}\mathrm{e}^{\psi-\nu}\right)^2}, \qquad P_{\rm K} \equiv \frac{2\pi}{\Omega_{\rm K}}, \tag{83}$$

which is to be evaluated at the star's equator (primes denote radial derivatives). Fig. 18 shows $P_{\rm K}$ as a function of rotating star mass. The rectangle indicates both the approximate

range of observed neutron star masses as well as the observed rotational periods which, currently, are $P \geq 1.6$ ms. One sees that all pulsars so far observed rotate below the mass shedding frequency and so can be interpreted as rotating neutron stars. Half-millisecond periods or even smaller ones are excluded for neutron stars of mass $1.4M_\odot$ [1,170,172]. The situation appears to be very different for stars made up of self-bound strange quark matter, the so-called strange stars which will be introduced in Section 5.2. Such stars can withstand stable rotation against mass shedding down to rotational periods in the half-millisecond regime or even below [148]. Consequently, the possible future discovery of a single submillisecond pulsar spinning at say 0.5 ms could give a strong hint that strange stars actually exist, and that the deconfined self-bound phase of three-flavor strange quark matter is in fact the true ground state of the strong interaction rather than nuclear matter. Strange stars of a canonical pulsar mass around $1.4M_\odot$ have Kepler periods in the range of 0.55 ms $\lesssim P_{\rm K} \lesssim$ 0.8 ms, depending on the thickness of the nuclear crust and the bag constant [10,11]. This range is to be compared with $P_{\rm K} \sim 1$ ms obtained for standard (i.e., no phase transition) neutron stars of the same mass. Phase transitions in neutron stars, however, may lower this value down to Kepler periods typical of strange stars [173].

4.5. *Moments of inertia of rotating compact stars*

To derive the expression for the moment of inertia of a rotationally deformed, axisymmetric star in hydrostatic equilibrium, we start from the following expression:

$$I(\mathcal{A}, \Omega) \equiv \frac{1}{\Omega} \int_{\mathcal{A}} {\rm d}r{\rm d}\theta{\rm d}\phi T_\phi{}^t(r, \theta, \phi, \Omega)\sqrt{-g(r, \theta, \phi, \Omega)}. \tag{84}$$

We assume stationary rotation, which is well justified for our investigations. The quantity $\mathcal{A}$ denotes an axially symmetric region in the interior of a stellar body where all matter is rotating with the same angular velocity Ω, and $\sqrt{-g} = {\rm e}^{\lambda+\mu+\nu+\psi}$. The component $T_\phi{}^t$ of the energy–momentum tensor is given by

$$T_\phi{}^t = (\epsilon + P)u_\phi u^t. \tag{85}$$

Let us focus next on the determination of the fluid's four-velocity, $u^\kappa = (u^t, u^r, u^\theta, u^\phi)$. From the general normalization relation $u^\kappa u_\kappa = -1$ one readily derives

$$-1 = (u^t)^2 g_{tt} + 2u^t u^\phi g_{t\phi} + (u^\phi)^2 g_{\phi\phi}. \tag{86}$$

This relation can be rewritten by noticing that

$$u^\phi = \Omega u^t, \tag{87}$$

which extremizes the total mass–energy of the stationary stellar fluid subject to the constraint that the angular momentum about the star's symmetry axis, J_z, and its baryon number, A, remain fixed [174]. Substituting (87) into (86) leads to

$$-1 = (u^t)^2(g_{tt} + 2g_{t\phi}\Omega + g_{\phi\phi}\Omega^2), \tag{88}$$

which can be solved for u^t. This gives

$$u^t = \left(-(g_{tt} + 2g_{t\phi}\Omega + g_{\phi\phi}\Omega^2)\right)^{-1/2}. \tag{89}$$

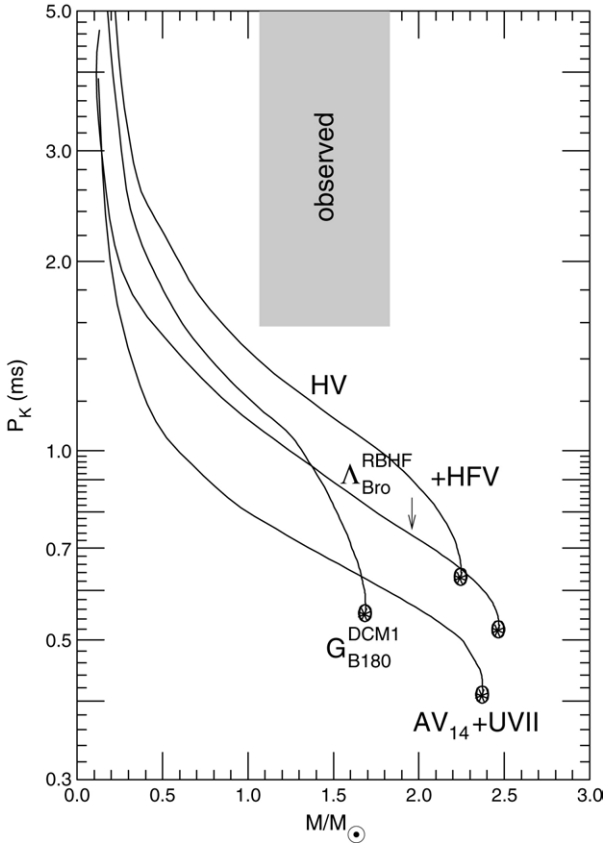

Fig. 18. The onset of mass shedding from rapidly spinning neutron stars, computed for a collection of equations of state (taken from Ref. [1]). The Kepler period is defined in Eq. (83).

Replacing g_{tt}, $g_{t\phi}$, and $g_{\phi\phi}$ with the expressions given in (76) and rearranging terms leads for (89) to

$$u^t = \mathrm{e}^{-\nu}\left(1-(\omega-\Omega)^2\mathrm{e}^{2\psi-2\nu}\right)^{-1}. \tag{90}$$

Last but not least we need an expression for u_ϕ of Eq. (85) in terms of the star's metric functions. To accomplish this we write u_ϕ as $u_\phi = g_{\phi\kappa}u^\kappa = g_{\phi t}u^t + g_{\phi\phi}u^\phi$. Upon substituting the expressions for $g_{\phi t}$ and $g_{\phi\phi}$ from (76) into this relation, we arrive at

$$u_\phi = (\Omega-\omega)\mathrm{e}^{2\psi}u^t. \tag{91}$$

Substituting the four-velocities (90) and (91) into (85) gives the required expression for the energy–momentum tensor:

$$T_\phi{}^t = (\epsilon+P)(\Omega-\omega)\mathrm{e}^{2\psi}\left(\mathrm{e}^{2\nu}-(\omega-\Omega)^2\mathrm{e}^{2\psi}\right)^{-1}. \tag{92}$$

Finally, inserting this expression into (84) leads for the moment of inertia of a rotationally deformed star to

$$I(\Omega) = 2\pi \int_0^{\pi} \mathrm{d}\theta \int_0^{R(\theta)} \mathrm{d}r\, \mathrm{e}^{\lambda+\mu+\nu+\psi} \frac{\epsilon + P(\epsilon)}{\mathrm{e}^{2\nu-2\psi} - (\omega-\Omega)^2} \frac{\Omega-\omega}{\Omega}. \tag{93}$$

Relativistic corrections to the Newtonian expression for I, which for a sphere of uniform mass density, $\epsilon(r) = \text{const}$, is given by $I = \frac{2}{5}MR^2$, come from the dragging of local inertial frames ($(\Omega-\omega)/\Omega < 1$) and the curvature of space.

5. Strangeness in compact stars

5.1. Neutron stars

Physicists know of three kinds of compact stars. These are black holes, neutron stars, and white dwarfs. Neutron stars and white dwarfs are in hydrostatic equilibrium, so at each point inside the star gravity is balanced by the degenerate particle pressure, as described mathematically by the Tolman–Oppenheimer–Volkoff equation (75). These stars, therefore, exhibit the generic mass–radius relationship shown in Fig. 19. Depending on composition, the maximum neutron star mass (marked '1') lies somewhere between $\sim$1.5 and $2.5M_\odot$ (see also Fig. 15). The minimum mass of neutron stars (marked '2') is around $0.1M_\odot$. These stars are considerably less dense ($\sim 0.1\epsilon_0$) and thus much bigger ($R \lesssim 300$ km) than the neutron stars of canonical mass, which is $\sim 1.4M_\odot$. White dwarfs at the Chandrasekhar mass limit (marked '3') have densities around 10^9 g/cm^3, which is five orders of magnitude smaller than the typical densities encountered in neutron stars.

5.1.1. Hyperons

Model calculations indicate that only in the most primitive conception is a neutron star made of only neutrons. In a more accurate representation, a neutron star may contain neutrons (n) and protons (p) whose charge is balanced by electrons (e^-) and muons (μ^-), strangeness-carrying hyperons (Σ, Λ, Ξ), meson condensates (K^- or p^-), u, d, s quarks, or possibly H-dibaryons. The particle composition is determined by the conditions of electric charge neutrality and chemical equilibrium as well as the in-medium properties of the constituents calculated for a given microscopic many-body theory (cf. Sections 2 and 3). In general, the population of negatively charged hadronic states is favored over the population of positively charged hadronic states since the negative charge carried by the hadrons can replace high energy electrons, by means of which a lower energy state is reached. Aside from electric charge, the isospin orientation of the possible constituents is of key importance for the population too. The reason is that neutron star matter constitutes a highly excited state of matter relative to isospin symmetric nuclear matter. Hence, as soon as there are new hadronic degrees of freedom accessible to neutron star matter which allow such matter to become more isospin symmetric, it will make use of them.

5.1.2. K^- meson condensate

The condensation of K^- mesons in neutron stars is initiated by the reaction

$$e^- \to K^- + \nu. \tag{94}$$

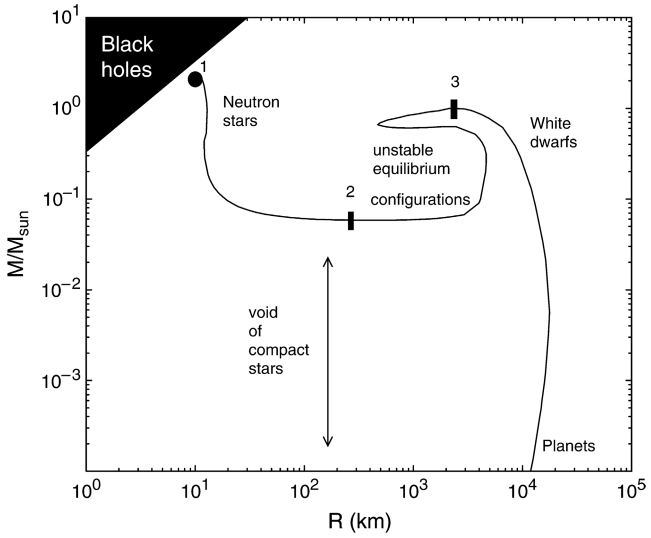

Fig. 19. Mass versus radius of neutron stars, white dwarfs, and planets. Stars located between the lightest neutron star (marked '2') and the heaviest white dwarf (marked '3') are unstable against radial oscillations and thus cannot exist stably in nature. If strange matter were to be more stable than nuclear matter, an enormous region in the M–R plane void of compact objects could be populated with strange matter configurations (see Fig. 28).

If this reaction becomes possible in a neutron star, it is energetically advantageous for the star to replace the fermionic electrons with the bosonic K^- mesons. Whether or not this happens depends on the behavior of the K^- mass in neutron star matter. Experiments which shed light on the properties of the K^- in nuclear matter have been performed with the Kaon Spectrometer (KaoS) and the FOPI detector at the heavy ion synchrotron SIS at GSI [175–178]. An analysis of the early K^- kinetic energy spectra extracted from Ni + Ni collisions [175] showed that the attraction from nuclear matter would bring the K^- mass down to $m^*_{K^-} \simeq 200$ MeV at $\rho \sim 3\rho_0$. For neutron-rich matter, the relation

$$m^*_{K^-}(\rho) \simeq m_{K^-}\left(1 - 0.2\frac{\rho}{\rho_0}\right) \tag{95}$$

was established [181–183], with $m_K = 495$ MeV the K^- vacuum mass. Values around $m^*_{K^-} \simeq 200$ MeV lie in the vicinity of the electron chemical potential, μ^e, in neutron star matter [1,14], so the threshold condition for the onset of K^- condensation, $\mu^e = m^*_K$, which follows from Eq. (94), could be fulfilled in the centers of neutron stars. The situation is illustrated graphically in Fig. 20. Eq. (94) is followed by

$$n + e^- \to p + K^- + \nu, \tag{96}$$

with the neutrinos leaving the star. By this conversion the nucleons in the cores of newly formed neutron stars can become half neutrons and half protons, which lowers the energy per baryon of the matter [184]. The relative isospin symmetric composition achieved in this way resembles that of atomic nuclei, which are made up of roughly equal

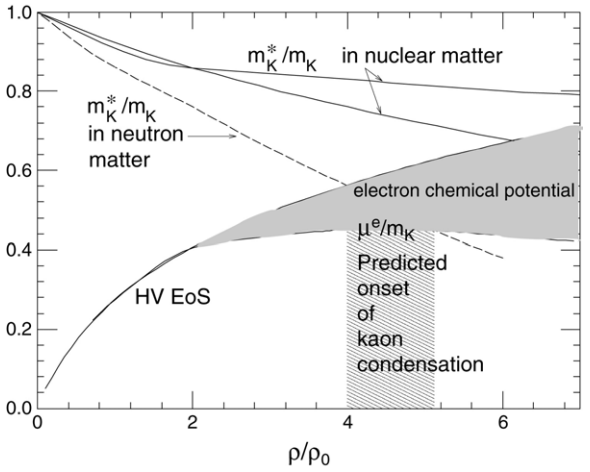

Fig. 20. The effective kaon mass in nuclear [179] and neutron star [180] matter. (Taken from Ref. [1].)

numbers of neutrons and protons. Neutron stars are therefore referred to, in this picture, as nucleon stars. The maximal possible mass of this type of star, where Eq. (96) has gone to completion, has been calculated to be around $1.5M_{\odot}$ [185]. Consequently, the collapsing core of a supernova (e.g. 1987A), if heavier than this value, should go into a black hole rather than forming a neutron star [168,181,182]. Another striking implication, pointed out by Brown and Bethe, would be the existence of a large number of low mass black holes in our galaxy [168].

5.1.3. Strange quarks

Several decades ago it had already been suggested that, because of the extreme densities reached in the cores of neutron stars, neutrons, protons, plus the heavier constituents may melt, creating quark matter being sought at the most powerful terrestrial heavy ion colliders [16–21]. At present one does not know from experiment at what density the expected phase transition to quark matter occurs, and one has no conclusive guide yet from lattice QCD simulations. From simple geometrical considerations it follows that nuclei begin to touch each other at densities of $\sim(4\pi r_N^3/3)^{-1} \simeq 0.24\ \mathrm{fm}^{-3}$, which, for a characteristic nucleon radius of $r_N \sim 1$ fm, is less than twice the baryon number density ρ_0 of ordinary nuclear matter [49]. Above this density, therefore, it appears plausible that the nuclear boundaries of hadrons dissolve and the originally confined quarks begin to populate free states outside of the hadrons. Depending on rotational frequency and stellar mass, densities as large as two to three times ρ_0 are easily surpassed in the cores of neutron stars, as can be seen from Figs. 21 and 22, so the neutrons and protons in the centers of neutron stars may have been broken up into their constituent quarks by gravity [1,186]. More than that, since the mass of the strange quark is so small, highly energetic up and down quarks are expected to readily transform to strange quarks at about the same density at which up and down quark deconfinement sets in [22,68]. Three-flavor quark matter could thus exist as a permanent component of matter in the centers of neutron stars [1,49,186].

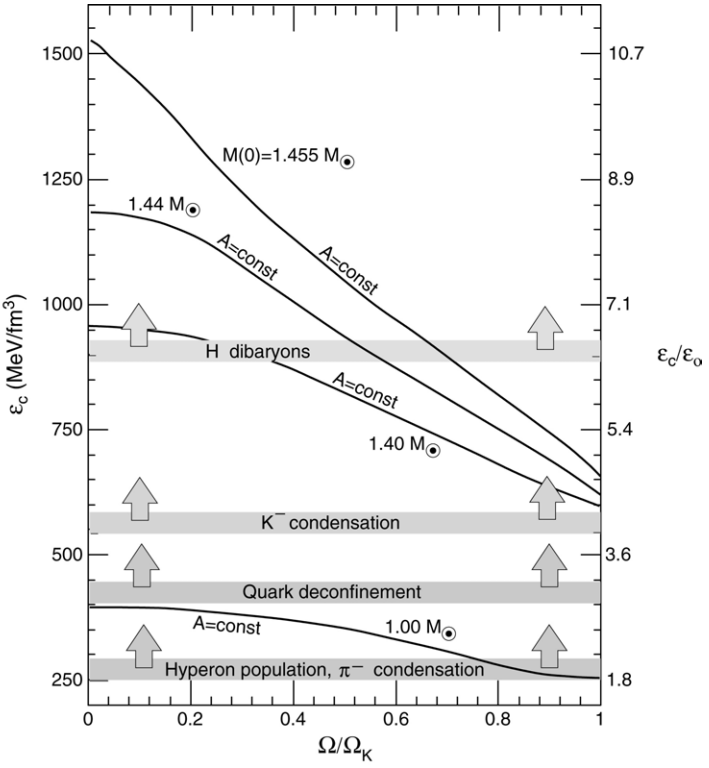

Fig. 21. Central density versus rotational frequency for several sample neutron stars. The stars' baryon number, A, is constant in each case. Theory predicts that the interior stellar density could become so great that the threshold densities of various novel phases of superdense matter are reached. $\epsilon_0 = 140\text{MeV/fm}^3$ denotes the density of nuclear matter, Ω_K is the Kepler frequency, and $M(0)$ is the stars' mass at zero rotation. (From Ref. [1].)

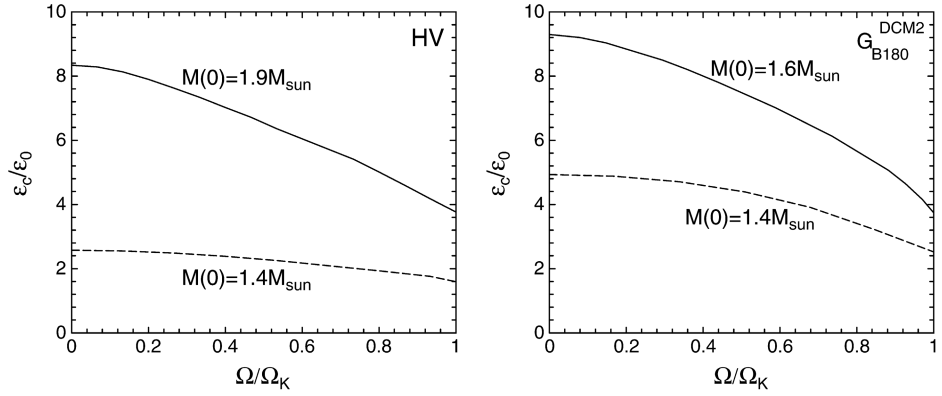

Fig. 22. Variation of central star density with rotational star frequency.

In passing we mention that the existence of a mixed phase depends decisively on the unknown surface tension. Alford et al. studied the CFL–nuclear mixed phase [187] and found that if the surface tension is above about 40 MeV/fm^2 then the mixed phase does not occur at all. This surface tension is completely unknown, but one might expect the 'natural scale' for it to be $(200\ \text{MeV})^3 = 200\ \text{MeV/fm}^2$. For what follows we will assume that the surface tension is such that a mixed phase of quark matter and nuclear matter exists above a certain density.

As pointed out by Glendenning [22,23], in all earlier work on the quark–hadron phase transition in neutron star matter, assumed to be a first-order transition, the possibility of reaching the lowest energy state by rearranging electric charge between the regions of confined hadronic matter and deconfined quark matter in phase equilibrium was ignored. This incorrectly yielded a description of the possible quark–hadron transition in neutron stars as a constant pressure one, which had the consequence of excluding the coexistence phase of hadrons and quarks from neutron stars. The microphysical agent behind this preference for charge rearrangement is the charge symmetric nuclear force which acts to relieve the high isospin asymmetry of neutron star matter as soon as it is in equilibrium with quark matter. This introduces a net positive charge on the hadronic regions and a compensatory net negative charge on quark matter. (The nuclear matter and quark matter phases are thus not separately charge neutral as assumed before Glendenning's work.) Because of this preference for charge rearrangement exploited by a neutron star, the pressure in the mixed quark–hadron phase varies as the proportions of the phases. Varying pressure in the mixed phase is of key importance for the existence of the mixed phase inside neutron stars, because hydrostatic equilibrium dictates that pressure drops monotonically from the center toward the surface. For that reason the mixed phase is not strictly—and incorrectly—excluded from neutron stars [22,23,49].

If the dense interior of a neutron star is converted to quark matter [1,22,49,188], it must be three-flavor quark matter (see Figs. 23 through 25) since it has lower energy than two-flavor quark matter (see Section 3). And just as for the hyperon content of neutron stars, strangeness is not conserved on macroscopic timescales which allows neutron stars to convert confined hadronic matter to three-flavor quark matter until equilibrium brings this process to a halt. Many of the earlier investigations have treated neutron stars as containing only neutrons, and the quark phase as consisting of the equivalent number of u and d quarks. Pure neutron matter, however, is not the ground state of a neutron star, nor is a mixture of u and d quarks the ground state of quark matter in compact stars. In fact the latter constitutes a highly excited state of quark matter, which will quickly weakly decay to a mixture of u, d, and s quarks in approximately equal proportions. Several other investigations have approximated the mixed phase as two components which are separately charge neutral, which hides the possible quark–hadron phase transition in neutron star matter [22,23] because the deconfinement transition is shifted to densities hardly reached in the cores of neutron stars of average mass, $M \sim 1.4 M_\odot$.

The Gibbs condition for phase equilibrium between quarks and hadrons is that the two associated, independent chemical potentials, μ^n and μ^e respectively, and the pressure in the two phases be equal:

$$P_{\rm H}(\mu^n, \mu^e, \{\phi\}, T) = P_{\rm Q}(\mu^n, \mu^e, T), \tag{97}$$

where μ^n and μ^e denote the chemical potentials of neutrons and electrons, respectively, and the subscripts H and Q refer to confined hadronic matter and deconfined quark matter. The quantity $\{\phi\}$ stands collectively for the particle fields and Fermi momenta which characterize a solution to the equations of confined hadronic matter discussed in Section 2. As known from Eq. (10), the quark chemical potentials are related to the baryon and charge chemical potentials in Eq. (97) as

$$\mu^u = \mu^c = \frac{1}{3}\mu^n - \frac{2}{3}\mu^e, \qquad \mu^d = \mu^s = \frac{1}{3}\mu^n + \frac{1}{3}\mu^e. \tag{98}$$

In accordance to what has been said just above, Eq. (97) is to be supplemented with the conditions of baryon charge conservation and electric charge conservation [22,23]. Mathematically, the global conservation of baryon charge within an unknown volume, V, containing A baryons is expressed as

$$\rho \equiv \frac{A}{V} = (1-\chi)\rho_{\rm H}(\mu^n, \mu^e, T) + \chi\rho_{\rm Q}(\mu^n, \mu^e, T), \tag{99}$$

where $\chi \equiv V_{\rm Q}/V$ denotes the volume proportion of quark matter, $V_{\rm Q}$, in the unknown volume V. By definition, the parameter χ varies between 0 and 1, determining how much confined hadronic matter exists as quark matter. The global neutrality of electric charge within the volume V is mathematically expressed as [22,23]

$$0 = \frac{Q}{V} = (1-\chi)q_{\rm H}(\mu^n, \mu^e, T) + \chi q_{\rm Q}(\mu^n, \mu^e, T) + q_{\rm L}, \tag{100}$$

where $q_{\rm H} = \sum_B q_B^{\rm el}\rho^B$ and $q_{\rm Q} = \sum_f q_f^{\rm el}\rho^f$ denote the net electric charge carried by hadronic and quark matter, respectively, and $q_{\rm L} = \sum_L q_L^{\rm el}\rho^L$ stands for the electric charge density of the leptons (see Sections 2 and 3). One sees that for a given temperature T, Eq. (97) through (100) serve to determine the two independent chemical potentials μ^n and μ^e, and the volume V for a specified volume fraction χ of the quark phase in equilibrium with the hadronic phase. After completion, $V_{\rm Q}$ is obtained as $V_{\rm Q} = \chi V$. Through Eq. (97) to (100) the chemical potentials μ^n and μ^e obviously depend on χ and thus on density ρ, which renders all properties that depend on μ^n and μ^e—from the energy density to the baryon and charge densities of each phase to the common pressure—density dependent, too.

Figs. 23 through 25 show sample quark–lepton populations computed for representative bag constants as well as different many-body approximations employed to model confined hadronic matter [1,186]. Three features emerge immediately from these populations. Firstly, one sees that the transition from pure hadronic matter to the mixed phase occurs at rather low density of about $3\rho_0$ or even somewhat less [22,23,189]. Depending on the bag constant and the underlying nuclear many-body approximation, threshold values even as small as about $2\rho_0$ are possible. Secondly, we emphasize the saturation of the number of electrons as soon as quark matter appears, for then electric charge neutrality can be achieved more economically among the baryon-charge-carrying particles themselves. This saturation is of very great importance for the possible formation of a K^- condensate in neutron stars [181–184], whose threshold condition is given by $\mu^e = m_K^*$. Fig. 20 shows that this condition may be fulfilled in neutron star matter, depending on the underlying many-body approximation and the structure of the many-body background. Thirdly, the

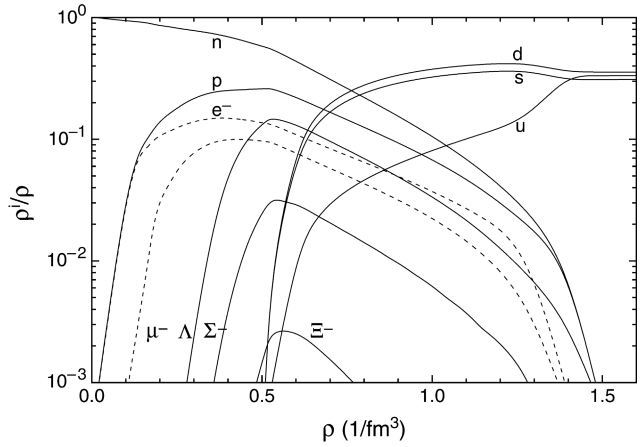

Fig. 23. The composition of chemically equilibrated, stellar quark–hadron (hybrid star) matter as a function of the baryon density. Hadronic matter is described by the relativistic Hartree model HV [1,44]; the bag constant is $B = 250$ MeV/fm^3. (From Ref. [1].)

presence of quark matter enables the hadronic regions of the mixed phase to arrange to be more isospin symmetric (i.e. closer equality in proton and neutron number is achieved) than in the pure phase by transferring charge to the quark phase in equilibrium with it. Symmetry energy will be lowered thereby at only a small cost in rearranging the quark Fermi surfaces. Electrons play only a minor role when neutrality can be realized among the baryon-charge-carrying particles. The stellar implication of this charge rearrangement is that the mixed phase region of the star will have positively charged regions of nuclear matter and negatively charged regions of quark matter.

Because of the competition between the Coulomb and the surface energies associated with the positively charged regions of nuclear matter and negatively charged regions of quark matter, the mixed phase will develop geometrical structures, similarly to what is expected of the subnuclear liquid–gas phase transition [190–192]. This competition establishes the shapes, sizes, and spacings of the rarer phase in the background of the other in order to minimize the lattice energy [22,23,193]. As known from the quark–hadron compositions shown above, the formation of quark (q) drops may set in around $3\rho_0$. At a somewhat greater density the drops are more closely spaced and slightly larger in size. Still deeper in the star, the drops are no longer the energetically favored configuration but merge together to form quark rods of varying diameter and spacing. At still greater depth, the rods grow together into quark slabs. Beyond this density the forms are repeated in reverse order until at the inner edge of the mixed phase hadronic (h) drops of finite size but separated from each other are immersed in quark matter. At densities between six to ten times ρ_0, the hadronic drops have completely dissolved into pure quark matter [22,23,49]. In all cases the geometric forms lie between about 10 and 25 fm [49,193]. The change in energy accompanied by developing such geometrical structures is likely to be very small in comparison with the volume energy [22,23,194,195] and, thus, cannot much affect the global properties of a neutron star. Nevertheless, the geometrical structure of the mixed

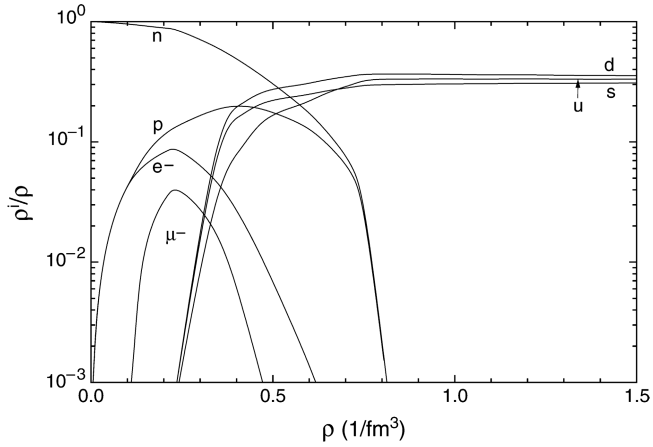

Fig. 24. The composition of chemically equilibrated, stellar quark–hadron matter as a function of the baryon density. Hyperons are artificially suppressed. Hadronic matter is described by HFV [1,44]; the bag constant is $B = 150$ MeV/fm^3. (Taken from Ref. [1].)

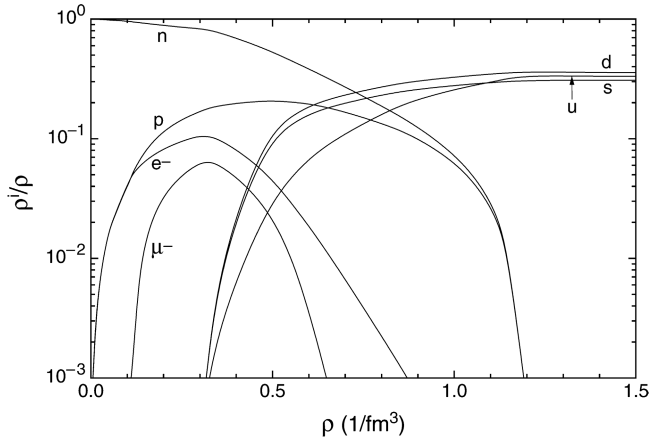

Fig. 25. The same as Fig. 24, but for $B = 250$ MeV/fm^3. (Taken from Ref. [1].)

phase may be very important for transport phenomena as well as irregularities (glitches) in the timing structure of pulsar spin down [22,23,49].

We conclude this section with presenting a representative model for the equation of state of a quark hybrid star, which is shown in Fig. 26 [189]. The hadronic phase is modeled, as in Fig. 23, in the framework of the relativistic Hartree approximation (model HV of Refs. [1,44,186]), the quark phase by the bag model with a bag constant of $B = 150$ MeV/fm^3 and a strange quark mass of 150 MeV. The only difference with respect to Fig. 23 is the smaller bag constant which lowers the onset of quark deconfinement from $3\rho_0$ to $2\rho_0$ [189]. Up to neutron chemical potentials of $\mu^n \sim 10^3$ MeV, the matter stays

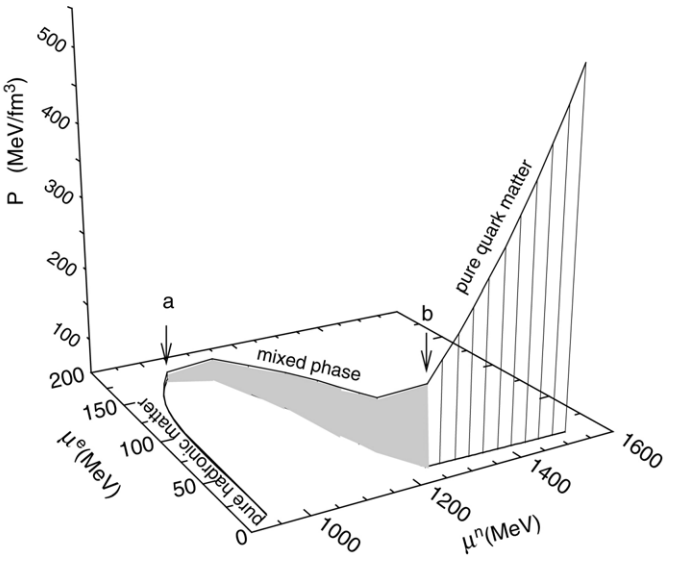

Fig. 26. The equation of state of neutron star matter accounting for quark deconfinement [1].

in the pure hadronic phase. The onset of quark deconfinement, which saturates the number of electrons (cf. Fig. 23), occurs at point a in the diagram where μ^e attains its maximum, $\mu^e \simeq 180$ MeV. As remarked just above, this value corresponds to a baryon number density of about $2\rho_0$. Beyond this density, μ^e decreases toward rather small values because fewer and fewer electrons are present in dense quark hybrid star matter. The mixed phase region (a–b) exists, in the direction of increasing density, for electron chemical potential in the range 180 MeV $\gtrsim \mu^e \gtrsim$ 25 MeV, which corresponds to neutron chemical potentials of 10^3 MeV $\lesssim \mu^n \lesssim 1.2 \times 10^3$ MeV. For this range the volume proportion of quark matter varies over $0 \leq \chi \leq 1$. The energy density in the mixed phase is the same linear combination of the two phases as the charge and baryon number [22,23,49], namely

$$\epsilon = (1-\chi)\epsilon_{\rm H}(\mu^n, \mu^e, \{\phi\}, T) + \chi\epsilon_{\rm Q}(\mu^n, \mu^e, T). \tag{101}$$

Most importantly, the pressure in the mixed phase region varies with density rather than being constant, which would be the case if the conservation of electron charge were ignored. The pure quark matter phase ($\chi = 1$) sets in at b where the density has grown to about $6\rho_0$. It is characterized by a relatively steep increase of pressure with density. Whether or not this phase exists in neutron stars constructed for this equation of state depends of the star's central density and thus on its mass.

5.1.4. H-dibaryons

A novel particle that could make its appearance in the center of a neutron star is the so-called H-dibaryon, a doubly strange six-quark composite with spin and isospin zero, and baryon number two [82]. Since its first prediction in 1977, the H-dibaryon has been the subject of many theoretical and experimental studies as a possible candidate for a strongly bound exotic state. In neutron stars, which may contain a significant fraction of

Λ hyperons, the Λ's could combine to form H-dibaryons, which could give way to the formation of H-dibaryon matter at densities somewhere above $\sim 3\epsilon_0$ [196–198] depending on the in-medium properties of the H-dibaryon. For an attractive optical potential, $U_{\rm H}$, of the H-dibaryon at normal nuclear density the equation of state is softened considerably, as shown in Fig. 27. H-dibaryon matter could thus exist in the cores of moderately dense neutron stars. H-dibaryons with a vacuum mass of about 2.2 GeV and a moderately attractive potential in the medium of about $U_{\rm H} = -30$ MeV, for instance, could go into a boson condensate in the cores of neutron stars if the limiting star mass is about that of the Hulse–Taylor pulsar PSR 1913 + 16, $M = 1.444 M_\odot$ [198]. Conversely, if the medium potential were moderately repulsive, around $U_{\rm H} = +30$ MeV, the formation of H-dibaryons may only take place in heavier neutron stars of mass $M \gtrsim 1.6 M_\odot$. If formed, however, H-matter may not remain dormant in neutron stars but, because of its instability against compression, could trigger the conversion of neutron stars into hypothetical strange stars [197,199,200].

5.2. Strange stars

5.2.1. General properties

If the strange matter hypothesis is true, a new class of compact stars called strange stars should exist. Possible strange star candidates are compiled in Table 5. They would form a distinct and disconnected branch of compact stars and are not a part of the continuum of equilibrium configurations that include white dwarfs and neutron stars (see Fig. 28). In principle, strange and neutron stars could coexist. However, if strange matter is the true ground state, the galaxy is likely to be contaminated by strange quark nuggets which, depending on their velocities [92], could convert neutron stars to strange stars [9,148,215]. This would mean that the objects known to astronomers as pulsars would be rotating strange stars (see Fig. 29) rather than rotating neutron stars. Another peculiar consequence of the hypothesis could be the existence of an entirely new class of dense white-dwarf-like strange stars, called strange dwarfs, plus an expansive range of planetary-like strange matter stars referred to as strange MACHOS. These objects could carry nuclear crusts that are between several hundred and several thousand kilometers thick [12]. The situation is graphically illustrated in Fig. 28. The important astrophysical implication of the existence of strange MACHOS would be that they occur as natural stellar candidates which effectively hide baryonic matter, linking strange quark matter to the fundamental dark matter problem, which is currently one of the problems of greatest importance to astrophysics and cosmology. Observationally, the strange MACHOS could be seen by the gravitational microlensing experiments [216], provided that such objects exist abundantly enough.

As described in Section 3, strange quark matter is expected to be a color superconductor which, at extremely high densities, should be in the CFL phase. This phase is rigorously electrically neutral with no electrons required [29]. For sufficiently large strange quark masses, however, the low density regime of strange quark matter is rather expected to form other condensation patterns (e.g. 2SC, CFL-K^0, CFL-K^+, CFL-$\pi^{0,-}$) in which electrons are present [24,25]. The presence of electrons causes the formation of an electric dipole layer on the surface of strange matter, as illustrated schematically in Fig. 30, which enables

Table 5
Possible strange star candidates

Compact object	Peculiar feature	References
RX J1856.5-3754	Small radius	[201–205]
4U 1728-34	Small radius	[206]
SAX J1808.4-3658	Small radius	[207]
Her X-1	Small radius	[208]
1E 1207.4-5209	Peculiar timing	[209]
PSR 0943 + 10	Microstorms	[210]
3C58 (J0205 + 6449)	Low temperature	[211]
GRO J1744-28	X-ray burst features	[212]
SGR 0526-66, SGR 1900 + 14, SGR 1806-20	X-ray burst features	[97,109,213,214]

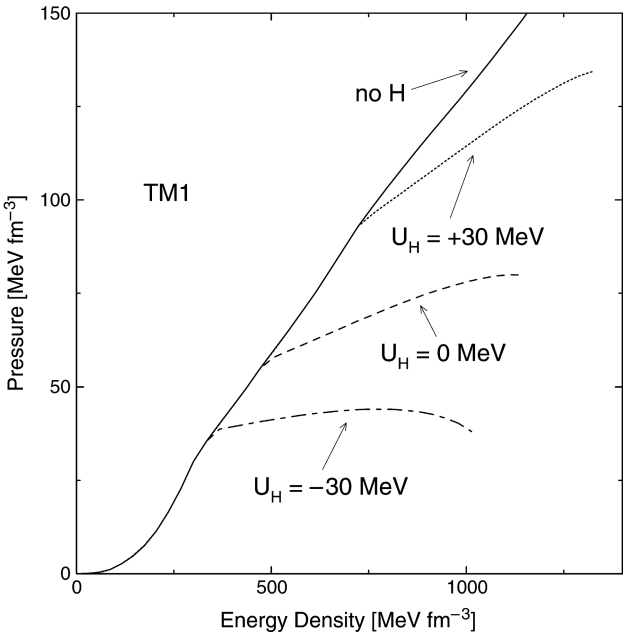

Fig. 27. Equations of state for neutron star matter accounting for a H-dibaryon condensate [198]. U_H is the optical potential of the H-dibaryon at normal nuclear density. Figure reprinted with permission from N.K. Glendenning and J. Schaffner-Bielich, Phys. Rev. C 58 (1998) 1298.

strange quark matter stars to carry nuclear crusts [7,8,68]. An analytical expression for the electron number density and the electric field on the surface of strange quark matter can be derived using the Thomas–Fermi model. One finds [217] that

$$n_e \sim \frac{9.5 \times 10^{35}}{(1.2z_{11}+4)^3}\ \mathrm{cm}^{-3}, \qquad E \sim \frac{7.2 \times 10^{18}}{(1.2z_{11}+4)^2}\ \mathrm{V\ cm}^{-1}, \tag{102}$$

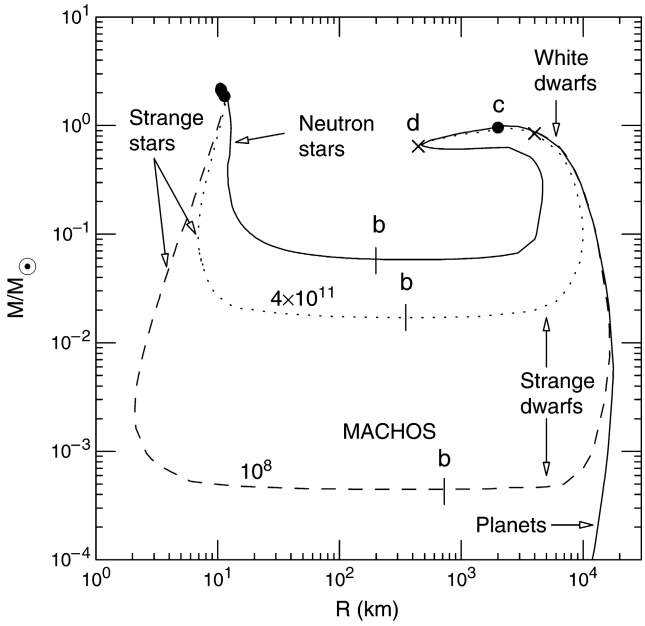

Fig. 28. Mass versus radius for strange star configurations with nuclear crusts (dashed and dotted curves) and gravitationally bound neutron stars and white dwarfs (solid curve). The strange stars carry nuclear crusts with chosen inner densities of $\epsilon_{\rm crust} = 4 \times 10^{11}$ g/cm^3 and $\epsilon_{\rm crust} = 10^8$ g/cm^3, respectively. Crosses denote the termination points of strange dwarf sequences, whose quark matter cores have shrunk to zero. Dots refer to maximum-mass stars; minimum-mass stars are located at the vertical bars labeled 'b'. (Taken from Ref. [1].)

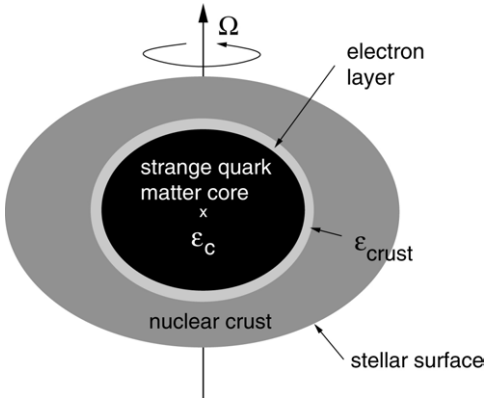

Fig. 29. A schematic illustration of the cross section of a rotating strange star carrying a nuclear crust. The quantities ϵ_c and $\epsilon_{\rm crust}$ denote the star's central density and the density at the base of the crust, respectively. (Taken from Ref. [1].)

where z is a measured height above the quark surface, $z_{11} = z/(10^{-11}$ cm). From Eq. (102) one sees that very strong electric fields, on the order of $\sim 10^{17}$ V/m, may be

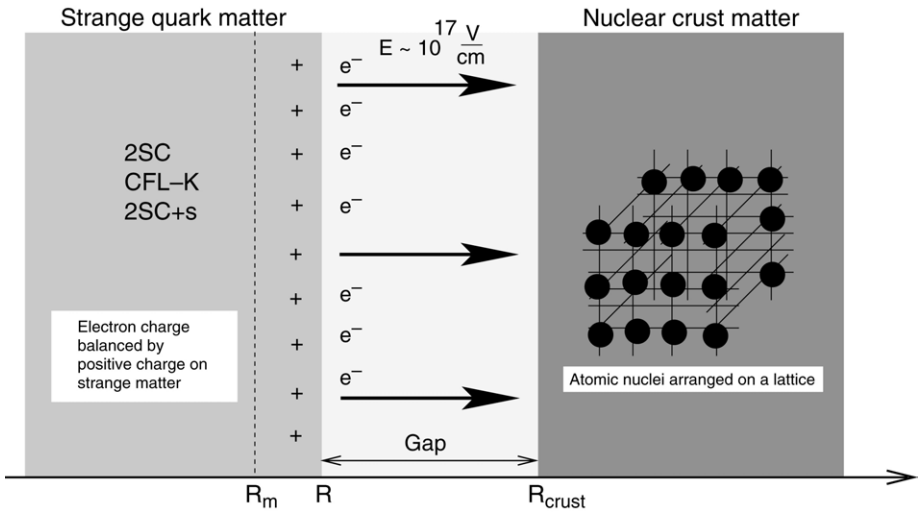

Fig. 30. A surface region of strange quark matter. The region between $R \leq r \leq R_{\rm crust}$ is filled with electrons that are bound to strange matter but extend beyond its surface, R, leading to a deficit of electrons in the range $R_{\rm m} \leq r \leq R$ and therefore a net positive charge in this region. The associated electric field, $E \sim 10^{17}$ V/cm, is sufficiently strong for avoiding contact between atomic matter and strange matter, enabling strange matter to be enveloped by ordinary atomic matter. (Taken from Ref. [1].)

expected near the quark surface. This makes it possible for a non-rotating star to support a nuclear crust with a mass up to $\sim 10^5 M_\odot$ [7]. The maximal possible density at the base of the crust, called the inner crust density, is determined by neutron drip, which occurs at about 4×10^{11} g/cm^3. This somewhat complicated situation of the structure of strange matter enveloped in a nuclear crust can be represented by a proper choice for the equation of state shown in Fig. 31. The equation of state is characterized by a discontinuity in density between strange quark matter and nuclear crust matter across the electric dipole gap where the pressure of the nuclear crust at its base equals the pressure of strange matter at its surface [1,10].

Since the nuclear crust surrounding the quark matter core of a strange star is bound to the core by the gravitational force rather than confinement, the mass–radius relationship of strange matter stars with nuclear crusts is qualitatively similar to those of neutron stars and white dwarfs, which are exclusively bound by gravity. The strange star sequences in Fig. 28 are computed for the maximal possible inner crust density set by neutron drip ($\epsilon_{\rm crust} = 4 \times 10^{11}$ g/cm^3) as well as for a considerably smaller sample density of 10^8 g/cm^3. Of course there are other possible sequences of strange stars with any smaller value of inner crust density [1,10,11]. From the maximum-mass star (solid dots), the central star density decreases monotonically through the sequence in each case. The fact that strange stars with nuclear crusts possess smaller radii than neutron stars leads to smaller Kepler (mass shedding) periods, $P_{\rm K}$, for strange stars. This is indicated by the classical expression $P_{\rm K} \propto \sqrt{R^3/M}$ and has its correspondence in the general relativistic expression for $P_{\rm K}$ derived in Eq. (83). Since the qualitative dependence of $P_{\rm K}$ on mass and radius

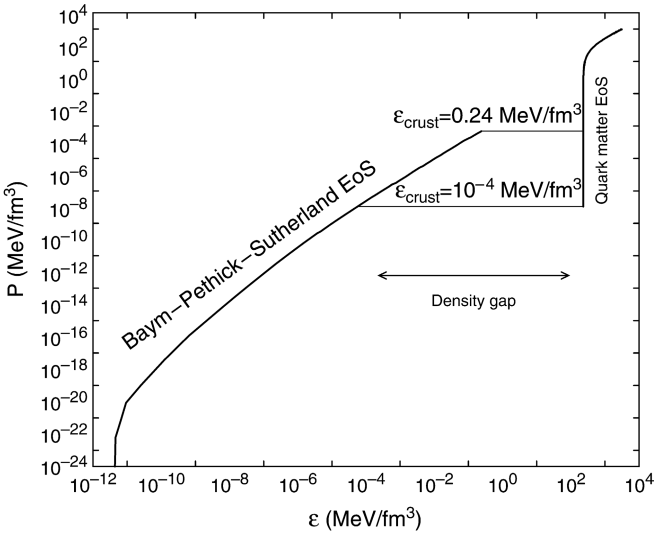

Fig. 31. The equation of state of strange quark matter surrounded by a nuclear crust [10]. The maximal possible nuclear matter density is determined by neutron drip which occurs at $\epsilon_{\rm crust} = 0.24$ MeV/fm^3 (4.3×10^{11} g/cm^3). Any nuclear density that is smaller than neutron drip is possible. As an example, we show the equation of state for a sample density of $\epsilon_{\rm crust} = 10^{-4}$ MeV/fm^3 (10^8 g/cm^3).

remains valid [218], one finds that the complete sequence of strange stars, and not just those close to the mass peak as is the case for neutron stars, can sustain extremely rapid rotation. In particular, a strange star with a typical pulsar mass of $\sim 1.4 M_\odot$ can rotate at Kepler periods as small as $P_{\rm K} \sim 0.5$ ms, depending on crust thickness and the modeling of strange quark matter [1]. This is to be compared with the larger limiting value of $P_{\rm K} \sim 1$ ms obtained for neutron stars of the same mass [1]. Exceptions to this, however, are possible if the nuclear matter exhibits a very strong softening at intermediate densities [173].

Of considerable relevance for the viability of the strange matter hypothesis is the question of whether strange stars can exhibit glitches in rotation frequency. Pulsar glitches are sudden changes in the rotational frequency of a rotating neutron star which otherwise decreases very slowly with time due to the loss of rotational energy through the emission of electromagnetic dipole radiation and an electron–positron wind. They occur in various pulsars at intervals of days to months or years, and in some pulsars are small (Crab), and in others large (Vela) and infrequent ($\Delta\Omega/\Omega \sim 10^{-8}$–$10^{-6}$, respectively). Glitches have been attributed to several factors related to the assumed structure of neutron stars. One such is the crust quake in which an oblate solid crust in its present shape slowly comes out of equilibrium with the forces acting on it as the period of rotation changes, and fractures when the built-up stress exceeds the sheer strength of the crust material [219,220]. The stellar frequency and rate of change of frequency, Ω and $\dot{\Omega}$ respectively, slowly heal to the trend preceding the glitch as the coupling between the crust and core re-establishes their co-rotation. The compatibility of pulsar glitches with the strange matter hypothesis will have a decisive impact on the question of whether or not strange matter is the true

ground state of strongly interacting matter [10,221]. From the study performed in Refs. [10,222] it is known that the ratio of the crustal moment of inertia to the total moment of inertia, $I_{\rm crust}/I_{\rm total}$, varies between 10^{-3} and $\sim 10^{-5}$. If the angular momentum of the pulsar is conserved in a stellar quake then the relative frequency change and moment of inertia change are equal, and one arrives for the change of the star's frequency at [10]

$$\frac{\Delta\Omega}{\Omega} = \frac{|\Delta I|}{I_0} > \frac{|\Delta I|}{I} \equiv f\,\frac{I_{\rm crust}}{I} \sim (10^{-5} - 10^{-3})\,f, \qquad \text{with } 0 < f < 1. \quad (103)$$

Here I_0 denotes the moment of inertia of that part of the star whose frequency is changed in the quake. It might be that of the crust only, or some fraction, or all of the star. The factor f in Eq. (103) represents the fraction of the crustal moment of inertia that is altered in the quake, i.e., $f \equiv |\Delta I|/I_{\rm crust}$. Since the observed glitches have relative frequency changes $\Delta\Omega/\Omega = (10^{-9}$–$10^{-6})$, a change in the crustal moment of inertia of $f \lesssim 0.1$ would cause a giant glitch even in the least favorable case [10]. Moreover, it turns out that the observed range of the fractional change in the spin down rate, $\dot{\Omega}$, is consistent with the crust having the small moment of inertia calculated and the quake involving only a small fraction f of that, just as in Eq. (103). For this purpose we write [10]

$$\frac{\Delta\dot{\Omega}}{\dot{\Omega}} = \frac{\Delta\dot{\Omega}/\dot{\Omega}}{\Delta\Omega/\Omega}\frac{|\Delta I|}{I_0} = \frac{\Delta\dot{\Omega}/\dot{\Omega}}{\Delta\Omega/\Omega}\,f\,\frac{I_{\rm crust}}{I_0} > (10^{-1}\text{ to }10)\,f, \quad (104)$$

where use of Eq. (103) has been made. Eq. (104) yields a small f value, i.e., $f < (10^{-4}$ to $10^{-1})$, in agreement with $f \lesssim 10^{-1}$ established just above. Here measured values of the ratio $(\Delta\Omega/\Omega)/(\Delta\dot{\Omega}/\dot{\Omega}) \sim 10^{-6}$ to 10^{-4} for the Crab and Vela pulsars, respectively, have been used.

5.2.2. SAX J1808.4-3658

As discussed just above, strange stars are self-bound objects at zero external pressure, which would exist stably even if gravity were switched off. The latter makes such objects even more compact. The radii of compact quark stars are thus expected to be smaller than those of neutron stars of comparable mass, which are bound solely by gravity. Figs. 15, 28 and 32 show that this difference in radius may be three to four kilometers for stars of canonical mass, $\sim 1.4 M_\odot$, and even bigger than that for less massive objects. One neutron star that may have such an unusually small radius is the transient x-ray burst source SAX J1808.4-3658 [207], which was discovered in September 1996 by the BeppoSAX satellite. Two bright type-I x-ray bursts were detected, each one lasting less than 30 seconds. An analysis of the bursts in SAX J1808.4-3658 indicates that it is 4 kpc distant and has a peak x-ray luminosity of 6×10^{36} erg/s in its bright state, and a x-ray luminosity lower than 10^{35} erg/s in quiescence [223]. Coherent pulsations at a period of 2.49 ms were also discovered [224]. The binary nature of SAX J1808.4-3658 was firmly established with the detection of a two-hour orbital period [225] as well as with the optical identification of the companion star. SAX J1808.4-3658 is the first pulsar that shows both coherent pulsations in its persistent emission and x-ray bursts.

Li et al. [207] extracted a mass–radius relationship for the compact star in SAX J1808.4-3658 from the following two requirements on the geometry of the stellar binary system (see also Section 7.2 where mass accretion onto a compact star is discussed in more detail).

Firstly, detection of x-ray pulsations requires that the inner radius, $r_{\rm m}$, of the accretion disk should be larger than the stellar radius R. Secondly, the inner radius must be smaller than the disk's co-rotation radius, $r_{\rm c}$; otherwise accretion will be inhibited by a centrifugal barrier. From these two conditions one finds that $r_{\rm m} \lesssim r_{\rm c} = (MP^2/(4\pi^2))^{1/3}$, with M and P the star's mass and rotational period, respectively. Expressing the location of the inner disk in terms of the Alfvén radius, $r_{\rm A}$, which is that distance from the neutron star at which the accreting matter is pulled by the magnetic fields to the poles of the star which happens when the kinetic energy density is comparable to the magnetic energy density [226], one arrives at $r_{\rm m} = \xi r_{\rm A} = \xi(B^2R^6/\dot{M}(2M)^{1/2})^{2/7}$. The symbols B and $\dot{M}$ stand for the surface magnetic field and the mass accretion rate of the rotating neutron star, respectively. The quantity $\xi \sim 1$ is a parameter which depends very weakly on the accretion rate [227]. Denoting the minimum and maximum accretion rates of SAX J1808.4-3658 as $\dot{M}_{\rm min}$ and $\dot{M}_{\rm max}$, the conditions discussed above can be expressed as

$$r \lesssim r_{\rm m}(\dot{M}_{\rm max}) < r_{\rm m}(\dot{M}_{\rm min}) \lesssim r_{\rm c}. \tag{105}$$

To connect this relation to the observed data, let us assume that the mass accretion rate is proportional to the x-ray flux F observed with the Rossi X-ray Timing Explorer (RXTE). This is supported by the fact that the x-ray spectrum of SAX J1808.4-3658 was remarkably stable and that there was only a slight increase in the pulse amplitude when the x-ray luminosity varied by a factor of ∼100 during the 1998 April/May outburst [228–230]. From this, an upper limit for the stellar radius of $R < (F_{\rm min}/F_{\rm max})^{2/7} r_{\rm c}$ was derived in [207]. This relation can be conveniently written as

$$R < 27.5 \left(\frac{F_{\rm min}}{F_{\rm max}}\right)^{2/7} \left(\frac{P}{2.49\ {\rm ms}}\right)^{2/3} \left(\frac{M}{M_\odot}\right)^{1/3} {\rm km}, \tag{106}$$

where $F_{\rm max}$ and $F_{\rm min}$ denote the x-ray fluxes measured for high and low x-ray emission states, respectively. Adopting a flux ratio of $F_{\rm max}/F_{\rm min} \sim 100$, Eq. (106) constrains the mass–radius values of SAX J1808.4-3658 to values that lie between the dashed curves in Fig. 32, which suggests that SAX J1808.4-3658 could be a strange star. The dashed line labeled $R = R_{\rm s} (= 2MR)$ denotes the Schwarzschild limit on the radius of a compact object set by gravitational collapse to a black hole. The curves labeled BBB1, BBB2, Hyp, and K^- denote the mass–radius relationships of conventional neutron stars computed for different models for the equation of state. Constraints on the mass–radius relationship which, if robust, are better described in terms of strange stars than neutron stars have also been obtained for the compact star in the x-ray source 4U 1728-34 ($M < 1.0 M_\odot$, $R < 9$ km) [231], for the isolated neutron star RX J1856.5-3754 [201], which will be discussed in the next section, as well as for the x-ray pulsar Her X-1 ($M = 1.1 - 1.8 M_\odot$, $R = 6.0 - 7.7$ km) [208]. (See also Table 5.)

In passing, we mention the recent discovery of significant absorption lines in the spectra of 28 bursts of the low mass x-ray binary EXO 0748–1676 [232]. These lines have been identified with iron and oxygen transitions, all with a gravitational red-shift of $z = 0.35$. As shown in Ref. [232], for a stellar mass range of $M \sim 1.3 - 2.0 M_\odot$ such a z value is completely consistent with conventional neutron star models, made of normal nuclear matter, and excludes even some models in which neutron stars are made of more exotic matter.

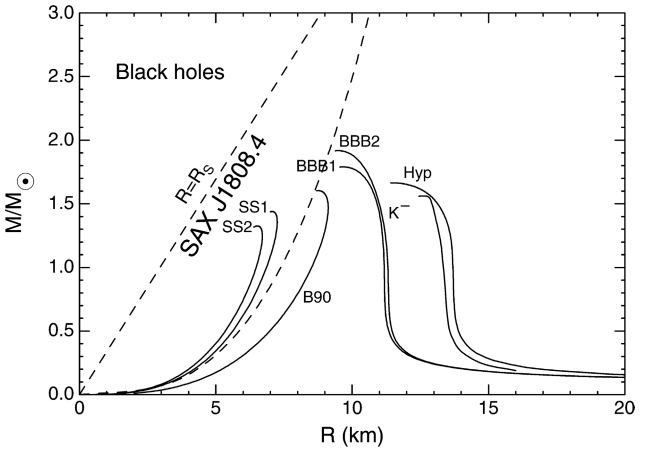

Fig. 32. Comparison of the mass–radius relationship of SAX J1808.4-3658 determined from RXTE observations (i.e. Eq. (106)) with theoretical models of neutron stars and strange stars [207]. The solid curves represent theoretical mass–radius relationships for neutron stars and strange stars. Figure reprinted with permission from X.D. Li et al., Phys. Rev. Lett. 83 (1999) 3776.

5.2.3. RX J1856.5-3754

In addition to x-ray emission from neutron stars in binaries, discussed in the previous section, the thermal emission from the surface of an isolated neutron star (INS) is of key importance for the determination of the mass and radius of a neutron star, too. ROSAT was the first satellite with a sufficient sensitivity in the x-ray band to perform a systematic search and study of such objects. The nearby neutron star RX J1856.5-3754, discovered in 1992 [233], is the brightest INS in x-rays. It does not show any signs of activity such as variability or pulsation. Since its discovery, RX J1856.5-3754 was studied in great detail in x-rays, UV, and the optical band, using a variety of different astrophysical observatories (ROSAT, EUVE, ASCA, HST, Chandra, XMM Newton, VLA). Detailed Chandra observations of RX J1856.5-3754 have shown that this neutron star has a featureless thermal spectrum for which a simple black-body distribution seems to provide a better fit to x-ray data than more sophisticated atmospheric models [234,235]. Several sets of observations taken with ROSAT, EUVE, NTT, Keck, HST, and Chandra have yielded a proper motion of 330 mas/yr and parallax 8.5 mas, which corresponds to a transverse stellar velocity of about 200 km/s and a distance from Earth of $D = 120$ pc [236,237]. These measurements could indicate that the star originated $\sim 10^6$ y ago in the Upper Scorpio Association at about the same time that a supernova ejected the runaway O star ζ Ophiuchus, suggesting that RX J1856.5-3754 and ζ Ophiuchus could have been members of a binary system and that RX J1856.5-3754 may be the remnant of the star that exploded. The apparent (red-shifted) radius of RX J1856.5-3754 can be calculated from [201]

$$R^{\infty} = 4.25\, f_A^{-1/2}\, f_E^{-1/2} \gamma^2 D_{100} (T_{\rm bb}^{\infty}/60\ {\rm eV})^{-2}\ {\rm km}. \tag{107}$$

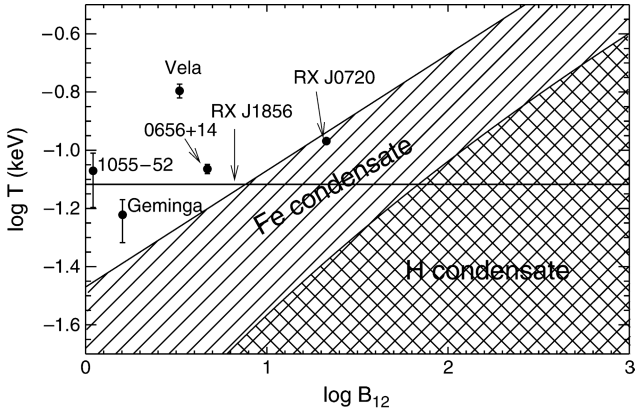

Fig. 33. The critical temperature for hydrogen (H) and iron (Fe) as a function of magnetic field, B [201]. A phase transition to a solid condensate is possible in the shaded region for Fe and in the cross-hatched region for H. The positions of five cool, isolated neutron stars (see table Table 7) are shown. The horizontal line is drawn in correspondence to the color temperature of RX J1856.5-3754. Figure reprinted with permission from R. Turolla, S. Zane, and J.J. Drake, Astrophys. J. 603 (2004) 265.

The true (coordinate) radius of the star, R, is connected to the apparent radius through

$$R = R^{\infty}(1 - 2M/R)^{1/2}. \tag{108}$$

The quantity f_A in Eq. (107) denotes the fraction of the stellar surface responsible for the observed emission, f_E is the ratio of emitted power to black-body power, γ stands for the spectral hardening, $D_{100} \equiv D/(100\ \text{pc})$ is the star's distance, and $T_{\rm bb} = T_{\rm bb}^{\infty}(1 - 2M/R)^{-1/2}$ its black-body temperature. If the emission comes from the entire stellar surface ($f_A = 1$) and the temperature distribution is uniform ($\gamma = 1$), Eq. (107) simplifies to

$$R^{\infty} = 4.25\, f_E^{-1/2} D_{100} (T_{\rm bb}/60\ \text{eV})^{-2}\ \text{km}. \tag{109}$$

On the basis of this relation Drake et al. [202] reported an apparent radius for RX J1856.5-3754 of $R^{\infty}/D_{100} = 4.12 \pm 0.68$ km, where the quoted uncertainty represents the combined temperature determination uncertainty (± 1 eV) and the dominant absolute effective area uncertainty of Chandra's Low Energy Transmission Grating (LETG) and High Resolution Camera–Spectroscopic Plate Detector Array (HRC-S) combination ($\pm 15\%$). Depending on the star's distance, which still appears to be an open issue [238], this implies a rather small apparent stellar radius in the range between about $R^{\infty} = 4$ km to 8 km. The latest distance measurement of 175 pc [238] combined with specific assumptions about the star's surface composition (see below) could favor $R^{\infty} \simeq 8$ km [239], which corresponds to a true radius of about 6 km. As can be seem from Figs. 15 and 32, such a value would be too small for conventional neutron star equations of state [202] which predict 12 km $\lesssim R^{\infty} \lesssim$ 17 km [3]. Proposed explanations for such a small radius include a reduced x-ray emitting region (such as a heated polar cap), or the presence of a more compact object such as a strange quark star [203–205]. An alternative possibility, suggested

in [201], is cold neutron stars ($T \lesssim 10^6$ K) endowed with rather strong magnetic fields ($B \gtrsim 10^{13}$ G) and with metal dominated outer layers. Depending on T and B, such stars may undergo a phase transition to a solid condensate in the outermost layers (Fig. 33), resulting in an x-ray spectrum that is featureless as observed for RX J1856.5-3754. The observed UV–optical enhanced emission could be explained by the presence of a gaseous, thin hydrogen shell on top of the iron condensate, where the optical flux is reprocessed. This model predicts a value for the apparent radius of RX J1856.5-3754 in the range of $R^\infty \sim 8$–12 km, depending on whether one assumes uniform or meridional variation temperature distributions on the star's surface.

For a canonical neutron star mass of $1.4M_\odot$, apparent radii in the range $R^\infty \sim 10$–12 km (true radii of $R \sim 7$–9 km for a $1.4M_\odot$ neutron star) can be accommodated by conventional models for the equations of state of superdense matter which exhibit a soft behavior at high densities [201]. The situation is different for $R^\infty \lesssim 8$ km which may indicate that such stars are made of self-bound hadronic matter, of which strange quark matter may be the most plausible state of matter. Sequences of such stars are shown in Figs. 15 and 32. While a strange star may be an intriguing conceivable option, present observations of RX J1856.5-3754 do not necessarily demand this interpretation and more conventional interpretations involving conventional neutron stars are certainly possible [201,240]. A conventional interpretation is also supported by models which fit the x-ray and optical data of RX J1856.5-3754 with a two-component black-body model [235]. The latter are best fitted with $T^\infty_{\mathrm{bb},X} \simeq 63.5$ eV and $R^\infty_{\mathrm{bb},X} \simeq 4.4(D/120\ \mathrm{pc})$ km for the hot x-ray emitting region, and $T^\infty_{\mathrm{bb,opt}} < 33$ eV and $R^\infty_{\mathrm{bb,opt}} > 17(D/120\ \mathrm{pc})$ km for the rest of the neutron star surface responsible for the optical flux [235].

5.2.4. The neutron star in 3C58

Murray et al. discovered the 65 ms pulsars PSR $0205+6449$ in the supernova remnant 3C58 located in the constellation Cassiopeia [241]. Historical evidence strongly suggests an association of the remnant with supernova SN 1181, which went off in 1181 AD. This renders PSR $0205+6449$ younger than B$0531+21$, the pulsar in the Crab nebula, born in a supernova explosion recorded by Chinese astronomers in 1045 AD. Using data provided by the Chandra x-ray observatory, Slane et al. inferred an upper limit on the effective surface temperature of PSR $0205+6449$ of only $T^\infty < 1.08\times10^6$ K which falls below predictions from standard cooling models [211]. On the basis of its low temperature, it was suggested that PSR $0205+6449$ may be a strange quark star rather than a neutron star [211]. We will discuss this issue in greater detail in Section 6.

5.2.5. X-ray, gamma ray burst, and SGR associations

X-ray bursts are sudden increases in the x-ray flux of x-ray sources, with rise times of $\leq$1 s, and subsequent decay with characteristic times ranging from 10 s to a few minutes. They are classified into two classes: type-I and type-II x-ray bursts. Type-I x-ray bursts are characterized by relatively long burst intervals (hours to days) and significant spectral softening during the burst decay as compared to their type-II counterparts. The differences between type-I (II) bursts and the HXRBs is discussed by [242].

Gamma ray bursts (GRBs) are most intense transient gamma ray events in the sky when they are on, but the nature of gamma ray bursts has remained a mystery since

their discovery [243]. The isotropic and inhomogeneous distribution of GRBs detected with BATSE and the identification of counterparts in radio, optical, and x-ray regions by BeppoSAX and other ground based telescopes supports the notion that they are located at cosmological distances, which make them the most energetic events ever known [244, 245]. Gamma ray bursts at truly cosmological distances could be due to collisions of two neutron or two strange stars in binary systems [246], depending on the true ground state of strongly interacting matter, and/or may also involve black holes [247]. Binary neutron star or strange star collisions could release $\sim 10^{52}$ ergs in the form of gamma rays over a time period of about 0.2 s. The central engine that powers gamma ray bursts should be capable of releasing a total energy of $\sim 10^{53}$ erg, which may or may not be possible in stellar collisions. The situation may be different for the conversion of a neutron star to a strange star [248]. Depending on the model for the equation of state, the total energy given off in such a conversion is $(1\text{–}4) \times 10^{53}$ erg [248].

Bare strange stars have also been associated with soft gamma repeaters (SGRs). Unlike gamma ray bursts, which emit large amounts of high energy gamma radiation, SGRs have a large proportion of lower energy x-ray radiation. Also, in contrast to gamma ray bursts, which can rumble on for many minutes, SGRs pop off in a fraction of a second. Conventional models associate SGRs with young neutron stars energizing a large cloud of gas cast off in a supernova explosion, or x-ray binary stars that accrete matter at irregular intervals and emit gamma rays when the accreted matter hits the surface. Most strikingly, the intensity of the outbursts is between 10^3 and 10^4 times the Eddington limit, $L_{\rm Edd}$. The latter is defined as the critical luminosity at which photon radiation pressure from the surface of a star of mass M equals gravity,

$$L_{\rm Edd} = 1.3 \times 10^{38} (M/M_\odot) \text{ erg s}^{-1}. \tag{110}$$

The Eddington limit does not apply to bare strange stars since quark matter is held in place by the strong interaction and not gravity (see Section 5.2.7). For that reason the bursting activity of SGRs can be comfortably explained by fast heating of the surfaces of bare quark stars up to temperatures of $\sim(1\text{–}2) \times 10^9$ K and subsequent thermal emission [97,108]. The fast heating mechanism of SGRs may be either impacts of comets onto bare strange stars [97,109,110] or fast decay of superstrong magnetic fields [249,111].

A very high luminosity flare took place in the Large Magellanic Cloud (LMC), some 55 kpc away, on 5 March 1979. Another giant flare was observed on 27 August 1998 from SGR 1900 + 14. The inferred peak luminosity for both events is $\sim 10^7$ (i.e. $\sim 10^{45}$ erg/s) times the Eddington limit for a solar mass object, and the rise time is very much smaller than the time needed to drop $\sim 10^{25}$ g (about $10^{-8} M_\odot$) of normal material onto a neutron star. Alcock et al. [7] suggested a detailed model for the 5 March 1979 event burst which involves the particular properties of strange matter (see also Horvath et al. [97, 107]). The model assumes that a lump of strange matter of $\sim 10^{-8} M_\odot$ fell onto a rotating strange star. Since the lump is entirely made up of self-bound high density matter, there would be only little tidal distortion of the lump, and so the duration of the impact can be very short, around $\sim 10^{-6}$ s, which would explain the observed rapid onset of the gamma ray flash. The light curves expected for such giant bursts [108,110,112,113] should possess characteristic features that are well within the capabilities of ESA's INTErnational

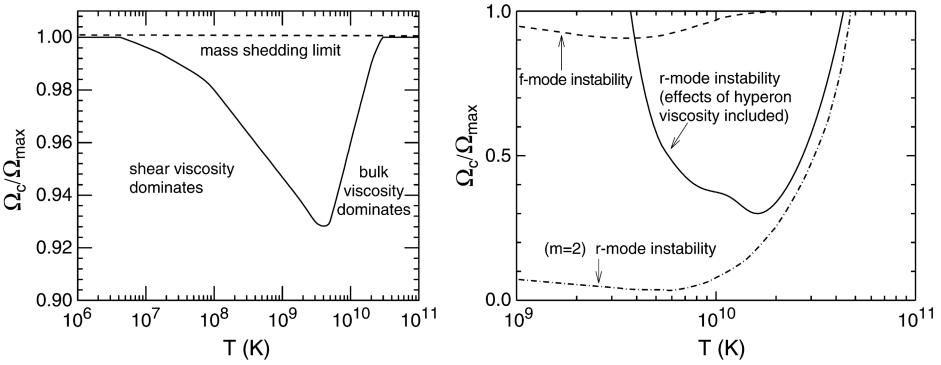

Fig. 34. The temperature dependence of the critical angular velocity Ω_c of rotating neutron stars. The left figure shows the gravitational radiation driven f-mode instability suppressed by shear and bulk viscosity (taken from Ref. [1]). Right figure: comparison of f-mode instability with r-mode instability. (Data from Refs. [251,252].)

Gamma-Ray Astrophysics Laboratory (INTEGRAL [250]) launched by the European Space Agency in October of 2002.

5.2.6. Rotational instabilities

An absolute limit on rapid rotation is set by the onset of mass shedding from the equator of a rotating star. However, rotational instabilities in rotating stars, known as gravitational radiation driven instabilities, set a more stringent limit on rapid stellar rotation than mass shedding. These instabilities originate from counter-rotating surface vibrational modes which at sufficiently high rotational star frequencies are dragged forward. In this case gravitational radiation, which inevitably accompanies the aspherical transport of matter, does not damp the instability modes but rather drives them. Viscosity plays the important role of damping these instabilities at a sufficiently reduced rotational frequency such that the viscous damping rate and power in gravity waves are comparable. The most critical instability modes that are driven unstable by gravitational radiation are f-modes and r-modes. Fig. 34 shows the stable neutron star frequencies if only f-modes were operative in neutron star. One sees that hot as well as cold neutron stars can rotate at frequencies close to mass shedding, because of the large contributions of shear and bulk viscosity, respectively, for this temperature regime. The more recently discovered r-mode instability may change the picture completely, as can be seen from Fig. 34. These modes are driven unstable by gravitational radiation over a considerably wider range of angular velocities than the f-modes (cf. the dashed curve labeled $(m = 2)$ r-mode instability). In stars with cores cooler than $\sim 10^9$ K, on the other hand, the r-mode instability may be completely suppressed by viscous phenomena, so stable rotation would be limited by the f-mode instability again [252].

Figs. 35 and 36 are the counterparts to Fig. 34 but calculated for strange stars made of CFL and 2SC quark matter, respectively [253,254]. The r-mode instability seems to rule out the possibility that pulsars are CFL strange stars, if the characteristic timescales for viscous damping of r-modes are exponentially increased by factors of $\sim \Delta/T$ as calculated in [253]. An energy gap as small as $\Delta = 1$ MeV was assumed. For much larger gaps of

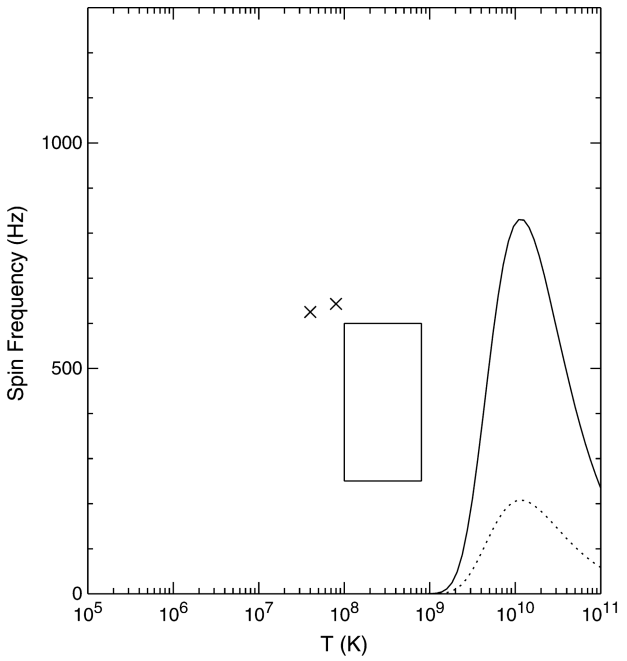

Fig. 35. Critical rotation frequencies versus stellar temperature for CFL strange stars [254]. Figure reprinted with permission from J. Madsen, Phys. Rev. Lett. 85 (2000) 10.

$\Delta \sim 100$ MeV, as expected for color superconducting quark matter (see Section 3.2), the entire diagram would be r-mode unstable. The full curve in Fig. 35 is calculated for a strange quark mass of $m_s = 200$ MeV, the dotted curve for $m_s = 100$ MeV. The box marks the positions of most low mass x-ray binaries (LMXBs) [255], and the crosses denote the most rapidly rotating millisecond pulsars known. All strange stars above the curves would spin down on a timescale of hours due to the r-mode instability, in complete contradiction to the observation of millisecond pulsars and LMXBs, which would rule out CFL quark matter in strange stars [330]. Fig. 36 shows the critical rotation frequencies of quark stars as a function of internal stellar temperature for 2SC quark stars. For such quark stars the situation is less conclusive. Rapid spin down, driven by the r-mode gravitational radiation instability, would happen for stars above the curves.

5.2.7. Surface properties of strange stars

Strange quark matter with a density of about two times the density of nuclear matter may exist up to the surface of a strange star [7]. Such a bare strange star differs qualitatively from a neutron star which has a density at the surface of about 0.1 to 1 g/cm^3. As is known from Section 5.2.1, the thickness of the quark surface would be just $\sim$1 fm, the length scale of the strong interaction. Electrons are held to quark matter electrostatically, and the thickness of the electron surface is several hundred fermis. Since neither component, electrons or quark

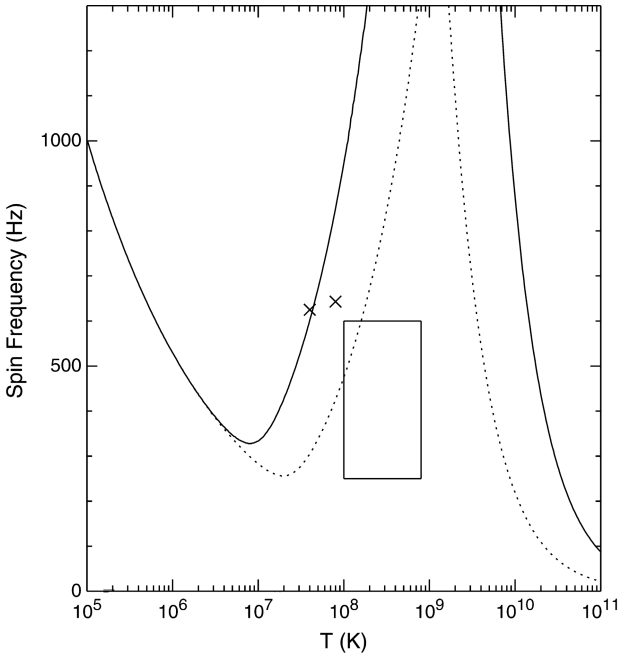

Fig. 36. The same as Fig. 35, but for 2SC quark stars [254]. Figure reprinted with permission from J. Madsen, Phys. Rev. Lett. 85 (2000) 10.

matter, is held in place gravitationally, the Eddington limit (Eq. (110)) to the luminosity that a static surface may emit does not apply, and thus the object may have photon luminosities much greater than 10^{38} erg/s. It was shown by Usov [112] that this value may be exceeded by many orders of magnitude by the luminosity of e^+e^- pairs produced by the Coulomb barrier at the surface of a hot strange star. For a surface temperature of $\sim 10^{11}$ K, the luminosity in the outflowing pair plasma was calculated to be as high as $\sim 3 \times 10^{51}$ erg/s. Such an effect may be a good observational signature of bare strange stars [108,110,112, 113]. If the strange star is enveloped by a nuclear crust however, which is gravitationally bound to the strange star, the surface made up of ordinary atomic matter would be subject to the Eddington limit. Hence the photon emissivity of such a strange star would be the same as for an ordinary neutron star. If quark matter at the stellar surface is in the CFL phase the process of e^+e^- pair creation at the stellar quark matter surface may be turned off, since cold CFL quark matter is electrically neutral, so no electrons are required and none are admitted inside CFL quark matter [29]. The situation may be different for the early stages of a hot CFL quark star [256].

5.3. Strange dwarfs

The strange white dwarfs constitute the strange counterparts of ordinary white dwarfs. They consist of a strange quark matter core in the star's center which is enveloped by a

nuclear crust made up of ordinary atomic matter [7]. The crust is suspended out of contact with the quark core due to the existence of an electric dipole layer on the core's surface [7,68], which insulates the crust from conversion to quark matter. Even so, the maximum density of the crust is strictly limited by the neutron drip density ($\epsilon_{\rm drip} = 4 \times 10^{11}$ g/cm^3), at which neutrons begin to drip out of the nuclei and would gravitate into the core where they would be dissolved into strange matter.

Strange white dwarfs comprise a largely unexplored consequence of the strange matter hypothesis. Depending on the amount of crust mass, their properties may differ considerably from those of ordinary white dwarfs. For instance, it is well known that the maximum density attained in the white dwarf of limiting mass is about $\epsilon_{\rm wd} = 10^9$ g/cm^3 [257,258]. Above this density, the electron pressure is insufficient to support the star, and there are no stable equilibrium configurations until densities of the order of the nuclear density ($\epsilon \gtrsim 10^{14}$ g/cm^3) are reached, which are neutron or strange stars. One class of strange dwarfs can be envisioned as consisting of a core of strange matter enveloped within what would otherwise be an ordinary white dwarf. They would be practically indistinguishable from ordinary white dwarfs. Of greater interest is the possible existence of a new class of white dwarfs that contain nuclear material up to the neutron drip density, which would not exist without the stabilizing influence of the strange quark core [12]. The density at the inner edge of the nuclear crust carried by these strange dwarfs could fall in the range of $\epsilon_{\rm wd} < \epsilon_{\rm crust} < \epsilon_{\rm drip}$. The maximum inner crust density therefore could be about 400 times the central density of the white dwarf of limiting mass and 4×10^4 times that of the typical $0.6 M_\odot$ white dwarf. An investigation of the stability of such very dense dwarf configurations against acoustic (radial) vibrations, which will be discussed below, reveals stability over an extensive mass range from $\sim 10^{-3} M_\odot$ to slightly more than $1 M_\odot$. This is the same range as for ordinary white dwarfs except that the lower mass limit is smaller by a factor of $\sim 10^{-2}$. This is because of the influence of the strange core, to which the entire class owes its stability. Whether or not a star is stable against radial oscillations is determined by an analysis of stability against radial oscillations [259,260]. The adiabatic motion of a star in its nth normal eigenmode ($n = 0$ is the fundamental mode) is expressed in terms of an amplitude $\xi_n(r)$ given by

$$\delta r(r,t) = \mathrm{e}^{2\Phi(r)}\, \xi_n(r)\, \mathrm{e}^{\mathrm{i}\omega_n t} r^{-2}, \tag{111}$$

where $\delta r(r,t)$ denotes small Lagrangian perturbations in r. The quantity ω_n is the star's oscillation frequency, which we want to compute. The eigenequation for $\xi_n(r)$, which governs the normal modes, is of Sturm–Liouville type:

$$\frac{\mathrm{d}}{\mathrm{d}r}\left(\Pi(r)\frac{\mathrm{d}\xi_n(r)}{\mathrm{d}r}\right) + (Q(r) + \omega_n^2 W(r))\,\xi_n(r) = 0, \tag{112}$$

which implies that the eigenvalues ω_n^2 are all real and form an infinite, discrete sequence $\omega_0^2 < \omega_1^2 < \omega_2^2 < \ldots$. Another consequence is that the eigenfunction ξ_n corresponding to ω_n^2 has n nodes in the radial interval $0 < r < R$. Hence, the eigenfunction ξ_0 is free of nodes in this interval. The functions $\Pi(r)$, $Q(r)$, and $W(r)$ are expressed in terms of the

equilibrium configurations of the star by

$$\begin{aligned} \Pi &= \mathrm{e}^{2\Lambda+6\Phi} r^{-2} \Gamma P, \\ Q &= -4\mathrm{e}^{2\Lambda+6\Phi} r^{-3} \frac{\mathrm{d}P}{\mathrm{d}r} - 8\pi \mathrm{e}^{6(\Lambda+2\Phi)} r^{-2} P(\epsilon + P) \\ &\quad + \mathrm{e}^{2\Lambda+6\Phi} r^{-2} (\epsilon + P)^{-1} \left(\frac{\mathrm{d}P}{\mathrm{d}r}\right)^2, \\ W &= \mathrm{e}^{6\Lambda+2\Phi} r^{-2} (\epsilon + P). \end{aligned} \tag{113}$$

The quantities ϵ and P denote the energy density and the pressure of the stellar matter. The pressure gradient, $\mathrm{d}P/\mathrm{d}r$, is obtained from the Tolman–Oppenheimer–Volkoff Eq. (75). The symbol Γ denotes the adiabatic index at constant entropy, s, given by

$$\Gamma = \frac{\partial \ln P(\rho, s)}{\partial \ln \rho} = \frac{(\epsilon + P)}{P} \frac{\partial P(\epsilon, s)}{\partial \epsilon}, \tag{114}$$

which varies throughout the star's interior. Solving (112) subject to the boundary conditions $\xi_n \propto r^3$ at the star's origin and $\mathrm{d}\xi_n/\mathrm{d}r = 0$ at the star's surface leads to the ordered frequency spectrum $\omega_n^2 < \omega_{n+1}^2$ $(n = 0, 1, 2, \ldots)$ of the normal radial stellar modes. If any of these is negative for a particular star, the frequency is imaginary, and to it there corresponds an exponentially growing amplitude of oscillation. Such stars are unstable. Figs. 37 and 38 show the solutions to Eq. (112) for the strange star sequence in Fig. 28 whose inner crust density is equal to neutron drip. It follows that all stars between 'c' and 'd' are unstable against radial pulsations since for them $\omega_0^2 < 0$. The situation is different for the stars to the left of 'c' whose eigenfrequencies are all positive [11].

At present there is neither a well studied model for the formation of hypothetical strange dwarfs, nor a study that determines their abundance in the universe. One possible scenario would be the formation of strange dwarfs from main sequence progenitors that have been contaminated with strange nuggets over their lifetimes. The capture of strange matter nuggets by main sequence stars would probably be an inevitable consequence if strange matter were more stable than hadronic matter [114] because then the galaxy would be filled with a flux of strange nuggets which would be acquired by every object they come into contact with, such as planets, white dwarfs, neutron stars, and main sequence stars. Naturally, due to the large radii of the latter, they arise as ideal, large surface, long integration time detectors for the strange matter flux [253]. Nuggets that are accreted onto neutron stars and white dwarfs, however, never reach their centers, where the gravitational potential is largest, because they are stopped in the lattice close to the surface due to the large structural energy density there. This prevents such stars from building up a core of strange matter. The situation is different for main sequence stars which are diffuse in comparison with neutron stars and white dwarfs. In this case the accreted nuggets may gravitate to the star's core, accumulate there, and form a strange matter core that grows with time until the star's demise as a main sequence star occurs [11,12]. An upper limit on the baryon number of strange matter that may accumulate in a main sequence star is given by [9,114]

$$A = 1.6 \times 10^{47} (M/M_\odot)^{-0.15} v_{250}^{-1} \rho_{24} (1 + 0.164 v_{250}^2 (M/M_\odot)^{-0.25}), \tag{115}$$

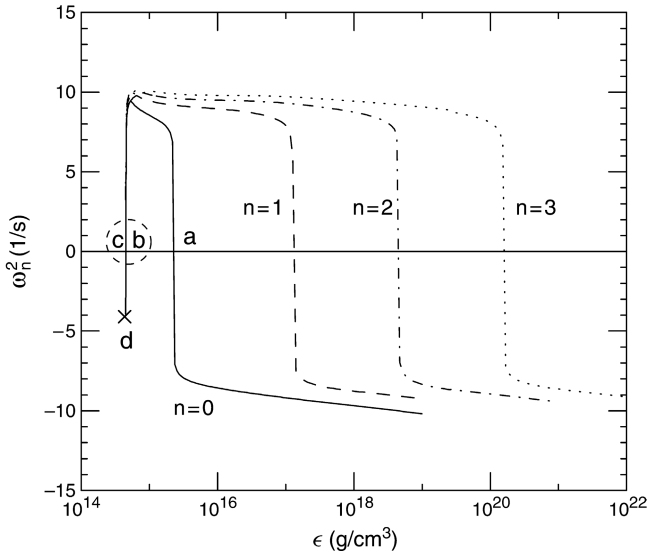

Fig. 37. Oscillation frequencies of the lowest four ($n = 0, 1, 2, 3$) normal radial modes of strange stars with $\epsilon_{\rm crust} = \epsilon_{\rm drip}$ as a function of central star density. The cross at 'd' refers to the termination point of the strange dwarf sequence shown in Fig. 28. (Taken from Ref. [11].)

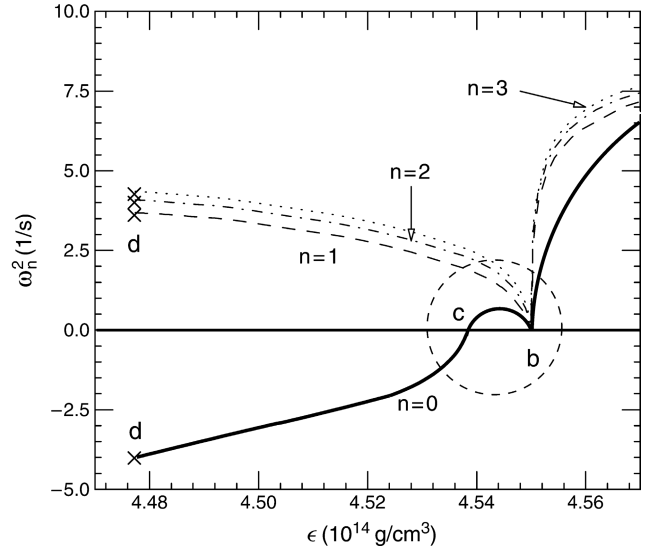

Fig. 38. The same as Fig. 37, but for strange dwarfs in the vicinity of the termination point, 'd', of the sequence. The labels 'b' and 'c' refer to the lightest and heaviest star, respectively, marked in Fig. 28. (Taken from Ref. [11].)

with $v_{250} \equiv v_\infty/(250\ \text{km/s})$ and $\rho_{24} \equiv \rho_\infty/(10^{-24}\ \text{g/cm}^3)$. The quantities v_∞ and ρ_∞ are the nugget speed and contribution to the density of the galactic halo far from the star,

respectively. If one assumes that all the dark matter in the halo of our galaxy consists of strange nuggets (certainly a crude overestimate), then $v_{250}^{-1}\rho_{24} \sim 1$, and Eq. (115) leads for typical progenitor star masses of $\sim 1 M_\odot$ to the upper limit of $A \sim 10^{48}$. The mass and radius of such a strange core are $\sim 2 \times 10^{21}$ kg ($\sim 10^{-9} M_\odot$ or about 10^{-3} times the mass of the Earth) and ~ 11 m. These values follow from the approximate relations $R = 4.35 \times 10^{26} (M/\text{kg})$ and $R/\text{km} = 1.12 \times 10^{-18} A^{1/3}$ for strange matter with $B^{1/4} = 145$ MeV.

Another plausible mechanism has to do with primordial strange matter bodies. Such bodies of masses between 10^{-2} and about $1 M_\odot$ may have been formed in the early universe and survived to the present epoch [261]. Such objects will occasionally be captured by a main sequence star and form a significant core in a single and singular event. The core's baryon number, however, cannot be significantly larger than $\sim 5 \times 10^{31} (M/M_\odot)^{-1.8}$ where M is the star's mass. Otherwise a main sequence star is not capable of capturing the strange matter core [9]. Finally we mention the possibility that in the very early evolution of the universe, primordial lumps [8,115] of hot strange matter will have evaporated nucleons which are plausibly gravitationally bound to the lump. The evaporation will continue until the quark matter has cooled sufficiently. Depending on the original baryon number of the quark lump, a strange star or dwarf, each with a nuclear crust, could have been formed.

For many years only rather vague tests of the theoretical mass–radius relationship of white dwarfs were possible. Recently, however, the quality and quantity of observational data on the mass–radius relation of white dwarfs has been reanalyzed and profoundly improved by the availability of Hipparcos parallax measurements for several white dwarfs [262]. In that work Hipparcos parallaxes were used to deduce luminosity radii for ten white dwarfs in visual binaries of common systems with proper motion as well as eleven field white dwarfs. Since that time, complementary follow-up HST observations have been made [263,264] to better determine the spectroscopy for Procyon B and pulsation of G226-29. Procyon B at first appeared as a rather compact star which, however, was later confirmed to lie on the normal mass–radius relation line of white dwarfs. Stars such as Sirius B and 40 Erin B fall nicely on the expected mass–radius relation line too. Several other stars from this sample (e.g. GD 140, EG 21, EG 50, G181-B5B, GD 279, WD2007-303, G238-44), however, appear to be unusually compact and thus could be strange dwarf candidates [265].

6. Neutrino emission and stellar cooling

The detection of thermal photons from the surfaces of neutron stars via x-ray observatories serves as the principal window on the properties of such objects. The surface temperatures of neutron stars are derivable from the measured photon flux and spectrum. The predominant cooling mechanism of hot (temperatures of several $\sim 10^{10}$ K) newly formed neutron stars immediately after formation is neutrino emission. Immediately after the birth of a (proto-) neutron star in a supernova explosion, neutrinos are trapped inside the star because their mean free paths are shorter than the stellar radius. About ten seconds after birth most of the neutrinos have left the star by diffusion. As shown in [266–268] the possible presence of quark matter in the core of a neutron star could modify the diffusion rate slightly. Depending on distance and stellar mass, the neutrino bursts will be detectable

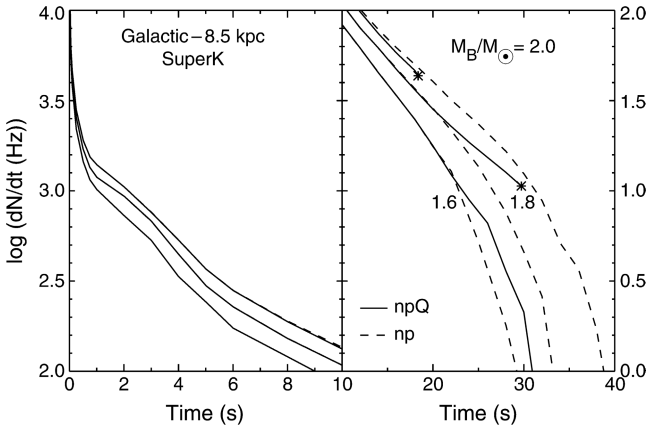

Fig. 39. A comparison of $\bar{\nu}_e$ count rates expected in SuperK from a proto-neutron star containing either np or $np + Q$ matter [270]. Figure reprinted with permission from J.A. Pons et al., Phys. Rev. Lett. 86 (2001) 5223. © 2001 by the American Physical Society.

by terrestrial neutrino detectors such as SuperK, IMB, Kamioka, SNO, and UNO [269]. The $\bar{\nu}_e$ count rates expected for SuperK from proto-neutron stars containing either only nucleons (np) or nucleons plus quark matter ($np + Q$) are shown in Fig. 39, where the left panel shows times less than 10 s, while the right panel shows times greater than 10 s. Fig. 40 shows the total neutrino luminosity for proto-neutron stars containing quark matter in their centers. The shaded bands illustrate the limiting luminosities corresponding to a count rate of 0.2 Hz, assuming a supernova distance of 50 kpc for IMB and Kamioka, and 8.5 kpc for SNO and SuperK. The widths of the shaded regions represent uncertainties in the average neutrino energy from the use of a diffusion scheme for neutrino transport (for details, see Refs. [270,271]). Observable effects of quarks only become apparent for stars older than 10 to 20 s. Sufficiently massive stars containing negatively charged, strongly interacting particles (such as quarks, but also including hyperons and kaon condensates) may collapse to black holes during the first minute of evolution. Since the neutrino flux vanishes when a black hole forms, this would constitute an obvious signal that quarks (or other types of strange matter) have appeared. The collapse timescales for stars containing quarks are predicted to be intermediate between those for stars containing hyperons and kaon condensates.

A few hours after birth, the internal neutron star temperature has already dropped to $\sim 10^9$ K. The cooling of the star is primarily dependent for the next several thousand years on the neutrino emissivity of the core's composition. Photon emission overtakes neutrinos only when the internal temperature has fallen to $\sim 10^8$ K, with a corresponding surface temperature roughly two orders of magnitude smaller. Being sensitive to the nuclear equation of state adopted, the neutron star mass, the assumed magnetic field strength, the possible existence of superfluidity, meson condensates, and quark matter, theoretical cooling calculations provide most valuable information about the interior matter and neutron star structure. The thermal evolution of a neutron star also yields information

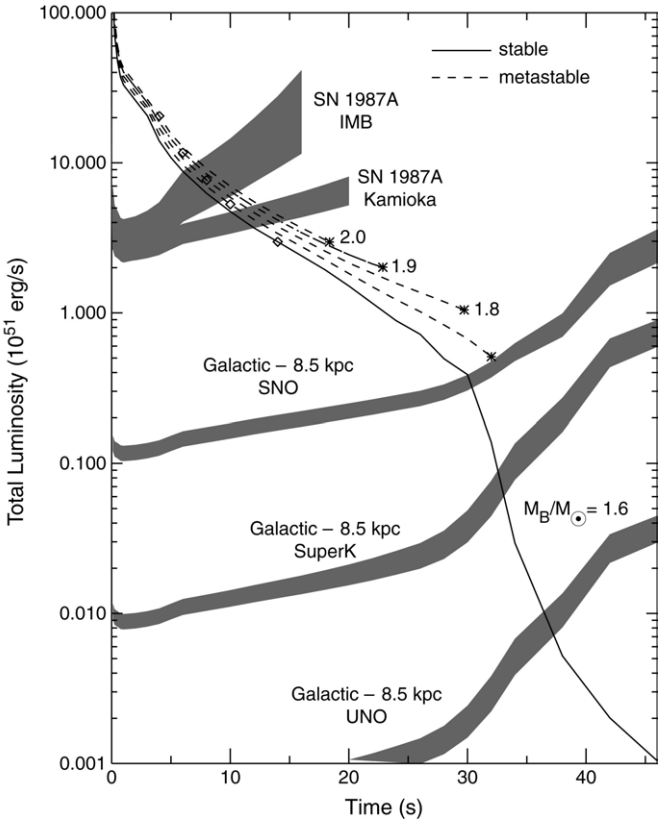

Fig. 40. Total neutrino luminosity for proto-neutron stars made of nucleons and quarks [270]. Figure reprinted with permission from J.A. Pons et al., Phys. Rev. Lett. 86 (2001) 5223.

about such temperature sensitive properties as transport coefficients, transition to superfluid states, crust solidification, and internal pulsar heating mechanisms such as frictional dissipation at the crust–superfluid interfaces [272]. In general, the possible existence of meson condensates and (certain phases of) quark matter would enhance the neutrino emissivity from the core, leading to a more rapid early cooling. An overview of processes of neutrino emission from the core and crust of a neutron star is given in Table 6. Superfluidity of nucleons, on the other hand, has the opposite effect on cooling. Quantitative constraints on cooling have been hampered by the relatively small number of young pulsars known, the complication that several of them also display non-thermal, beamed x-ray emission from their magnetospheres, and uncertainties in distance and interstellar absorption. Table 7 summarizes the temperatures of a collection of neutron stars. To compare the observations with theory, one needs mainly the neutron star effective temperatures T_s and ages τ, which are compiled in Table 7 for a representative collection of neutron stars. The thermal photon luminosity in the local reference frame of the star is given by $L_\gamma = 4\pi R^2 \sigma T_s^4$ with σ the

Table 6
Overview of neutrino emitting processes relevant for neutron star cooling [1]

Name	Processes	Emissivity	Efficiency
Modified Urca	$n+n \to n+p+e^- + \bar{\nu}_e$ $n+p+e^- \to n+n+\nu_e$	$\sim 10^{20} T_9^8$	slow
Direct Urca	$n \to p+e^- + \bar{\nu}_e$ $p+e^- \to n+\nu_e$	$\sim 10^{27} T_9^6$	fast
Quark modified Urca	$d+u+e^- \to d+d+\nu_e$ $u+u+e^- \to u+d+\nu_e$ $d+u+e^- \to d+s+\nu_e$ $u+u+e^- \to u+s+\nu_e$	$\sim 10^{20} T_9^8$	slow
Quark direct Urca	$d \to u+e^- + \bar{\nu}_e$ $u+e^- \to d+\nu_e$ $s \to u+e^- + \bar{\nu}_e$ $u+e^- \to s+\nu_e$	$\sim 10^{26} T_9^6$	fast
π^- condensate	$n+ <\pi^-> \to n+e^- + \bar{\nu}_e$	$\sim 10^{26} T_9^6$	fast
K^- condensate	$n+ <K^-> \to n+e^- + \bar{\nu}_e$	$\sim 10^{26} T_9^6$	fast
Quark bremsstrahlung	$Q_1+Q_2 \to Q_1+Q_2+\nu+\bar{\nu}$	$\sim 10^{20} T_9^8$	slow
Core bremsstrahlung	$n+n \to n+n+\nu_e+\bar{\nu}_e$ $n+p \to n+p+\nu_e+\bar{\nu}_e$ $e^-+p \to e^-+p+\nu_e+\bar{\nu}_e$	$\sim 10^{19} T_9^8$	slow
Crust bremsstrahlung	$e^- + (A,Z) \to e^- + (A,Z)$ $+\nu_e + \bar{\nu}_e$		slow

Stefan–Boltzmann constant. The apparent (red-shifted) effective surface temperature T_s^∞ and luminosity L_γ^∞, as detected by a distant observer, are given by

$$T_s^\infty = T_s\sqrt{1-R_s/R} \quad \text{and} \quad L_\gamma^\infty = 4\pi (R^\infty)^2 \sigma (T_s^\infty)^4 = L_\gamma (1-R_s/R), \qquad (116)$$

where $R_s = 2M = 2.95\, M/M_\odot$ km is the Schwarzschild radius. The coordinate radius R is connected to the apparent radius according to Eq. (108).

As already mentioned in Section 5.2.4, recent Chandra x-ray observations have identified pulsar PSR 0205 + 6449 at the center of the young Crab-like supernova remnant 3C58. Historical evidence suggests an association of the remnant with supernova SN 1181, which makes 3C58 younger than the Crab (see Table 7). The Chandra observation indicates that the thermal component must be very small, since the radiation is nearly completely fitted by a power-law spectrum [211]. The temperature of a possible residual thermal component is thereby limited to an effective black-body value of $T^\infty < 95$ eV (surface temperature of <6.0334) [211] which, as can be seen from Fig. 41, falls well below predictions of standard cooling calculations [211]. As pointed out by Prakash et al. [269], this upper limit can be fitted with standard neutrino cooling (such as $n+n \to n+p+\mathrm{e}^- + \bar{\nu}_e$) plus pair breaking and formation, but the luminosity and ages of other neutron stars cannot be simultaneously fitted using the same equation of state [293,294] which has the interesting consequence that more exotic, rapid cooling processes may exist in the core of PSR 0205 + 6449. Physical processes which would enable such a rapid drop in temperature range from the presence of meson condensates [184,295], to quark matter

Table 7
Surface temperatures of neutron stars at infinite distances from the stars

Source	P (ms)	$\log_{10}\ \tau$ (y)	$\log_{10}\ T_s^\infty$ (K)	Refs.
B1706–44	102.45	4.23	$5.91^{+0.01}_{-0.23}$	[273]
B1823–13	101.45	4.33	6.01 ± 0.02	[274]
2334 + 61	495.24	4.61	$5.92^{+0.15}_{-0.09}$	[275]
B0531 + 21 (Crab pulsar)	33.40	2.97	< 6.3	[276]
B1509–58 (MSH 15–52)	150.23	3.19	6.11 ± 0.1	[277,278]
0540–69	50.37	3.22	$6.77^{+0.03}_{-0.04}$	[279]
1951 + 32 (CTB 80)	39.53	5.02	$6.14^{+0.03}_{-0.05}$	[280]
1929 + 10	226.51	6.49	5.52	[281,282]
0950 + 08	253.06	7.24	$4.93^{+0.07}_{-0.05}$	[283]
J0437–47	5.75	8.88	5.36 ± 0.1	[284]
0833–45 (Vela pulsar)	89.29	4.05	6.24 ± 0.03	[285]
0656 + 14	384.87	5.05	5.98 ± 0.05	[286]
0630 + 18 (Geminga)	237.09	5.53	$5.75^{+0.05}_{-0.08}$	[287]
B1055–52	197.10	5.73	$5.90^{+0.06}_{-0.12}$	[288]
J0205 + 6449 (3C58)	65.86	2.91	<6.04	[211]
J0822–4300	not known	3.3–3.7	6.20–6.28	[289]
1E 1207.4–5209	424.13	$\gtrsim 3.85$	6.04–6.18	[290]
J1856.4–3754	$\sim$220	5.7	<5.7	[291]
J0720.4–3125	8391.11	$\sim$6.11	$\sim$5.7	[292]

τ denotes the age of the star.

[38,296,297], to the direct Urca process [298]. (For a very recent overview on neutron star cooling, see Ref. [293].)

Before the discovery of color superconductivity of quark matter, it was believed that depending on the density of electrons in quark matter, the temperature of quark stars could drop much more rapidly than for neutron stars [1,299,300]. The density of electrons is crucial since the fast quark direct Urca processes (see Table 6),

$$d \to u + e^- + \bar{\nu}_e,\ u + e^- \to d + \nu_e,\ s \to u + e^- + \bar{\nu}_e,\ u + e^- \to s + \nu_e, \quad (117)$$

are only possible if the electron Fermi momentum in quark matter is sufficiently high that energy and momentum conservation in the above reactions is guaranteed. If the electron Fermi momentum is too small for this to happen, a bystander quark is needed to ensure energy and momentum conservation in the scattering process. The emissivity in the latter case is considerably smaller than the emissivities associated with the direct Urca processes in (117), because of the different phase spaces associated with two-quark scattering and quark decay. If the electron fraction in quark matter vanishes entirely, both the quark direct and the quark modified Urca processes become unimportant. The neutrino emission is then entirely dominated by bremsstrahlung,

$$Q_1 + Q_2 \longrightarrow Q_1 + Q_2 + \nu + \bar{\nu}, \quad (118)$$

where Q_1, Q_2 denote any pair of quark flavors. In this case quark star cooling would proceed rather slowly, at about the same rate as cooling of conventional neutron stars

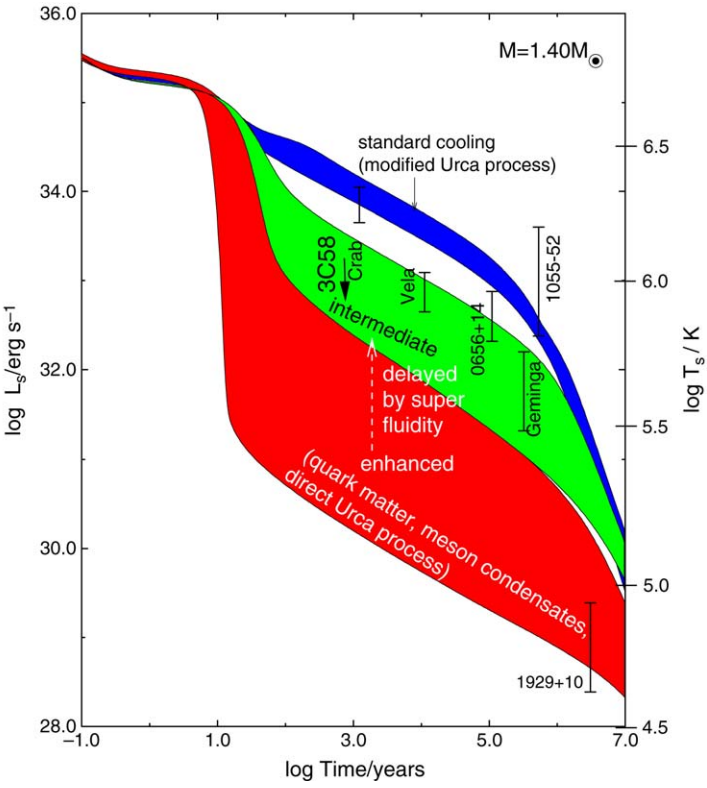

Fig. 41. Cooling behavior of a $1.4M_{\odot}$ neutron star for competing assumptions about the properties of superdense matter. Three distinct cooling scenarios, referred to as 'standard', 'intermediate', and 'enhanced', can be distinguished. The band-like structures reflect the uncertainties inherent in the equation of state of superdense matter [1].

[1,299,300]. The same would be the case if quark matter were to be superfluid with gaps on the order of a few MeV, as described in the paper by Bailin and Love [301,302]. The neutrino emissivities would then be suppressed by a factor of $\exp(-\Delta/T)$, with Δ the gap energy.

The situation is more complicated if quark matter forms a color superconductor [24]. If, as in the CFL phase, all quarks have a gap $\Delta \gg T$, then both the heat capacity C_V and neutrino luminosity L_ν are suppressed by $\sim\exp(-\Delta/T)$ which would render quarks in the centers of compact stars invisible. Vanishingly small quark gaps, on the other hand, would lead to cooling behaviors indistinguishable from those of ordinary neutron stars made of either nucleons or nucleons and hyperons. In Ref. [303], the rates of photon and neutrino emission from the decay of photons and Nambu–Goldstone (NG) bosons associated with the spontaneous breaking of baryon number, $U(1)_B$, in the CFL phase were calculated. The emission rates were found to be very small, so these emissions would be inefficient for core cooling of neutron stars containing quark matter in the CFL phase, rendering quark pairing in the CFL phase invisible to telescopes. This finding is in accordance with the

quantitative determination of the mean free paths and thermal conductivities of photons (γ) and NG bosons (ϕ) in the CFL phase performed in [304]. The total conductivity associated with these particles was found to be $\kappa_{\rm CFL} = \kappa_\phi + \kappa_\gamma \simeq (2\pi^2/9)T^3R_0$ which can be conveniently written as

$$\kappa_{\rm CFL} \simeq 1.2 \times 10^{32} (T/{\rm MeV})^3 (R_0/{\rm km}) \ {\rm erg\ cm^{-1}\ s^{-1}\ K^{-1}}, \tag{119}$$

where R_0 is the radius of the quark matter core. This expression reveals that the thermal conductivity of the CFL phase from photons and NG bosons is many orders of magnitude larger than the thermal conductivity of regular nuclear matter in a neutron star. The cooling of the quark matter core in the center of a compact star thus arises primarily from the heat flux across the surface of direct contact with the nuclear matter enveloping the CFL quark matter core. Since the thermal conductivity of the neighboring layer is also high, the entire interior of the star should be nearly isothermal [304]. The results in Ref. [304] confirm that the cooling time for neutron stars with CFL quark matter cores is similar to that of conventional neutron stars.

Finally we mention briefly the cooling behavior of compact stars hiding color superconducting 2SC quark matter in their cores. The cooling of such stars is complicated by the fact that up and down quarks may pair with a gap $\Delta \sim 100$ MeV that is orders of magnitude larger than the stellar temperature, $\lesssim$1 MeV, and are therefore inert with respect to the star's temperature evolution. In contrast to the CFL phase, where diquark condensation produces gaps for quarks of all three flavors and colors, there exist quark pairing channels that lead to weak pairing with gaps on the order of several keV to about 1 MeV, which is of the same order of magnitude as the star's temperature. These quarks may thus not pair but, instead, may radiate neutrinos rapidly via the quark direct Urca process shown in Table 6. If this is the case, the 2SC quark matter core will cool rapidly and determine the cooling history of the star [24,297]. Examples of cooling curves of neutron stars containing quark matter in the 2SC phase are shown in Figs. 42 and 43 for different star masses. A quark gap of 1 MeV, as chosen in Fig. 42, leads to too slow a cooling, while a reduced gap of 50 keV reproduces the observed data quite well.

7. Signals of quark matter in rotating neutron stars

In this section we explore possible signals of quark deconfinement in neutron stars, assuming that the densities in the centers of such objects are high enough that quark deconfinement occurs. A convincing discovery of the kinds of signals described in this section could indicate that strange quark matter is not absolutely stable, ruling out the absolute stability of strange quark matter and the existence of strange quark stars, since it is impossible for (quark hybrid) neutron stars and strange quark stars to coexist stably. The signals described below require rather pronounced modifications of the equation of state caused by quark confinement and depend on the rate at which the mixed phase of quarks and hadrons gives way to pure quark matter. In addition great care is to be taken as regards the numerical modeling [305] of rotating stars as well as the properties of the nuclear crust [306]. We shall begin our discussion with isolated rotating neutron stars, which spin down because of the loss of rotational energy caused by the emission

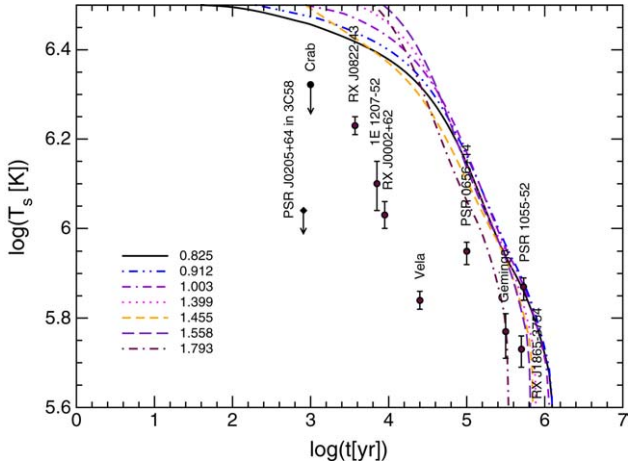

Fig. 42. Cooling curves of 2SC quark hybrid stars for a quark pairing gap of 1 MeV. (From Ref. [297].)

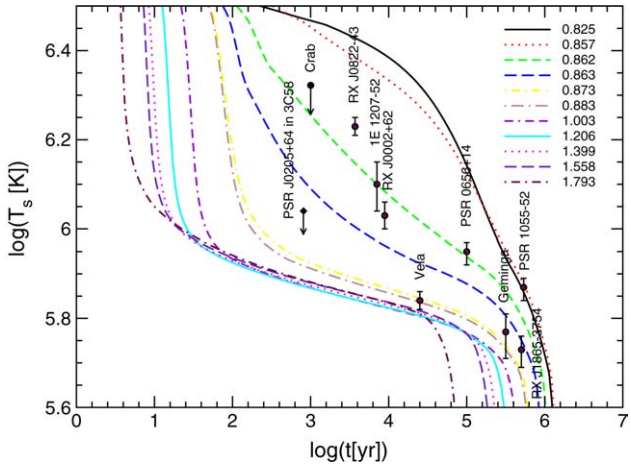

Fig. 43. The same as Fig. 42, but for a quark pairing gap of 50 keV. (From Ref. [297].)

of an electron–positron wind from the star and by the emission of electromagnetic dipole radiation. This is followed by a discussion of accreting neutron stars in binary systems. The spin period of such neutron stars increases over time. The densities inside both neutron stars that are spinning down as well as neutron stars that are being spun up by mass accretion changes dramatically, which could lead to signals of quark matter in observable data.

7.1. Isolated pulsars

It is known from Figs. 21 and 22 that the weakening of the centrifugal force accompanied by the slowing down of a rotating neutron star causes a significant increase

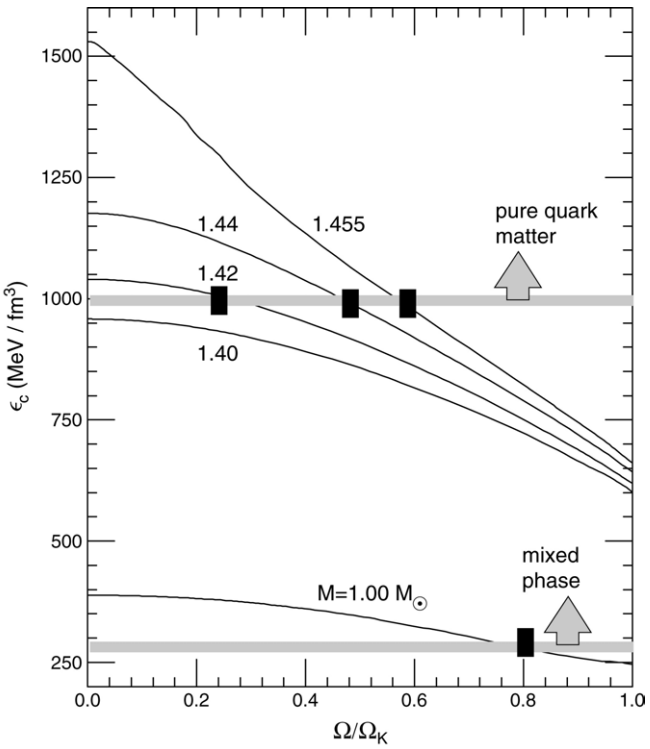

Fig. 44. Central star density versus rotational frequency for neutron stars of different masses. The vertical bars mark the density where quark matter is produced. (From Ref. [1].)

of its central density. From Fig. 21, for instance, one reads off that the central density of a neutron star model of mass $M = 1.42 M_\odot$, computed for a soft equation of state (G_{B180}^{K300} in the present case [307]), increases from about 450 MeV/fm^3 for rotation at the mass shedding frequency, Ω_K, to more than 1500 MeV/fm^3 for zero rotation, which is a ∼66% effect. Such dramatic changes in the interior density of a neutron star driven by changes in frequency modify the stellar composition considerably. If the mass and initial rotational frequency of a pulsar are such that during its slowing down phase the interior density rises from below to above the critical density for the quark–hadron phase transition, first at the center where the density is highest (Figs. 44–46 through 49) and then in a region expanding in the radial outward direction away from the star's center, matter will be gradually converted from the relatively incompressible nuclear matter phase to the more compressible quark matter phase, as shown in Fig. 50. The tremendous weight of the overlying layers of nuclear matter tends to compress the quark matter core, which causes the entire star to shrink on a length scale of several hundred meters, as shown in Figs. 48 through 47. The mass concentration in the core will be further enhanced by the increasing gravitational attraction of the quark core on the overlying nuclear matter. The moment of inertia thus decreases anomalously with decreasing rotational frequency as the

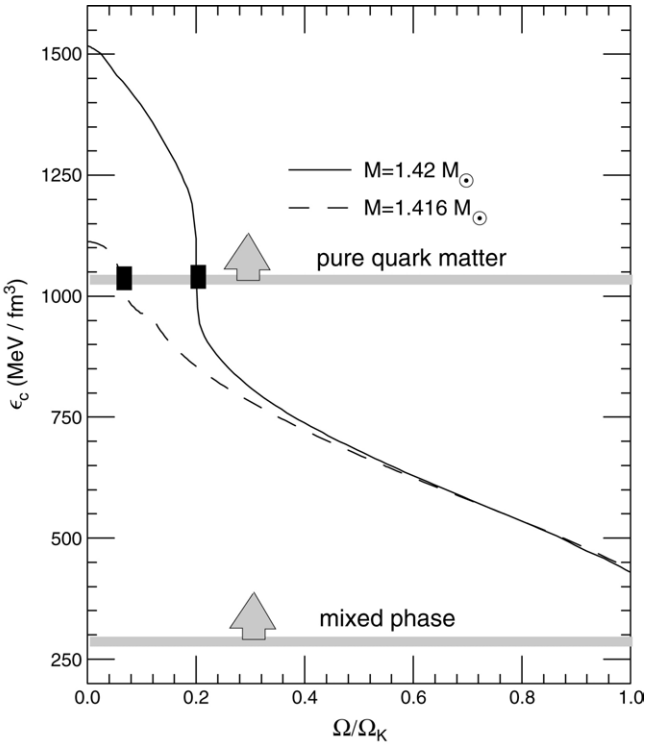

Fig. 45. The same as Fig. 44, but for equation of state G^{K300}_{B180}. (From Ref. [1].)

new phase slowly engulfs a growing fraction of the star [307], as can be seem from Figs. 51 and 52. Fig. 51 shows the moment of inertia, I, computed self-consistently from Eq. (93) for several sample stars having the same baryon number but different internal constitutions [308]. The curve labeled $M = 1.420 M_\odot$, computed for G^{K300}_{B180}, shows the moment of inertia of the quark hybrid star of Figs. 48 and 49. The other curves correspond to a standard hyperon star (n, p, H) constructed for G^{K240}_{M78} and a standard neutron star (n, p) where hyperons (H) have been ignored purposely. In accordance with what has been said just above, the smaller the quark matter cores which are being built up in their centers, the less pronounced the shrinkage of quark hybrid stars driven by the development of quark matter cores. Correspondingly, the dip in I weakens with decreasing star mass, as shown in Fig. 51 for several sample masses in the range $1.416 \leq M/M_\odot \leq 1.420$. Model calculations indicate that very strong reductions of I, such as are found for the $1.421 M_\odot$ model, for instance, may hardly be obtainable for physical scenarios other than the hypothetical quark–hadron phase transition [1]. Hyperon populations alone, as calculated in Ref. [14] (Figs. 51, 53 and 54), for instance, appear to modify the equation of state far too little to cause significant changes in I. Nevertheless, there are models for the equation of state of hyperonic matter which also can strongly affect the spin evolution of isolated neutron stars [309,310]. As shown in these references, depending on the nucleon–hyperon interaction

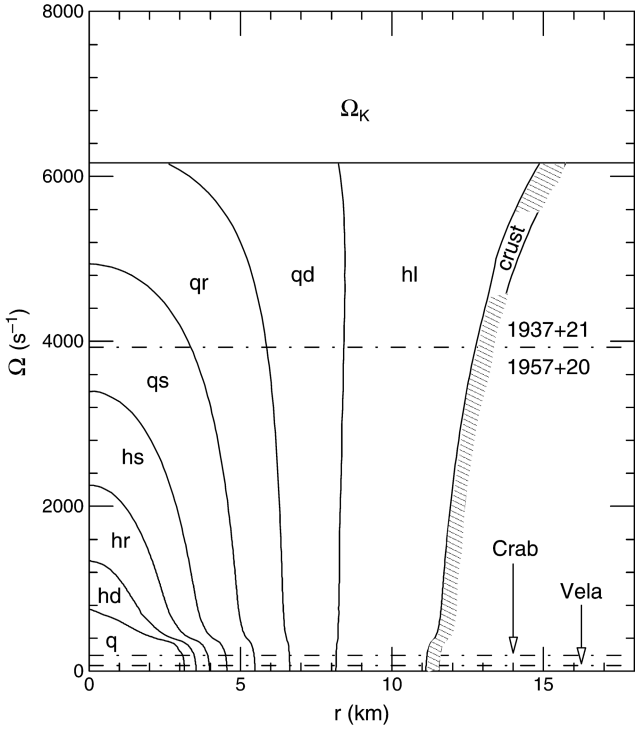

Fig. 46. The frequency dependence of quark structures in the equatorial star direction for equation of state G^{K300}_{B180} and a non-rotating star mass of $1.416 M_\odot$ [1].

and the hyperon–hyperon interaction in matter, hyperons can even cause back-bending. The back-bending episode can terminate either unstably or through a stable continuous transition to a standard spin down behavior. The observation of back-bending in the timing behavior of isolated pulsars, or of spin clustering on accreting neutron stars discussed in Section 7.2, is therefore not unambiguous evidence for quark deconfinement. It is also explored to what extent back-bending may be caused by other competing particle processes (cf. Figs. 1 and 21).

The decrease of the moment of inertia caused by the quark–hadron phase transition, shown in Fig. 51, is superimposed on the response of the stellar shape to a decreasing centrifugal force as the star spins down due to the loss of rotational energy. In order to conserve angular momentum not carried off by particle radiation from the star, the deceleration rate $\dot{\Omega}(<0)$ must respond correspondingly by decreasing in absolute magnitude. More than that, $\dot{\Omega}$ may even change sign, as shown in Fig. 52 [307], which carries the important astrophysical information that an isolated pulsar may spin up during a certain period of its stellar evolution. The situation may be compared with an ice skater who spins up upon contraction of the arms before air resistance and friction of the skate on the ice re-establishes spin down again. Such an anomalous decrease of I is analogous to the ‘back-bending’ phenomenon known from nuclear physics, in which case the moment

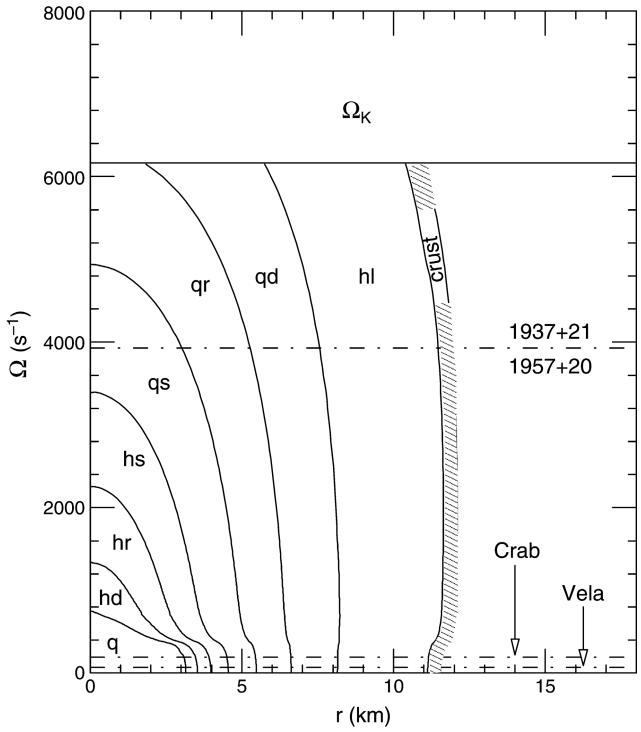

Fig. 47. The same as Fig. 46, but in the polar direction [1].

of inertia of an atomic nucleus changes anomalously because of a change in phase from a nucleon spin-aligned state at high angular momentum to a pair-correlated superfluid phase at low angular momentum. In the nuclear physics case, the back-bending in the rotational bands of nuclei was predicted by Mottelson and Valatin [311] and then observed years later by Stephens and Simon [312], and Johnson, Ride, and Hjorth [313]. For neutron stars, the stellar back-bending of I is shown in Fig. 52. Stars evolving from 'b' to 'a' are rotationally accelerated ($\dot{\Omega} > 0$), while stars evolving from 'a' to 'b', which could be part of the evolutionary track of pulsars accreting matter from companions (see Section 7.2), are rotationally decelerated ($\dot{\Omega} < 0$). As we shall see next, the structure in the moment of inertia and, specifically, the back-bending phenomenon dramatically modifies the timing structure of pulsar spin down, rendering the observation of quark matter in neutron stars accessible to radio astronomy. Pulsars are identified by their periodic signal, believed to be due to a strong magnetic field fixed in the star and oriented at an angle from the rotation axis. The period of the signal is therefore that of the rotation of the star. The angular velocity of rotation decreases slowly but measurably over time, and usually the first and occasionally the second time derivative can also be measured. Various energy loss mechanisms could be at play such as the magnetic dipole radiation, part of which is detected on each revolution, as well as other losses such as ejection of charged particles [314]. If one assume that pulsar slow down is governed by a single mechanism, or several

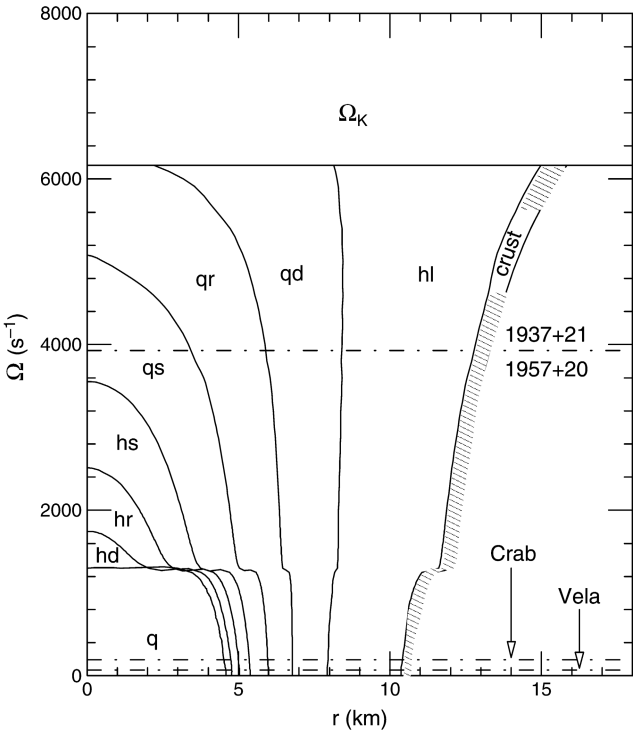

Fig. 48. The frequency dependence of the quark structure in the equatorial neutron star direction computed for G_{B180}^{K300} and a non-rotating star mass of $1.42 M_{\odot}$ [308].

mechanisms having the same power law, the energy balance equation can then be written in the form

$$\frac{\mathrm{d}E}{\mathrm{d}t} = \frac{\mathrm{d}}{\mathrm{d}t}\left(\frac{1}{2} I(\Omega)\Omega^2\right) = -C\Omega^{n+1}. \tag{120}$$

In the case of magnetic dipole radiation, the constant C is equal to $C = \frac{2}{3}\mu^2 \sin^2\alpha$ where μ denotes the star's magnetic dipole moment. The quantity n in Eq. (120) is called the braking index. It is $n = 3$ if I is kept constant during spin up (down). If, as is customary, the star's angular velocity Ω is regarded as the only time dependent quantity, one obtains the usual formula for the rate of change of pulsar frequency, given by

$$\dot{\Omega} = -K\Omega^n, \tag{121}$$

with $K = C/I$ a constant. With the braking formula (121) one can define the spin down age of a pulsar given by

$$\tau = -(n-1)^{-1}\Omega/\dot{\Omega}, \tag{122}$$

with $n = 3$ for energy loss governed by magnetic dipole radiation. However, the moment of inertia is not constant in time but responds to changes in rotational frequency, as shown

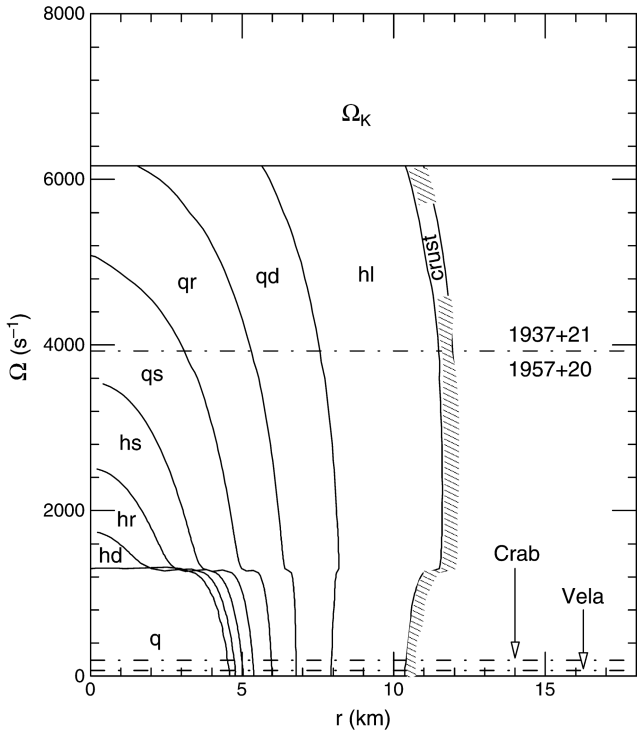

Fig. 49. The same as Fig. 48, but in the polar direction [308].

in Figs. 51 and 52, more or less in accord with the softness or stiffness of the equation of state and according to whether the stellar mass is small or large. This response changes the value of the braking index in a frequency dependent manner, that is $n = n(\Omega)$, even if the sole energy loss mechanism were pure magnetic dipolar, as expressed in Eq. (120). Thus during any epoch of observation, the braking index will be measured to be different from it canonical value $n = 3$ by a certain amount. How much less depends, for any given pulsar, on its rotational frequency and, for different pulsars of the same frequency, on their mass and on their internal constitution [1,186,316–318]. When the frequency response of the moment of inertia is taken into account, Eq. (121) is replaced with [1,307]

$$\dot{\Omega} = -2C\Omega^n(2I + \Omega(\mathrm{d}I/\mathrm{d}\Omega))^{-1}. \tag{123}$$

This explicitly shows that the frequency dependence of $\dot{\Omega}$ corresponding to any mechanism that absorbs (or deposits) rotational energy cannot be a simple power law as given in Eq. (121) (with K a constant). It must depend on the mass and internal constitution of the star through the response of the moment of inertia to rotation as expressed in (123). Eq. (123) can be represented in the form of (121), but now with a frequency dependent prefactor, by evaluating

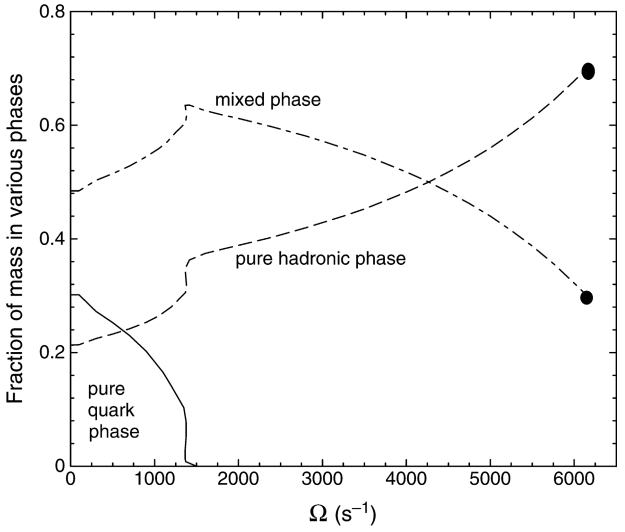

Fig. 50. The fraction of mass existing in the form of pure quark matter, pure hadronic matter, and in the mixed phase of quarks and hadrons for the star of Fig. 48. (From Ref. [1].)

$$n(\Omega) \equiv \frac{\Omega\ddot{\Omega}}{\dot{\Omega}^2} = 3 - \left(3\frac{\mathrm{d}I}{\mathrm{d}\Omega}\Omega + \frac{\mathrm{d}^2 I}{\mathrm{d}\Omega^2}\Omega^2\right)\left(2I + \frac{\mathrm{d}I}{\mathrm{d}\Omega}\Omega\right)^{-1}. \tag{124}$$

One sees that this braking index depends explicitly and implicitly on Ω. This relation reduces to the canonical expression $n = 3$ only if I is independent of frequency, which may not the case, as seen above, if there are compositional changes driven by a varying star frequency. As an example, we show in Fig. 55 the variation of the braking index with frequency for two selected quark hybrid stars of Figs. 51 and 52. For illustrational purposes we assume dipole radiation. Because of the response of the moment of inertia to quark deconfinement, the braking index deviates dramatically from the canonical value $n = 3$ at rotational frequencies where quark deconfinement leads to the build-up of pure quark matter cores in the centers of these stars. Such anomalies in $n(\Omega)$ are not obtained for conventional neutron stars or hyperon stars because their moments of inertia increase smoothly with Ω, as known from Fig. 51. The observation of such an anomaly in the timing structure of pulsar spin down could thus be interpreted as a signal of quark deconfinement in the centers of pulsars. Of course, because of the extremely small temporal change of a pulsar's rotational period, one cannot measure the shape of the curve which is in fact not necessary. Just a single anomalous value of n that differed significantly from the canonical value of $n = 3$ would suffice [307,319].

Carried over to the observed pulsar data for Ω and $\dot{\Omega}$, it appears that the change in centrifugal force over the life of a canonical, slowly rotating pulsar could eventually be too meager to span a significant change. The significant braking anomaly, therefore, could be restricted to millisecond pulsars. For them, the phase change may occur only in such millisecond pulsars as rotate near the maximum-mass peak determined by the underlying

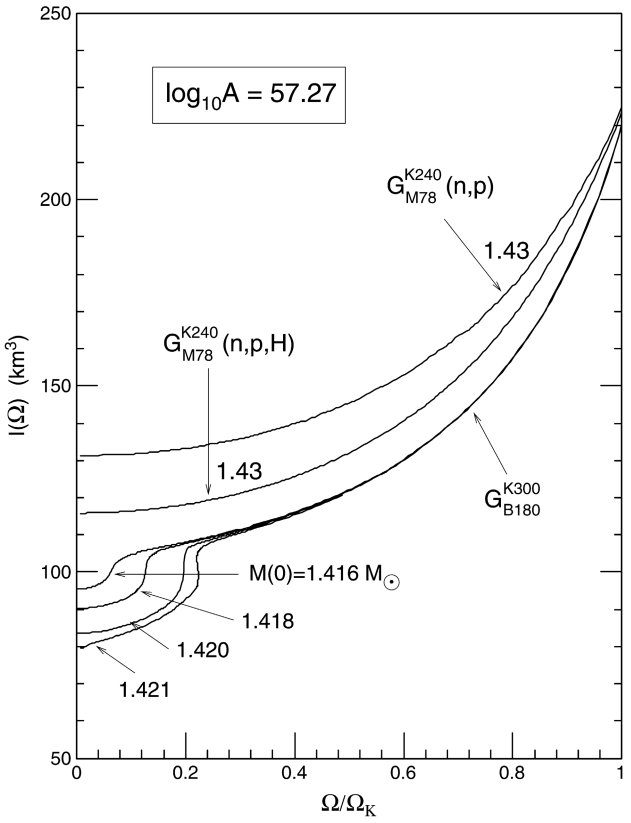

Fig. 51. Moment of inertia versus rotational frequency for neutron stars having the same baryon number, A, but different internal constitutions. The dips at low Ω's are caused by quark deconfinement [186].

equation of state. Otherwise the fraction of pure quark matter in their centers may not be sufficient to cause the required shrinkage. The phase change itself may be first (as in our example) or second order. Both orders will cause a signal as long as quark deconfinement causes a sufficient softening of the equation of state and quark matter is generated at the center of the star at a sufficiently high rate. On the observational side, a serious drawback may be that the braking indices of millisecond pulsars are very hard to measure, because of timing noise which renders the determination of $\ddot{\Omega}$ very complicated. As a final but very important point on the subject of quark deconfinement, we estimate the typical duration over which the braking index is anomalous if quark deconfinement is well pronounced, as for the quark hybrid star of mass $M(0) = 1.421 M_\odot$. The time span can be estimated from $\Delta T \simeq -\Delta\Omega/\dot{\Omega} = \Delta P/\dot{P}$, where $\Delta\Omega$ is the frequency interval of the anomaly. The range over which $n(\Omega)$ is smaller than zero and larger than six (Fig. 55) is $\Delta\Omega \approx -100$ s^{-1}, or $\Delta P \approx -2\pi\Delta\Omega/\Omega^2 \approx 3 \times 10^{-4}$ s at $\Omega = 1370$ s^{-1}. Hence, for a millisecond pulsar whose period derivative is typically $\dot{P} \simeq 10^{-19}$ one has $\Delta T \simeq 10^8$ y, as graphically illustrated in Fig. 56. The dipole age of such pulsars is about 10^9 y. So, as a rough estimate

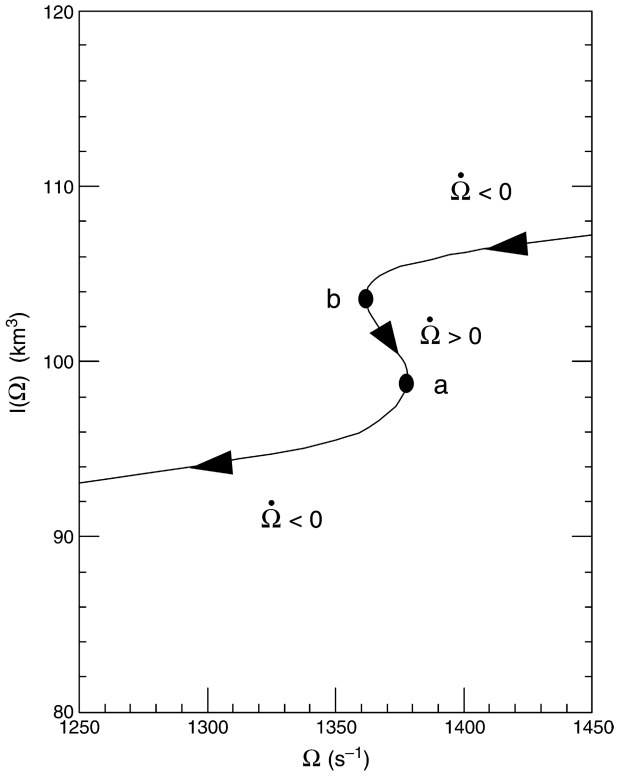

Fig. 52. Am enlargement of the lower left portion of Fig. 51 for the quark hybrid star of mass $M = 1.421 M_{\odot}$, which is characterized by a back-bending of I for frequencies between 'a' and 'b' [1,186,307].

we expect about 10% of the ∼30 currently known solitary millisecond pulsars to be in the transition epoch during which pure quark matter cores are gradually being built up in their centers. These pulsars could be signaling the ongoing process of quark deconfinement in their cores. Last but not least we note that the spin up time (region *b–a* in Fig. 52) is about $1/5$ of the time span ΔT, or about $1/50$ of the dipole age. To avoid confusion, we point out that the spin up has nothing to do with the minuscule spin ups known as pulsar glitches. In the latter case the relative change of the moment of inertia is very small, $\Delta I/I \simeq -\Delta\Omega/\Omega \simeq 10^{-6}$ or smaller, and approximates closely a continuous response of the star to changing frequency on any timescale that is large compared to the glitch and recovery interval. Excursion of such a magnitude as quoted would fall within the thickness of the line in Fig. 52.

7.2. Accreting neutron stars

The signal of quark deconfinement described in Section 7.1 is computed for isolated neutron stars, where deconfinement is driven by the gradual stellar contraction as the star spins down. The situation is reversed in neutron stars in binary systems, which experience

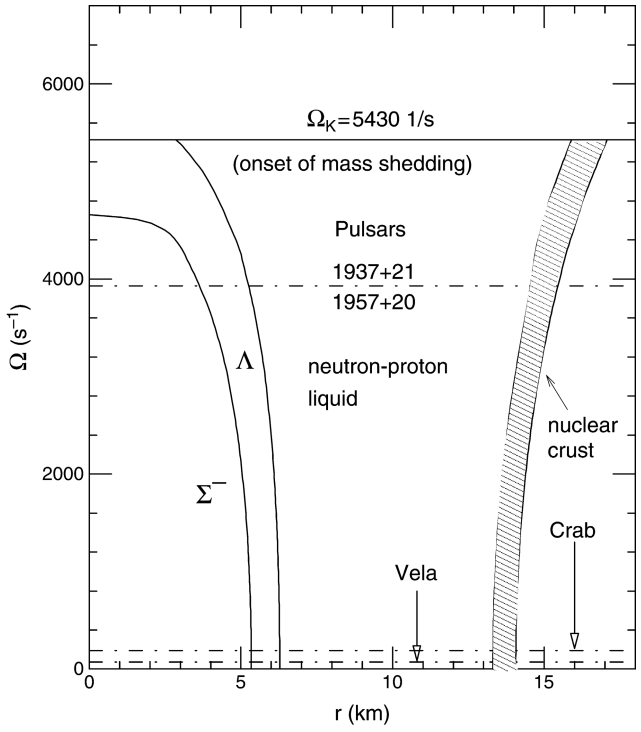

Fig. 53. The frequency dependence of hyperon thresholds in the equatorial neutron star direction computed for HV. The star's non-rotating mass is $1.40 M_\odot$ [1].

a spin up torque because of the transfer of angular momentum carried by the matter picked up by the star's magnetic field from the surrounding accretion disk [315–317,320,321]. The spin up torque causes a change in the stars' angular momentum that can be expressed as [315]

$$\mathrm{d}J/\mathrm{d}t = \dot{M}\tilde{l}(r_\mathrm{m}) - N(r_\mathrm{c}), \tag{125}$$

where $\dot{M}$ denotes the accretion rate and

$$\tilde{l}(r_\mathrm{m}) = \sqrt{M r_\mathrm{m}} \tag{126}$$

is the angular momentum added to the star per unit mass of accreted matter. The quantity N stands for the magnetic plus viscous torque term,

$$N(r_\mathrm{c}) = \kappa \mu^2 r_\mathrm{c}^{-3}, \tag{127}$$

with $\mu \equiv R^3 B$ the star's magnetic moment. The quantities r_m and r_c denote the radius of the inner edge of the accretion disk and the co-rotating radius, respectively, and are given by

$$r_\mathrm{m} = \xi r_\mathrm{A}, \qquad r_\mathrm{c} = (M\Omega^{-2})^{1/3}, \tag{128}$$

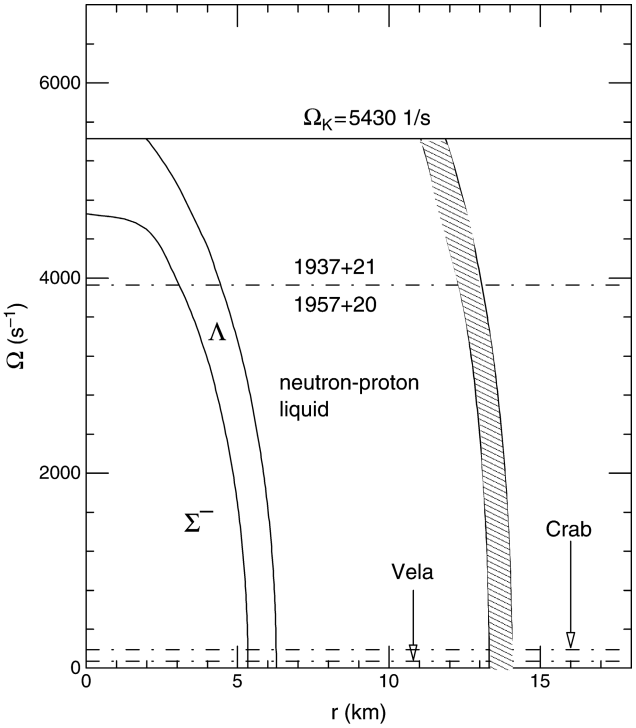

Fig. 54. The same as Fig. 53, but in the polar direction [1].

with ($\xi \sim 1$). The Alfvén radius r_A is defined by

$$r_A = (\mu^4(2M\dot{M}^2)^{-1})^{1/7}. \tag{129}$$

Accretion will be inhibited by a centrifugal barrier if the neutron star's magnetosphere rotates faster than the Kepler frequency at the magnetosphere. Hence $r_m < r_c$; otherwise accretion onto the star will cease. The rate of change of a star's angular frequency Ω then follows from Eq. (125) as

$$I(t)\frac{d\Omega(t)}{dt} = \dot{M}\tilde{l}(t) - \Omega(t)\frac{dI(t)}{dt} - \kappa\mu(t)^2 r_c(t)^{-3}, \tag{130}$$

with the explicit time dependences as indicated. There are two terms on the right-hand side of Eq. (130) that grow linearly and quadratically with Ω. Ignoring the linear term shows that mass transfer can spin up a neutron star to an equilibrium period of [226]

$$P_{eq} = 2.4\ \text{ms}\left(\frac{\dot{M}}{\dot{M}_{Edd}}\right)^{-3/7}\left(\frac{M}{M_\odot}\right)^{-5/7} R_6^{15/7} B_9^{6/7}, \tag{131}$$

where R_6 and B_9 are the star's radius and its magnetic field in units of 10^6 cm and 10^9 G, respectively. $\dot{M}_{Edd}$ in Eq. (131) denotes the maximum possible accretion rate, defined by the Eddington limit (see Eq. (110)), at which the accretion luminosity equals the luminosity

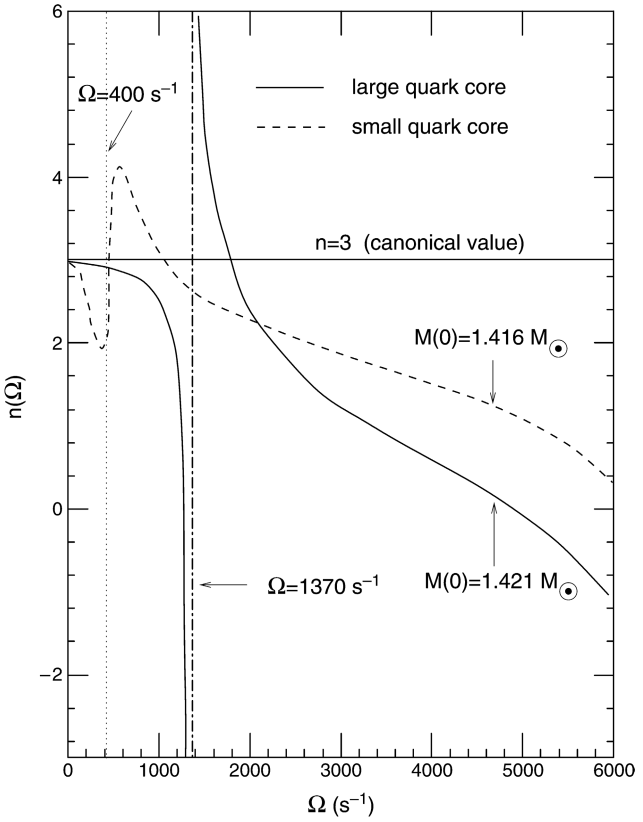

Fig. 55. The braking index, n, of quark hybrid stars of Figs. 51 and 52. The anomalies in n at $\Omega \sim 400$ s^{-1} and $\Omega \sim 1370$ s^{-1} are caused by quark deconfinement. The overall reduction of n below 3 is due to rotation. (From Ref. [1].)

at which the radiation pressure force on ionized hydrogen plasma near the star balances the gravitational acceleration force exerted by the star on the plasma. This condition leads to an Eddington accretion rate of $\dot{M}_{\rm Edd} = 1.5 \times 10^{-8} R_6 M_\odot$ y^{-1}. For a typical accretion rate of $\dot{M}_{-10} \equiv \dot{M}/(10^{-10} M_\odot$ y$^{-1})$, the Eddington rate can be expressed as $\dot{M}_{\rm Edd} = 150 R_6 \dot{M}_{-10}^{-1} \dot{M}$. The low mass x-ray binaries (LMXBs) observed with the RXTE are divided into Z sources and A(toll) sources, which accrete at rates of $\dot{M}_{-10} \sim 200$ and $\dot{M}_{-10} \sim 2$, respectively [255].

The solution of Eq. (130) in combination with the expression for the moment of inertia derived in Eq. (93) for the quark hybrid model $\rm G^{K300}_{B180}$ ($M(0) = 1.42 M_\odot$) is shown in Fig. 57. The magnetic field is assumed to evolve according to

$$B(t) = B(\infty) + (B(t=0) - B(\infty)) {\rm e}^{-t/t_{\rm d}}, \tag{132}$$

with $t = 0$ at the start of accretion, $B(t=0) = 10^{12}$ G, $B(\infty) = 10^8$ G, and $t_{\rm d} = 10^6$ y. Such a decay to an asymptotic value seems to be a feature of some treatments of the

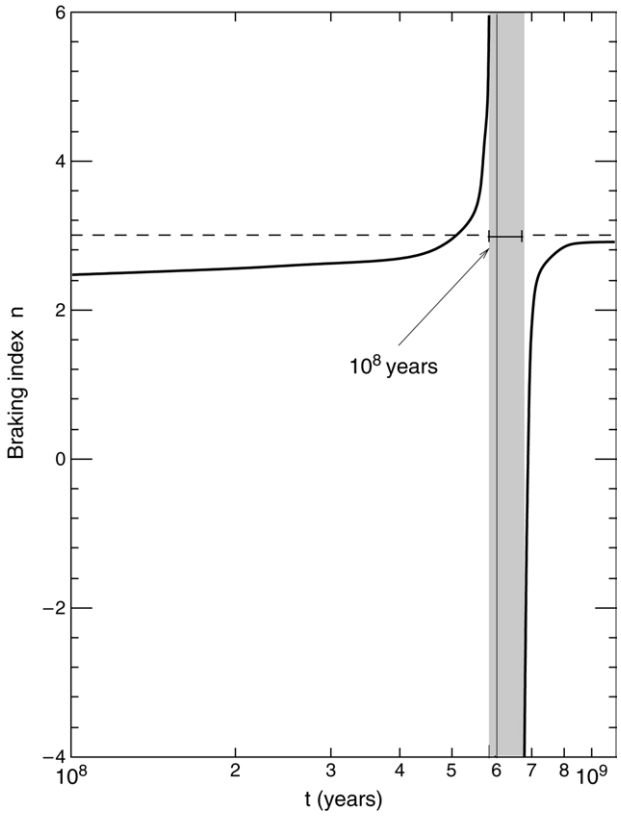

Fig. 56. Braking index versus time for the quark hybrid star of mass $M = 1.421 M_\odot$ of Fig. 55. The epoch over which n is anomalous because of quark deconfinement, $\sim 10^8$ y, is indicated by the shaded area. (From Ref. [1].)

magnetic field evolution of accreting neutron stars [322]. Moreover, it expresses the fact that canonical neutron stars have high magnetic fields, $\sim 10^{12}$ G, and millisecond pulsars have low fields of $\sim 10^8$ G. The result for the spin up of the quark hybrid stars is most striking. One sees that quark matter remains relatively dormant in the stellar core until the star has been spun up to frequencies at which the central density is about to drop below the threshold density at which quark matter is predicted to exist for this model. As known from Fig. 52, this manifests itself in a significant increase of the star's moment of inertia. The angular momentum added to a neutron star during this phase of evolution is therefore consumed by the star's expansion, inhibiting a further spin up until the entire quark matter core has been spun out of the center, leaving the star with a mixed phase of quarks and hadrons made up of hadrons and quarks surrounded by ordinary nuclear matter (see Figs. 48 and 49). Such accreters, therefore, tend to spend a much greater length of time in the critical frequency range than otherwise. There will be an anomalous number of accreters that appear near the same frequency, as shown in Fig. 58. Evidence that accreting neutron stars pile up at certain frequencies, which are well below the mass shedding

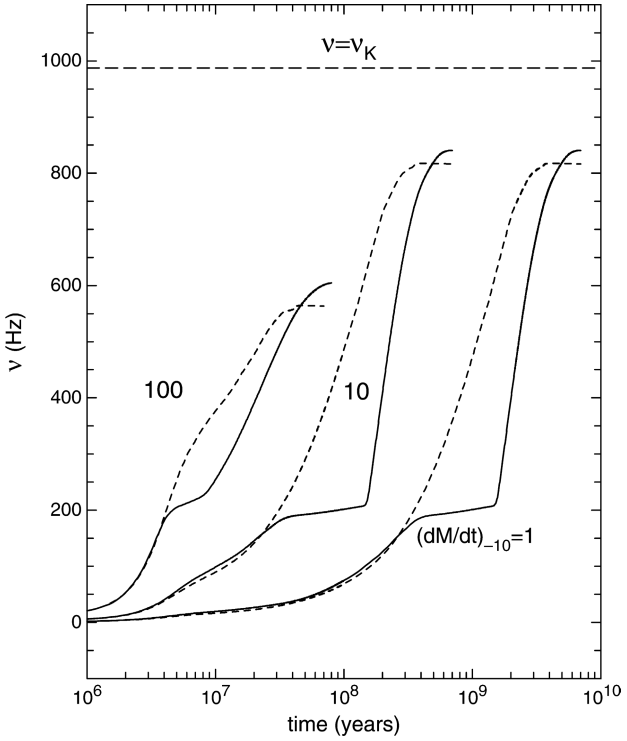

Fig. 57. Spin distribution of x-ray neutron stars. The spike in the calculated distribution corresponds to the spinout of quark matter. Otherwise the spike would be absent.

limit, is provided by the spin distribution of accreting millisecond pulsars in 57 Tuc and neutron stars in low mass x-ray binaries observed with the Rossi X-ray Timing Explorer. The proposed limiting mechanisms responsible for this behavior could be gravity-wave emission caused by the r-mode instability, or a small stellar mass quadrupole moment [324,325,331]. As shown here, quark reconfinement may be linked to this phenomenon as well [315,316,320,323].

8. Summary

The tremendous pressures in the cores of neutron stars might be able to break neutrons, protons, plus other hadronic constituents in the centers of neutron stars into their quark constituents, creating a new state of matter known as quark matter which is being sought at the most powerful colliders. If quark matter exists in the cores of neutron stars, it will be a color superconductor whose complex condensation pattern is likely to change with density inside the star. The exploration of the numerous astrophysical facets of (color superconducting) quark matter is therefore of uppermost importance and is pursued by physicists from different, complementing fields of physics. Their joint scientific efforts,

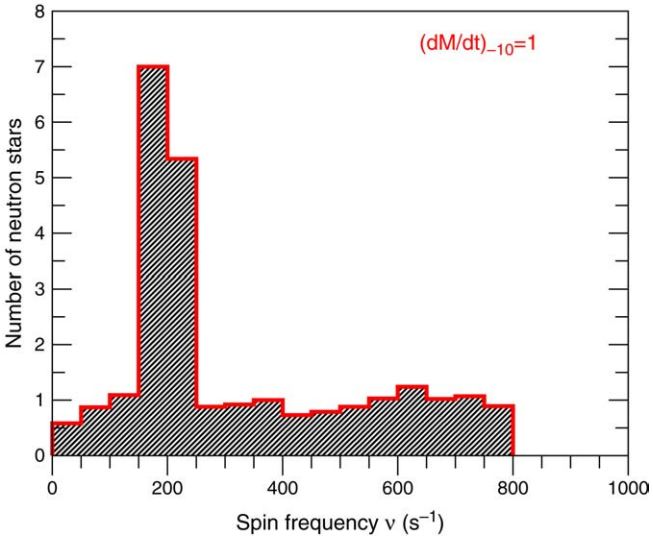

Fig. 58. The spin distribution of x-ray neutron stars. The spike in the calculated distribution (unshaded diagram) corresponds to the spin-out of quark matter. Otherwise the spike would be absent. The shaded histogram displays the observed data [315], which have been questioned recently, however. (Taken from Ref. [315].)

surveyed in this review, provide most valuable information about the phase diagram of nuclear matter at high baryon number density but low temperature, which is not accessible to relativistic heavy ion collision experiments, and may ultimately provide us with a glimpse of the kind of matter that filled our universe just milliseconds after is was born.

Acknowledgments

I thank the Institute for Nuclear Theory at the University of Washington for its hospitality and the Department of Energy for partial support during the completion of this work. Mark Alford deserves my special thanks for discussions and communications.

References

[1] F. Weber, Pulsars as Astrophysical Laboratories for Nuclear and Particle Physics, High Energy Physics, Cosmology and Gravitation Series, IOP Publishing, Bristol, Great Britain, 1999.
[2] H. Heiselberg, V. Pandharipande, Ann. Rev. Nucl. Part. Sci. 50 (2000) 481.
[3] J.M. Lattimer, M. Prakash, Astrophys. J. 550 (2001) 426.
[4] A.R. Bodmer, Phys. Rev. D 4 (1971) 1601.
[5] E. Witten, Phys. Rev. D 30 (1984) 272.
[6] H. Terazawa, INS-Report-338, INS, Univ. of Tokyo, 1979; J. Phys. Soc. Japan, 58 (1989) 3555; 58 (1989) 4388; 59 (1990) 1199.
[7] C. Alcock, E. Farhi, A.V. Olinto, Astrophys. J. 310 (1986) 261.
[8] C. Alcock, A.V. Olinto, Ann. Rev. Nucl. Part. Sci. 38 (1988) 161.
[9] J. Madsen, Lecture Notes in Physics 516 (1999) 162.
[10] N.K. Glendenning, F. Weber, Astrophys. J. 400 (1992) 647.

[11] N.K. Glendenning, Ch. Kettner, F. Weber, Astrophys. J. 450 (1995) 253.
[12] N.K. Glendenning, Ch. Kettner, F. Weber, Phys. Rev. Lett. 74 (1995) 3519.
[13] G.E. Brown, in: A. Griffin, D.W. Snoke, S. Stringari (Eds.), Bose–Einstein Condensation, Cambridge University Press, Cambridge, 1995, p. 438.
[14] N.K. Glendenning, Astrophys. J. 293 (1985) 470.
[15] N.K. Glendenning, F. Weber, S.A. Moszkowski, Phys. Rev. C 45 (1992) 844.
[16] D.D. Ivanenko, D.F. Kurdgelaidze, Astrophys. 1 (1965) 251.
[17] H. Fritzsch, M. Gell-Mann, H. Leutwyler, Phys. Lett. B 47 (1973) 365.
[18] G. Baym, S. Chin, Phys. Lett. B 62 (1976) 241.
[19] B.D. Keister, L.S. Kisslinger, Phys. Lett. B 64 (1976) 117.
[20] G. Chapline, M. Nauenberg, Phys. Rev. D 16 (1977) 450; Ann. New York Acad. Sci. 302 (1977) 191.
[21] W.B. Fechner, P.C. Joss, Nature 274 (1978) 347.
[22] N.K. Glendenning, Phys. Rev. D 46 (1992) 1274.
[23] N.K. Glendenning, Phys. Rep. 342 (2001) 393.
[24] K. Rajagopal, F. Wilczek, in: M. Shifman (Ed.), The Condensed Matter Physics of QCD, At the Frontier of Particle Physics/Handbook of QCD, World Scientific, 2001.
[25] M. Alford, Ann. Rev. Nucl. Part. Sci. 51 (2001) 131.
[26] M. Alford, K. Rajagopal, F. Wilczek, Phys. Lett. B 422 (1998) 247.
[27] R. Rapp, T Schäfer, E.V. Shuryak, M. Velkovsky, Phys. Rev. Lett. 81 (1998) 53; Ann. Physics 280 (2000) 35.
[28] C. Aubin et al., HPQCD Collaboration, First determination of the strange and light quark masses from full lattice QCD, hep-lat/0405022 (2004).
[29] K. Rajagopal, F. Wilczek, Phys. Rev. Lett. 86 (2001) 3492.
[30] P.F. Bedaque, T. Schäfer, Nucl. Phys. A 697 (2002) 802.
[31] T. Schäfer, Phys. Rev. D 62 (2000) 094007.
[32] M. Alford, S. Reddy, Phys. Rev. D 67 (2003) 074024.
[33] M. Alford, J. Phys. G 30 (2004) S441.
[34] K. Rajagopal, Acta Phys. Polon. B 31 (2000) 3021.
[35] M. Alford, J.A. Bowers, K. Rajagopal, Phys. Rev. D 63 (2001) 074016.
[36] M. Alford, J.A. Bowers, K. Rajagopal, J. Phys. G 27 (2001) 541.
[37] D. Blaschke, D.M. Sedrakian, K.M. Shahabasyan, Astron. Astrophys. 350 (1999) L47.
[38] D. Blaschke, H. Grigorian, D.N. Voskresensky, Astron. Astrophys. 368 (2001) 561.
[39] The AMS home page is, http://ams.cern.ch.
[40] Information about ECCO can be found at, http://ultraman.berkeley.edu.
[41] J. Madsen, Phys. Rev. Lett. 87 (2001) 172003.
[42] J.D. Walecka, Ann. Physics. 83 (1974) 491.
[43] B.D. Serot, J.D. Walecka, Adv. Nucl. Phys. 16 (1986) 1.
[44] F. Weber, M.K. Weigel, Nucl. Phys. A 505 (1989) 779.
[45] J. Boguta, A.R. Bodmer, Nucl. Phys. A 292 (1977) 413.
[46] D.B. Kaplan, A.E. Nelson, Phys. Lett. B 175 (1986) 57;
D.B. Kaplan, A.E. Nelson, Nucl. Phys. A 479 (1988) 273.
[47] G.E. Brown, K. Kubodera, M. Rho, Phys. Lett. B 192 (1987) 273.
[48] H. Huber, F. Weber, M.K. Weigel, Phys. Rev. C 51 (1995) 1790.
[49] N.K. Glendenning, Compact Stars, Nuclear Physics, Particle Physics, and General Relativity, 2nd edition, Springer-Verlag, New York, 2000.
[50] N.K. Glendenning, S.A. Moszkowski, Phys. Rev. Lett. 67 (1991) 2414.
[51] K. Oyamatsu, K. Iida, Prog. Theor. Phys. 109 (2003) 631.
[52] H. Lenske, C. Fuchs, Phys. Lett. B 345 (1995) 355.
[53] C. Fuchs, H. Lenske, H.H. Wolter, Phys. Rev. C 52 (1995) 3043.
[54] S. Typel, H.H. Wolter, Nucl. Phys. A 656 (1999) 331.
[55] T. Nikšić, D. Vretenar, P. Finelli, P. Ring, Phys. Rev. C 66 (2002) 024306.
[56] S.F. Ban, J. Li, S.Q. Zhang, H.Y. Jia, J.P. Sang, J. Meng, Phys. Rev. C 69 (2004) 045805.
[57] M. Baldo, F. Burgio, Microscopic Theory of the Nuclear Equation of State and Neutron Star Structure, Lecture Notes in Physics, vol. 578, Springer-Verlag, Berlin, 2001, p. 1.

[58] M. Baldo, G.F. Burgio, Int. J. Mod. Phys. B 17 (2003) 5127.
[59] W.D. Myers, W.J. Swiatecki, Nucl. Phys. A 601 (1996) 141.
[60] K. Strobel, F. Weber, M.K. Weigel, Ch. Schaab, Int. J. Mod. Phys. E 6 (4) (1997) 669.
[61] H. Müther, A. Polls, Prog. Part. Nucl. Phys. 45 (2000) 243.
[62] R.B. Wiringa, V. Fiks, A. Fabrocini, Phys. Rev. C 38 (1988) 1010.
[63] A. Akmal, V.R. Pandharipande, Phys. Rev. C 56 (1997) 1997.
[64] A. Akmal, V.R. Pandharipande, D.G. Ravenhall, Phys. Rev. C 58 (1998) 1804.
[65] A. Chodos, R.L. Jaffe, K. Johnson, C.B. Thorne, V.F. Weisskopf, Phys. Rev. D 9 (1974) 3471.
[66] A. Chodos, R.L. Jaffe, K. Johnson, C.B. Thorne, Phys. Rev. D 10 (1974) 2599.
[67] G. Giacomelli, M. Sioli, Astroparticle Physics, hep-ex/0211035 (2002).
[68] Ch. Kettner, F. Weber, M.K. Weigel, N.K. Glendenning, Phys. Rev. D 51 (1995) 1440.
[69] D.B. Kaplan, S. Reddy, Phys. Rev. D 65 (2002) 054042.
[70] M. Alford, C. Kouvaris, K. Rajagopal, Phys. Rev. Lett. 92 (2004) 222001.
[71] M. Buballa, J. Hosek, M. Oertel, Phys. Rev. Lett. 90 (2003) 182002.
[72] A. Schmitt, Spin-one Color Superconductivity in Cold and Dense Quark Matter, nucl-th/0405076 (2004).
[73] J.A. Bowers, K. Rajagopal, Phys. Rev. D 66 (2002) 065002.
[74] R. Casalbuoni, G. Nardulli, Rev. Modern Phys. 76 (2004) 263.
[75] M. Alford, K. Rajagopal, F. Wilczek, Nucl. Phys. B 537 (1999) 443.
[76] D.T. Son, Phys. Rev. D 59 (1999) 094019.
[77] J. Madsen, P. Haensel (Eds.), Proc. of the International Workshop, Nucl. Phys. B (Proc. Suppl.) 24 (1991).
[78] J.D. Bjorken, L. McLerran, Phys. Rev. D 20 (1979) 2353.
[79] S.A. Chin, A.K. Kerman, Phys. Rev. Lett. 43 (1979) 1292.
[80] Brazil–Japan Collaboration, J.A. Chinellato et al., in: R.J. Protheroe (Ed.), Proc. of the 21st International Cosmic Ray Conference, Adelaide, Australia, vol. 8, Graphic Services, Northfield, South Australia, 1990, p. 259.
[81] G. Wilk, Z. Wlodarczyk, J. Phys. G: Nucl. Part. Phys. 22 (1996) L105;
G. Wilk, Z. Wlodarczyk, J. Phys. G: Nucl. Part. Phys. 32 (1996) 105; Nucl. Phys. B (Proc. Suppl.) 52 (1997) 215.
[82] R.L. Jaffe, Phys. Lett. 38 (1977) 195.
[83] G. Baym, E.W. Kolb, L. McLerran, T.P. Walker, R.L. Jaffe, Phys. Lett. B 160 (1985) 181.
[84] A. De Rújula, S.L. Glashow, Nature 312 (1984) 734.
[85] D. Larousserie, Les quarks font trembler la Terre, Sciences et Avenir, September, 2002, p. 84.
[86] D.P. Anderson, E.T. Herrin, V.L. Teplitz, I.M. Tibuleac, BSSA 93 (6) (2003) 2363. astro-ph/0205089.
[87] H. Terazawa, J. Phys. Soc. Japan 60 (1991) 1848.
[88] H. Terazawa, J. Phys. Soc. Japan 62 (1993) 1415.
[89] E. Gladysz-Dziadus, Z. Wlodarczyk, J. Phys. G: Nucl. Part. Phys. 23 (1997) 2057.
[90] M. Rybczynski, Z. Wlodarczyk, G. Wilk, Nuovo Cimento C 24 (2001) 645.
[91] M. Rybczynski, Z. Wlodarczyk, G. Wilk, Acta Phys. Polon. B 33 (2002) 277.
[92] J Madsen, J.M. Larsen, Phys. Rev. Lett. 90 (2003) 121102;
J. Madsen, Phys. Rev. Lett. 92 (2004) 119002.
[93] F.C. Michel, Phys. Rev. Lett. 60 (1988) 677.
[94] O.G. Benvenuto, J.E. Horvath, H. Vucetich, Int. J. Mod. Phys. A 4 (1989) 257;
O.G. Benvenuto, J.E. Horvath, Phys. Rev. Lett. 63 (1989) 716.
[95] J.E. Horvath, O.G. Benvenuto, H. Vucetich, Phys. Rev. D 45 (1992) 3865.
[96] P. Haensel, J.L. Zdunik, R. Schaeffer, Astron. Astrophys. 160 (1986) 121.
[97] V.V. Usov, Phys. Rev. Lett. 87 (2001) 021101.
[98] P. Haensel, J.L. Zdunik, Nature 340 (1989) 617.
[99] N.K. Glendenning, Ch. Kettner, F. Weber, in: J. Rafelski (Ed.), Proc. of the International Conference on Strangeness in Hadronic Matter, AIP 340, American Institute of Physics, New York, 1995, p. 46.
[100] P.F.C. Romanelli, Strange star crusts, B.S. Thesis, MIT, 1986.
[101] O.G. Benvenuto, L.G. Althaus, Astrophys. J. 462 (1996) 364; Phys. Rev. D 53 (1996) 635.
[102] F. Weber, Ch. Schaab, M.K. Weigel, N.K. Glendenning, in: F. Giovannelli, G. Mannocchi (Eds.), Frontier Objects in Astrophysics and Particle Physics, Editrice Compositori, Bologna, 1997, 88-7794-096-4, p. 87.
[103] S.K. Ghosh, S.C. Phatak, P.K. Sahu, Nucl. Phys. A 596 (1996) 670.

[104] A.V. Olinto, Phys. Lett. B 192 (1987) 71.
[105] J.A. Frieman, A.V. Olinto, Nature 341 (1989) 633.
[106] J.E. Horvath, O.G. Benvenuto, Phys. Lett. B 213 (1988) 516.
[107] J.E. Horvath, H. Vucetich, O.G. Benvenuto, Mon. Not. R. Astron. Soc. 262 (1993) 506.
[108] V.V. Usov, Astrophys. J. 550 (2001) L179.
[109] B. Zhang, R.X. Xu, G.J. Qiao, Astrophys. J. 545 (2000) L127.
[110] V.V. Usov, Astrophys. J. 559 (2001) L137.
[111] R. Ouyed, O. Elgaroy, H. Dahle, P. Keranen, Meissner Effect and Vortex Dynamics in Quark Stars–A Model for Soft Gamma-Ray Repeaters, astro-ph/0308166 (2003).
[112] V.V. Usov, Phys. Rev. Lett. 80 (1998) 230.
[113] K.S. Cheng, T. Harko, Astrophys. J. 596 (2003) 451.
[114] J. Madsen, Phys. Rev. Lett. 61 (1988) 2909.
[115] J. Madsen, H. Heiselberg, K. Riisager, Phys. Rev. D 34 (1986) 2947.
[116] J. Madsen, M.L. Olesen, Phys. Rev. D 43 (1991) 1069;
J. Madsen, M.L. Olesen, Phys. Rev. D 44 (1991) 566 (erratum).
[117] S.J. Cho, K.S. Lee, U. Heinz, Phys. Rev. D 50 (1994) 4771.
[118] G.L. Shaw, M. Shin, R.H. Dalitz, M. Desai, Nature 337 (1989) 436.
[119] H.-C. Liu, G.L. Shaw, Phys. Rev. D 30 (1984) 1137.
[120] C. Greiner, P. Koch, H. Stöcker, Phys. Rev. Lett. 58 (1987) 1825.
[121] C. Greiner, D.-H. Rischke, H. Stöcker, P. Koch, Phys. Rev. D 38 (1988) 2797.
[122] J. Sandweiss, J. Phys. G: Nucl. Part. Phys. 30 (2004) S51.
[123] T. Saito, Y. Hatano, Y. Fukuda, H. Oda, Phys. Rev. Lett. 65 (1990) 2094.
[124] T. Saito, in: G. Vassiliadis, A.D. Panagiotou, B.S. Kumar, J. Madsen (Eds.), Proc. of the International Symposium on Strangeness and Quark Matter, World Scientific, Singapore, 1995, p. 259.
[125] M. Ichimura et al., Nuovo Cimento A 36 (1993) 843.
[126] S.B. Shaulov, N.S. APH, Heavy Ion Physics 4 (1996) 403.
[127] A. De Rújula, S.L. Glashow, R.R. Wilson, G. Charpak, Phys. Rep. 99 (1983) 341.
[128] O. Miyamura, Proc. of the 24th International Cosmic Ray Conference, Rome, vol. 1, 1995, p. 890.
[129] J.J. Lord, J. Iwai, Paper 515, Presented at the International Conference on High Energy Physics, Dallas, 1992;
H. Wilczynski et al., Proceedings of the XXIV International Cosmic Ray Conference, HE Sessions, Rome, vol. 1, 1995, p. 1.
[130] MACRO Collaboration, Phys. Rev. Lett. 69 (1992) 1860.
[131] M. Ambrosio et al., Eur. J. Phys. C13 (2000) 453.
[132] M. Ambrosio et al., for the MACRO Collaboration, Status Report of the MACRO Experiment for the year 2001, hep-ex/0206027.
[133] G. Giacomelli, for the MACRO Collaboration, hep-ex/0210021 (2002).
[134] Z.-T. Lu, R.J. Holt, P. Mueller, T.P. O'Connor, J.P. Schiffer, L.-B. Wang, Searches for Stable Strangelets in Ordinary Matter: Overview and a Recent Example, nucl-ex/0402015 (2004).
[135] P.B. Price, Phys. Rev. Lett. 52 (1984) 1265.
[136] M. Brügger, K. Lützenkirchen, S. Polikanov, G. Herrmann, M. Overbeck, N. Trautmann, A. Breskin, R. Chechik, Z. Fraenkel, U. Smilansky, Nature 337 (1989) 434.
[137] M.C. Perillo Isaac et al., Phys. Rev. Lett. 81 (1998) 2416;
M.C. Perillo Isaac et al., Phys. Rev. Lett. 82 (1999) 2220 (erratum).
[138] J. Thomas, P. Jacobs, A Guide to the High Energy Heavy Ion Experiments, UCRL-ID-119181 (1995).
[139] A. Rusek et al., E886 Collaboration, Phys. Rev. C 54 (1996) R15.
[140] G. Van Buren, E864 Collaboration, J. Phys. G: Nucl. Part. Phys. 25 (1999) 411.
[141] J. Belz et al., BNL E888 Collaboration, Phys. Rev. D 53 (1996) R3487.
[142] J. Belz et al., BNL E888 Collaboration, Phys. Rev. Lett. 76 (1996) 3277.
[143] F. Dittus et al., NA52 Collaboration, in: J. Rafelski (Ed.), International Conference on Strangeness in Hadronic Matter, AIP 340, American Institute of Physics, New York, 1995, p. 24.
[144] G. Appelquist et al., Phys. Rev. Lett. 76 (1996) 3907.
[145] G. Ambrosini et al., Nucl. Phys. A 610 (1996) 306c.
[146] R. Klingenberg, J. Phys. G: Nucl. Part. Phys. 25 (1999) R273.

[147] P.B. Price, Phys. Rev. D 38 (1988) 3813.
[148] N.K. Glendenning, Mod. Phys. Lett. A 5 (1990) 2197.
[149] M. Brügger et al., Nature 337 (1989) 434.
[150] B.S. Kumar, in: G. Vassiliadis, A.D. Panagiotou, B.S. Kumar, J. Madsen (Eds.), Proc. of the Int. Symposium on Strangeness and Quark Matter, World Scientific, Singapore, 1995, p. 318.
[151] K. Pretzl, NA52 collaboration November 1997 (private communication).
[152] E. Gladysz-Dziaduś, A.D. Panagiotou, in: G. Vassiliadis, A.D. Panagiotou, B.S. Kumar, J. Madsen (Eds.), Proc. of the Int. Symposium on Strangeness and Quark Matter, World Scientific, Singapore, 1995, p. 265.
[153] C.G.M. Lattes, Y. Fujimoto, S. Hasegawa, Phys. Rep. 65 (1980) 151;
S. Hasegawa, ICRR Report, 1987, p. 151-87-5.
[154] L. McLerran, in: W. Greiner, H. Stöcker (Eds.), The Nuclear Equation of State (Part B), NATO ASI Series, Phys., vol. 216B, Plenum Press, New York, 1989, p. 155.
[155] J.D. Bjorken, Int. J. Mod. Phys. A 7 (1992) 4189.
[156] S.B. Shaulov, April, 2004 (private communication).
[157] P.B. Price, Phys. Rev. D 18 (1978) 1382.
[158] T. Saito, Proc. of the 24th International Cosmic Ray Conference, Rome, vol. 1, 1995, p. 898.
[159] J.N. Capdevielle, Proc. of the 24th International Cosmic Ray Conference, Rome, vol. 1, 1995, p. 910.
[160] E.T. Herrin, V.L. Teplitz, Phys. Rev. D 53 (1996) 6762.
[161] K.S. Thorne, in: L. Gratton (Ed.), Proc. Int. School of Phys. “Enrico Fermi”, Course 35, High Energy Astrophysics, Academic Press, New York, 1966, p. 166.
[162] J.R. Oppenheimer, G.M. Volkoff, Phys. Rev. 55 (1939) 374.
[163] R.C. Tolman, Phys. Rev. 55 (1939) 364.
[164] O. Barziv, L. Kaper, M.H. van Kerkwijk, J.H. Telting, J. van Paradijs, Astron. Astrophys. 377 (2001) 925.
[165] J.A. Orosz, E. Kuulkers, Mon. Not. R. Astron. Soc. 305 (1999) 132.
[166] J.H. Taylor, J.M. Weisberg, Astrophys. J. 345 (1989) 434.
[167] S.E. Thorsett, D. Chakrabarty, Astrophys. J. 512 (1999) 288.
[168] G.E. Brown, H.A. Bethe, Astrophys. J. 423 (1994) 659.
[169] H.A. Bethe, G.E. Brown, Astrophys. J. 445 (1995) L129.
[170] J.L. Friedman, J.R. Ipser, L. Parker, Astrophys. J. 304 (1986) 115.
[171] J.B. Hartle, Astrophys. J. 150 (1967) 1005.
[172] J.L. Friedman, J.R. Ipser, L. Parker, Phys. Rev. Lett. 62 (1989) 3015.
[173] G.F. Burgio, H.-J. Schulze, F. Weber, Astron. Astrophys. 408 (2003) 675.
[174] J.B. Hartle, D.H. Sharp, Astrophys. J. 147 (1967) 317.
[175] R. Barth et al., Phys. Rev. Lett. 78 (1997) 4007.
[176] P. Senger, Nucl. Phys. A 685 (2001) 312c.
[177] C. Sturm et al., Phys. Rev. Lett. 86 (2001) 39.
[178] A. Devismes, J. Phys. G: Nucl. Part. Phys. 28 (2002) 1591.
[179] G. Mao, P. Papazoglou, S. Hofmann, S. Schramm, H. Stöcker, W. Greiner, Phys. Rev. C 59 (1999) 3381.
[180] T. Waas, M. Rho, W. Weise, Nucl. Phys. A 617 (1997) 449.
[181] G.Q. Li, C.-H. Lee, G.E. Brown, Nucl. Phys. A 625 (1997) 372.
[182] G.Q. Li, C.-H. Lee, G.E. Brown, Phys. Rev. Lett. 79 (1997) 5214.
[183] G.E. Brown, Phys. Bl. 53 (1997) 671.
[184] G.E. Brown, in: S. Zuxun, X. Jincheng (Eds.), Proceedings of the Nuclear Physics Conference, INPC’95, World Scientific, Singapore, 1996, p. 623.
[185] V. Thorsson, M. Prakash, J.M. Lattimer, Nucl. Phys. A 572 (1994) 693.
[186] F. Weber, J. Phys. G: Nucl. Part. Phys. 25 (1999) R195.
[187] M. Alford, K. Rajagopal, S. Reddy, F. Wilczek, Phys. Rev. D 64 (2001) 074017.
[188] J. Ellis, J.I. Kapusta, K.A. Olive, Nucl. Phys. B 348 (1991) 345.
[189] B. Hermann, Master Thesis, University of Munich, 1996 (unpublished).
[190] D.G. Ravenhall, C.J. Pethick, J.R. Wilson, Phys. Rev. Lett. 50 (1983) 2066.
[191] D.G. Ravenhall, C.J. Pethick, J.M. Lattimer, Nucl. Phys. A 407 (1983) 571.
[192] R.D. Williams, S.E. Koonin, Nucl. Phys. A 435 (1985) 844.
[193] N.K. Glendenning, S. Pei, Phys. Rev. C 52 (1995) 2250.
[194] H. Heiselberg, C.J. Pethick, E.F. Staubo, Phys. Rev. Lett. 70 (1993) 1355.

[195] H. Heiselberg, in: G. Vassiliadis, A.D. Panagiotou, B.S. Kumar, J. Madsen (Eds.), Proc. of the International Symposium on Strangeness and Quark Matter, World Scientific, Singapore, 1995, p. 298.
[196] R. Tamagaki, Prog. Theor. Phys. 85 (1991) 321.
[197] T. Sakai, J. Mori, A.J. Buchmann, K. Shimizu, K. Yazaki, Nucl. Phys. A 625 (1997) 192.
[198] N.K. Glendenning, J. Schaffner-Bielich, Phys. Rev. C 58 (1998) 1298.
[199] A. Faessler, A.J. Buchmann, M.I. Krivoruchenko, B.V. Martemyanov, Phys. Lett. B 391 (1997) 255.
[200] A. Faessler, A.J. Buchmann, M.I. Krivoruchenko, Phys. Rev. C 56 (1997) 1576.
[201] R. Turolla, S. Zane, J.J. Drake, Astrophys. J. 603 (2004) 265;
S. Zane, R. Turolla, J.J. Drake, Advances Space Res. 33 (2004) 531. astro-ph/0302197.
[202] J. Drake et al., Astrophys. J. 572 (2002) 996.
[203] D. Gondek-Rosińska, W. Kluźniak, N. Stergioulas, An unusually low mass of some “neutron” stars?, astro-ph/0206470 (2002).
[204] P. Haensel, Astron. Astrophys. 380 (2001) 186.
[205] R.X. Xu, Astrophys. J. 570 (2002) L65.
[206] I. Bombaci, A possible signature for quark deconfinement in the compact star in 4U 1828-34, astro-ph/0307522 (2003).
[207] X.D. Li, I. Bombaci, M. Dey, J. Dey, E.P.J. van den Heuvel, Phys. Rev. Lett. 83 (1999) 3776.
[208] M. Dey, I. Bombaci, J. Dey, S. Ray, B.C. Samanta, Phys. Lett. B 438 (1998) 123.; 467 (1999) 303.
[209] R.X. Xu, 1E 1207.4-5209: a low-mass bare strange star?, astro-ph/0402659 (2004).
[210] R.X. Xu, G.J. Qiao, B. Zhang, Astrophys. J. 522 (1999) L109.
[211] P.O. Slane, D.J. Helfand, S.S. Murray, Astrophys. J. 571 (2002) L45.
[212] K.S. Cheng, Z.G. Dai, D.M. Wei, T. Lu, Science 280 (1998) 407.
[213] K.S. Cheng, Z.G. Dai, Phys. Rev. Lett. 77 (1996) 1210.; 80 (1998) 18.
[214] K.K. Cheng, Z.G. Dai, Astropart. Phys. 16 (2002) 277.
[215] R.R. Caldwell, J.L. Friedman, Phys. Lett. B 264 (1991) 143.
[216] C. Alcock et al., Astrophys. J. 542 (2000) 281.
[217] R.X. Xu, G.J. Qiao, Chin. Phys. Lett. 16 (1999) 778.
[218] N.K. Glendenning, F. Weber, Phys. Rev. D 50 (1994) 3836.
[219] M.A. Ruderman, Nature 223 (1969) 597.
[220] G. Baym, D. Pines, Ann. Phys. (NY) 66 (1971) 816.
[221] M.A. Alpar, Phys. Rev. Lett. 58 (1987) 2152.
[222] J.L. Zdunik, P. Haensel, E. Gourgoulhon, Astron. Astrophys. 372 (2001) 535.
[223] J.J.M. in’t Zand et al., Astron. Astrophys. 331 (1998) L25.
[224] R. Wijnands, M. van der Klis, Nature 394 (1998) 344.
[225] D. Chakrabarty, E.H. Morgan, Nature 394 (1988) 346.
[226] D. Bhattacharya, E.P.J. van den Heuvel, Phys. Rep. 203 (1991) 1.
[227] X.-D. Li, Astrophys. J. 476 (1997) 278.
[228] M. Gilfanov et al., Astron. Astrophys. 338 (1998) L83.
[229] W. Cui, E.H. Morgan, L. Titarchuk, Astrophys. J. 504 (1998) L27.
[230] D. Psaltis, D. Chakrabarty, Astrophys. J. 521 (1999) 332.
[231] X.-D. Li, S. Ray, J. Dey, M. Dey, I. Bombaci, ApJ 527 (1999) L51.
[232] J. Cottam, F. Paerels, M. Mendez, Nature 420 (2002) 51.
[233] F.M. Walter, S.J. Wolk, R. Neuhäuser, Nature 379 (1996) 233.
[234] V. Burwitz et al., Astron. Astrophys. 379 (2001) L35.
[235] V. Burwitz et al., Astron. Astrophys. 399 (2003) 1109.
[236] D.L. Kaplan, M.H. van Kerkwijk, J. Anderson, Astrophys. J. 571 (2001) 447.
[237] F.W. Walter, J. Lattimer, Astrophys. J. 576 (2002) L145.
[238] D.L. Kaplan, International Workshop in Astro-Hadron Physics on Compact Stars: Quest For New States of Dense Matter, http://beauty.phys.pusan.ac.kr/~astro/KIAS-APCTP.html.
[239] J. Drake, International Workshop in Astro-Hadron Physics on Compact Stars: Quest For New States of Dense Matter, http://beauty.phys.pusan.ac.kr/~astro/KIAS-APCTP.html.
[240] M.H. Thoma, J. Trümper, V. Burwitz, SQM 2003 Proceedings (to be published). astro-ph/0305249.
[241] S.S. Murray, P.O. Slane, F.D. Seward, S.M. Ransom, B.G. Gaensler, Astrophys. J. 568 (2002) 226.

[242] W.H.G. Lewin, R.E. Rutledge, J.M. Kommers, J. van Paradijs, C. Kouveliotou, Astrophys. J. 462 (1996) L39.
[243] R.W. Klebesadel, I.B. Strong, R.A. Olson, Astrophys. J. 182 (1973) L85.
[244] G.J. Fishman, Ch.A. Meegan, Ann. Rev. Astron. Astrophys. 33 (1995) 415.
[245] T. Piran, Phys. Rep. 314 (1999) 575.
[246] P. Haensel, B. Paczynski, P. Amsterdamski, Astrophys. J. 375 (1991) 209.
[247] G.E. Brown, C.-H. Lee, R.A.M.J. Wijers, H.K. Lee, G. Israelian, H.A. Bethe, New Astronomy 5 (4) (2000) 191.
[248] I. Bombaci, B. Datta, Astrphys. J. 530 (2000) L69.
[249] V.V. Usov, Astrophys. Space Sci. 107 (1984) 191;
C. Thompson, R.C. Duncan, Mon. Not. R. Astron. Soc. 275 (1995) 255;
J.S. Heyl, S.R. Kulkarni, Astrophys. J. 506 (1998) L61.
[250] See, for instance, astro-ph/0207527.
[251] L. Lindblom, in: V. Ferrari, J.C. Miller, and L. Rezzolla (Eds.) Gravitational Waves: A Challenge to Theoretical Astrophysics, ICTP, Lecture Notes Series, (in press), astro-ph/0101136.
[252] L. Lindblom, B. Owen, Phys. Rev. D 65 (2002) 063006.
[253] J. Madsen, Phys. Rev. Lett. 81 (1998) 3311.
[254] J. Madsen, Phys. Rev. Lett. 85 (2000) 10.
[255] M. van der Klis, Ann. Rev. Astron. Astrophys. 38 (2000) 717.
[256] C. Vogt, R. Rapp, R. Ouyed, Nucl. Phys. A 735 (2004) 543.
[257] B.K. Harrison, J.A. Wheeler, in: B.K. Harrison, K.S. Thorne, M. Wakano, J.A. Wheeler (Eds.), Gravitation Theory and Gravitational Collapse, University of Chicago Press, Chicago, 1965.
[258] G. Baym, C. Pethick, P. Sutherland, Astrophys. J. 170 (1971) 299.
[259] S. Chandrasekhar, Phys. Rev. Lett. 12 (1964) 114.
[260] J.M. Bardeen, K.S. Thorne, D.W. Meltzer, Astrophys. J. 145 (1966) 505.
[261] W.N. Cottingham, D. Kalafatis, R. Vinh Mau, Phys. Rev. Lett. 73 (1994) 1328.
[262] J.L. Provencal, H.L. Shipman, E. Hog, P. Thejll, Astrophys. J. 494 (1998) 759.
[263] J.L. Provencal, H.L. Shipman, D. Koester, F. Wesemael, P. Bergeron, Astrophys. J. 568 (2002) 324.
[264] S.O. Kepler et al., Astrophys. J. 539 (2000) 379.
[265] G.J. Mathews, B. O'Gorman, K. Otsuki, I. Suh, F. Weber, Univ. of Notre Dame preprint, 2003.
[266] G.W. Carter, S. Reddy, Phys. Rev. D 62 (2000) 103002.
[267] A.W. Steiner, M. Prakash, J.M. Lattimer, Phys. Lett. B 509 (2001) 10.
[268] S. Reddy, M. Sadzikowski, M. Tachibana, Nucl. Phys. A 714 (2003) 337. nucl-th/0203011.
[269] M. Prakash, J.M. Lattimer, A.W. Steiner, D. Page, Nucl. Phys. A 715 (2003) 835.
[270] J.A. Pons, A.W. Steiner, M. Prakash, J.M. Lattimer, Phys. Rev. Lett. 86 (2001) 5223.
[271] J.A. Pons, A.W. Steiner, M. Prakash, J.M. Lattimer, Phys. Rev. Lett. 80 (1998) 230.
[272] Ch. Schaab, A. Sedrakian, F. Weber, M.K. Weigel, Astron. Astrophys. 346 (1999) 465.
[273] K.E. McGowan, S. Zane, M. Cropper, J.A. Kennea, F.A. Córdova, C. Ho, T. Sasseen, W.T. Vestrand, Astrophys. J. 600 (2004) 343.
[274] J. Finley, H. Ögelman, IAU Circular 5787 (1993).
[275] W. Becker, IAU Circular 5805 (1993).
[276] M.C. Weisskopf, S.L. O'Dell, F. Paerels, R.F. Elsner, W. Becker, A.F. Tennant, D.A. Swartz, Astrophys. J. 601 (2004) 1050.
[277] F. Seward, F. Harnden, P. Murdin, D. Clark, Astrophys. J. 267 (1983) 698.
[278] E. Trussoni, W. Brinkmann, H. Ögelman, G. Hasinger, B. Aschenbach, Astron. Astrophys. 234 (1990) 403.
[279] J.P. Finley, H. Ögelman, G. Hasinger, J. Trümper, Astrophys. J. 410 (1993) 323.
[280] S. Safi-Harb, H. Ögelman, in: M.A. Alpar, Ü Kiziloglu, J. Van Paradijs (Eds.), The Lives of Neutron Stars, Kluwer, Dordrecht, 1995, p. 53.
[281] H. Ögelman, in: M.A. Alpar, Ü Kiziloglu, J. Van Paradijs (Eds.), The Lives of Neutron Stars, Kluwer, Dordrecht, 1995, p. 101.
[282] S.D. Yancopoulos, T.D. Hamilton, D.J. Helfland, Bull. Am. Astron. Soc. 25 (1993) 912.
[283] F. Seward, Z.-R. Wang, Astrophys. J. 332 (1988) 199.
[284] W. Becker, J. Trümper, Nature 365 (1993) 528.

[285] G.G. Pavlov, V.E. Zavlin, D. Sanwal, V. Burwitz, G.P. Garmire, Astrophys. J. 552 (2001) L129.
[286] A. Possenti, S. Mereghetti, M. Colpi, Astron. Astrophys. 313 (1996) 565.
[287] J.P. Halpern, F.Y.-H. Wang, Astrophys. J. 477 (1997) 905.
[288] C. Greiveldinger et al., Astrophys. J. 465 (1996) L35.
[289] V.E. Zavlin, J. Trümper, G.G. Pavlov, Astrophys. J. 525 (1999) 959.
[290] V.E. Zavlin, G.G. Pavlov, J. Trümper, Astron. Astrophys. 331 (1998) 821.
[291] G.G. Pavlov, V.E. Zavlin, in: R. Bandiera, R. Maiolino, F. Mannucci (Eds.), XXI Texas Symposium on Relativistic Astrophysics, World Scientific, Singapore, 2003, p. 319.
[292] C. Motch, V.E. Zavlin, F. Haberl, Astron. Astrophys. 408 (2003) 323.
[293] D.G. Yakovlev, C.J. Pethick, Ann. Rev. Astron. Astrophys. (2004) (in press). astro-ph/0402143.
[294] D.G. Yakovlev, A.D. Kaminker, P. Haensel, O.Y. Gnedin, Astron. Astrophys. 389 (2002) L24.
[295] D. Page, in: R. Buccheri, J. van Paradijs, M.A. Alpar (Eds.), The Many Faces of Neutron Stars, Kluwer Academic Publishers, Dordrecht, 1998, p. 539.
[296] D. Page, V.V. Usov, Phys. Rev. Lett. 89 (2002) 131101.
[297] D. Blaschke, D.N. Voskresensky, H. Grigorian, Cooling of Neutron Stars with Color Superconducting Quark Cores, astro-ph/0403171 (2004).
[298] J.M. Lattimer, C.J. Pethick, M. Prakash, P. Haensel, Phys. Rev. Lett. 66 (1991) 2701.
[299] Ch. Schaab, F. Weber, M.K. Weigel, N.K. Glendenning, Nucl. Phys. A 605 (1996) 531.
[300] Ch. Schaab, B. Hermann, F. Weber, M.K. Weigel, Astrophys. J. Lett. 480 (1997) L111.
[301] D. Bailin, A. Love, J. Phys. A 12 (1979) L283.
[302] D. Bailin, A. Love, Phys. Rep. 107 (1984) 325.
[303] P. Jaikumar, M. Prakash, T. Schäfer, Phys. Rev. D 66 (2002) 063003.
[304] I.A. Shovkovy, P.J. Ellis, Phys. Rev. C 66 (2002) 015802.
[305] N.K. Spyrou, N. Stergioulas, Astron. Astrophys. 395 (2002) 151.
[306] K.S. Cheng, Y.F. Yuan, J.L. Zhang, Astrophys. J. 564 (2002) 909.
[307] N.K. Glendenning, S. Pei, F. Weber, Phys. Rev. Lett. 79 (1997) 1603.
[308] F. Weber, N.K. Glendenning, S. Pei, in: B.C. Sinha, D.K. Srivastava, Y.P. Viyogi (Eds.), Signal for the Quark–Hadron Phase Transition in Rotating Hybrid Stars, Proc. of the 3rd International Conference on Physics and Astrophysics of Quark–Gluon Plasma, Narosa Publishing House, New Delhi, 1998, p. 237.
[309] S. Balberg, I. Lichtenstadt, G.P. Cook, Astrophys. J. 121 (1999) 515.
[310] J.L. Zdunik, P. Haensel, E. Gourgoulhon, M. Bejger, Astron. Astrophys. 2004 (in press). astro-ph/0311470.
[311] B.R. Mottelson, J.G. Valatin, Phys. Rev. Lett. 5 (1960) 511.
[312] F.S. Stephens, R.S. Simon, Nucl. Phys. A 183 (1972) 257.
[313] A. Johnson, H. Ryde, S.A. Hjorth, Nucl. Phys. A 179 (1972) 753.
[314] M.A. Ruderman, in: F. Pacini (Ed.), High Energy Phenomena around Collapsed Stars, D. Reidel Publishing Company, Dodrecht, 1987.
[315] N.K. Glendenning, F. Weber, Astrophys. J. 559 (2001) L119.
[316] E. Chubarian, H. Grigorian, G. Poghosyan, D. Blaschke, Astron. Astrophys. 357 (2000) 968.
[317] D. Blaschke et al., in: D. Blaschke, F. Karsch, C.D. Roberts (Eds.), Modeling Deconfinement & Quark Matter Phase Diagram, Proceedings of the International Workshop on Understanding of Deconfinement in QCD, Trento, Italy, March 1 through 12, 1999, World Scientific, 1999, (to be published).
[318] H. Heiselberg, M. Hjorth-Hensen, Phys. Rev. Lett. 80 (1998) 5485.
[319] N.K. Glendenning, Nucl. Phys. A 638 (1998) 239c.
[320] N.K. Glendenning, F. Weber, Signal of Quark Deconfinement in Millisecond Pulsars and Reconfinement in Accreting X-ray Neutron Stars, Lecture Notes in Physics, vol. 578, Springer-Verlag, Berlin, 2001, p. 305.
[321] N.K. Glendenning, F. Weber, Spin Clustering as Possible Evidence of Quark Matter in Accreting X-ray Neutron Stars, AIP conf. proc., vol. 610, 2002, p. 470.
[322] S. Konar, D. Bhattacharya, Mon. Not. R. Astron. Soc. 303 (1999) 588;
S. Konar, D. Bhattacharya, Mon. Not. R. Astron. Soc. 308 (1999) 795.
[323] G. Poghosyan, H. Grigorian, D. Blaschke, Astrophys. J. 551 (2001) L73.
[324] L. Bildsten, Astrophys. J. 501 (1998) L89.
[325] N. Andersson, D.I. Jones, K.D. Kokkotas, N. Stergioulas, Astrophys. J. 534 (2000) L75.
[326] N. Itoh, Progr. Theor. Phys. 44 (1970) 291.

[327] M.S. Berger, R.L. Jaffe, Phys. Rev. C 35 (1987) 213.
[328] E.P. Gilson, R.L. Jaffe, Phys. Rev. Lett. 71 (1993) 332.
[329] E. Farhi, R.L. Jaffe, Phys. Rev. D 30 (1984) 2379.
[330] C. Manuel, A. Dobado, F.J. Llanes-Estrada, Shear viscosity in a CFL quark star, hep-ph/0406058 (2004).
[331] D. Chakrabarty et al., Nature 424 (2003) 42.